COLLINEAR DIVERGENCES AND FACTORIZATION IN PERTURBATIVE QCD

BY

ROBERT EDWARD PUTMAN

DISSERTATION

Submitted in partial fulfillment of the requirements
for the degree of Doctor of Philosophy in Physics
in the Graduate College of the
University of Illinois at Urbana-Champaign, 2010

Urbana, Illinois

Doctoral Committee:

Professor John Stack, Chair
Professor Scott Willenbrock, Director of Research
Professor Eduardo Fradkin
Professor Mats Selen

Abstract

The issue of choosing a factorization scale in perturbative QCD is examined in detail. First a previously defined factorization scheme called the collinear scheme is implemented on Higgs production by bottom quark fusion, and then extended to Higgs production by gluon fusion. After this the issue of gauge invariance in this collinear scheme is addressed and it is realized that the collinear scheme fails to be gauge invariant. A more general analysis of collinear divergences and the phase space integrated over to calculate cross sections is performed and a new scheme called the generalized collinear scheme is presented for factorization of radiated gluons. Virtual corrections are considered and a possible method of dealing with them is suggested. This generalized collinear scheme is then tested on three $2 \to 1$ processes with encouraging results.

To God. Thanks for giving us such a fun sandbox to play around in.

"It is the glory of God to conceal things, but the glory of kings is to search things out."

Prov 25:2

Acknowledgments

Clearly the work put in to complete a doctoral degree goes far beyond what any single person can do. This thesis would not have been written without the support of my family and friends and the advice and input of my coworkers.

First I must thank my wife. Without her continual emotional, spiritual and financial support I don't know how I would have stayed focused long enough to make it through. Thank you for putting your dreams on hold for mine. She truly is deserving of a Ph.T. degree.

Secondly I must thank my parents for valuing my education above many of their own comforts and conveniences. If you had made different choices I know I couldn't possibly be here. Thanks as well for the continual support and constant prayers. Thanks for supporting my interest in science from the beginning and letting me be the geek that I am. I must also thank my brother for demonstrating a work ethic that goes far beyond mine. You're an inspiration to what people can accomplish when they stick to it and give 100% continually.

I also want to thank many of my friends who gave me outlets to be myself when I needed it the most. Thanks to Andrew for considering me to be a 'leading scientist' from day one. Thanks as well for always being an excellent person to process the mystically bizarre with and for many early morning Kung Fu lessons. Thanks to Tim for always keeping laughter in my life, many conversations about cults, and never letting my focus get too far from video games. Thanks to James for the old school days of playing Legos. I probably learned as much about physics doing that as in the classroom. Thanks to Orion for understanding my dark sense of humor and giving me an outlet to be 'the worst person ever.' Thanks to Brad and Katie for being brothers and sisters from day one; I've known few people that are amazing as you two. You are all amazing people to do life with.

I must thank many of my friends from the Vineyard. Thanks to Yu-Yu for realizing the leadership potential I had and for getting me first plugged in, as well as for taking me to China twice. That changed my life for sure. Alan and Arlene, thanks for being mentors and equippers and sold out on the prophetic. Hap and Di, thanks for many early Sunday mornings of prayer. The two of you and Ben have built an

amazing place and I hope we can live up to the foundation you have laid. I also want to thank my small group for being sold out for Jesus and hungry for the Holy Spirit. I've learned more from you than you from me for sure.

Thanks to my Kung Fu teacher, Santanu, for being an inspiration and a fantastic teacher. Every time we train together I get pushed to a new level. Thanks to my Kung Fu students for training hard and providing a healthy outlet for the at times overwhelming stress in my life.

Many thanks must be extended to Scott. Thanks for being a fantastic advisor. You know how to ask the right question even when it doesn't seem like there is one to ask. Thanks for all your flexibility and letting me run around and do all the extra things as well as physics. Thanks to Tom for being a genius and having thought of most things ahead of me. The work we've done wouldn't have gotten nearly as far without you. Thanks to Josh for explaining to me why most of my crazy GUT ideas won't work. Thanks to Will for so many amazing stories, you live life to the extreme. Thanks to Cen and Harrison for your dedication to physics. I know you guys will be better than I was for sure.

Thanks as well to the Physics Education Research group. You guys are so much fun to work with and thanks for grabbing me and putting me in an environment where I can try new things.

Thanks to my professors and fellow students at Bethel. Without the foundational knowledge I gained there I couldn't have made it through graduate school. Professors Beecken, Greenlee, Peterson and Stein - you are all fantastic and Bethel is lucky to have you. Thanks for a unique balance of brilliance, humor and wisdom.

Finally thanks to the Department of Energy for believing in Physics enough to fund it. This work was supported in part by the U.S. Department of Energy under contract No. DE-FG02-91ER40677 and in part by the University of Illinois at Urbana-Champaign.

Table of Contents

List of Tables

List of Figures

List of Symbols

d	$= 4 - 2\epsilon$, the dimensionality of spacetime in dimensional regularization
γ_E	Euler-Mascheroni constant
S	Collider center-of-mass energy squared.
v	Electroweak vaccuum expectation value.
μ	Factorization scale.
μ_{UV}	Renormalization scale.
s	$= (p_1 + p_2)^2$
t	$= (p_1 - p_3)^2$
u	$= (p_1 - p_4)^2$
z	$= \frac{Q^2}{s}$
z_0	$= \frac{Q^2}{S}$
$\{q \otimes \bar{q}\}$	$= q \otimes \bar{q} + \bar{q} \otimes q$
$\{g \otimes q\}$	$= q \otimes g + g \otimes q + \bar{q} \otimes g + g \otimes \bar{q}$
$\{g \otimes g\}$	$= g \otimes g$
$P_{qq}(z)$	$= C_F \left(\frac{1+z^2}{1-z}\right)_+$
$P_{qg}(z)$	$= T_R \left(z^2 + (1-z)^2\right)$
$P_{gq}(z)$	$= C_F \frac{1+(1-z)^2}{z}$
$P_{gg}(z)$	$= 2C_A \frac{(1-z+z^2)^2}{z(1-z)_+} + \left(\frac{11}{6}C_A - \frac{2n_f T_F}{3}\right)\delta(1-z)$
$P^d_{qq}(z)$	$= C_F \left[\left(\frac{1+z^2}{1-z}\right)_+ - \epsilon(1-z)\right]$
$P^d_{qg}(z)$	$= T_R \left(z^2 + (1-z)^2\right) - 2\epsilon T_R z(1-z)$
$P^d_{gq}(z)$	$= C_F \left[\frac{1+(1-z)^2}{z} - \epsilon z\right]$
$P^d_{gg}(z)$	$= P_{gg}(z)$

Chapter 1

Introduction

Calculations in perturbative QCD are performed in the parton model. In this model all of the hadronic physics is parameterized by probability distributions, $f_i(x)$, the probability density of choosing one parton (of index i) out of the parton with momentum fraction x ($0 \leq x \leq 1$), called the parton distribution function.[1] The form of the hadronic cross section for hard scattering is then the convolution of these parton distrubution functions with the calculable hard scattering matrix element, called the partonic cross section, $\hat{\sigma}$:

$$\sigma = \sum_{i,j} \int_0^1 dx_1 \int_0^1 dx_2 \, f_i(x_1) f_j(x_2) \hat{\sigma}_{ij}(x_1, x_2) \tag{1.1}$$

If the energy scale of the scattering is high enough, the partonic cross section can be calculated perturbatively. At next-to-leading order in pertrubation theory, the perturbation series begins to break down. If the calculation is performed with massless quarks there are divergences that aren't handled by the renormalization procedure. Keeping the quark masses finite regulates these divergence and produces logarithms of the form $\log(Q/m)$, where Q is the relevant scale in the process and m is the quark mass. These problematic terms arise from the regions in phase space where an initial parton radiates another parton that is nearly collinear to the first.

The solution to this problem is to consider the collinear terms as corrections to the parton distribution functions rather than the hard scattering matrix element. Indeed for sufficently inclusive processes it has been shown that all collinearly divergent terms can be subtracted back into the PDFs. Like the renormalization process, this introduces a momentum scale, μ, called the factorization scale, into the PDFs. The PDFs obey an evolution equation called the DGLAP equation [1], [6], [7]:

$$\frac{dq_i(x,\mu)}{d\log\mu^2} = \frac{\alpha_s}{2\pi} \int_z^1 \frac{dz}{z} \left[g(x,\mu) P_{qg}(z) + q_i(x,\mu) P_{qq}(z) \right] \tag{1.2}$$

[1] Usually abreviated PDF.

$$\frac{dg(x,\mu)}{d\log\mu^2} = \frac{\alpha_s}{2\pi}\int_z^1 \frac{dz}{z}\left[g(x,\mu)P_{gg}(z) + \sum_i q_i(x,\mu)P_{gq}(z)\right] \tag{1.3}$$

where the integration kernels are called the DGLAP splitting functions, and are predicted by QCD alone.[2] The method used to determine what to subtract into the PDFs is called a factorization scheme. Surprisingly little work has been done on the subject of factorization schemes and choosing a factorization scale. To that end this work attempts to be more systematic in factorization and the issue of choosing a factorization scale.

In general the leading order hard scattering cross section is independent of μ, but depends logarithmically on μ at next to leading order and higher. If the hard scattering contains only one momentum scale, Q, then the factorization scale is chosen to be of order Q, because there are no other scales in the problem. This doesn't determine a precise value for μ, though, and it is common practice to vary the scale between $\frac{Q}{2} \leq \mu \leq 2Q$, although this variation is arbitrarily chosen as well.

The issue of choosing a scale depends largely on how one chooses to interpret μ. If we decide to interpret μ agnostically because it is a completely unphysical scale, we are left with very little idea of how to choose the scale. At best one can try to examine properties of the convergence of the perturbation series, such as Fastest Apparent Convergence, or the Principle of Minimal Sensitivity [13]. The other choice is to interpret the scale μ as the momentum scale that separates the short distance hard scattering physics from the long distance collinear physics [3]. This interpretation has been implemented in the context of Higgs production by bottom quark fusion [12], [2], [10]. This method of choosing the scale was then further refined and examined, resulting in a factorization scheme called the collinear scheme that was proposed in [9] and [11].

In Chapter 2 this previously defined factorization scheme and method for choosing the factorization scale is implemented on the $b\bar{b} \to H$ process. The results found here are consistent with our previous findings in Drell-Yan production. Chapter 3 then extends this factorization scheme and scale choice to the $gg \to H$ process in the effective theory. This fully defines the scheme, providing all four PDF counterterms and a method of choosing the factorization scale. Chapter 4 then addresses the issue of gauge invariance of this factorization scheme. It is found that this method of factorization is not gauge invariant.

Chapter 5 then returns to the drawing board and looks at the problem more generally. A generalized scheme that is independent of the scattering process is derived, with one method for handling the infrared issues that arise implemented. This scheme and scale choice is implemented on the Drell-Yan, $gg \to H$, and $b\bar{b} \to H$ processes, with some discussion of the differences between the proposed collinear factorization scheme and the $\overline{\text{MS}}$ factorization scheme.

[2] Though beyond leading order, they depend on the scheme used to subtract the divergences.

Chapter 2

The Prelim: Bottom Quark Fusion

The first new calculation in my research was to apply the collinear scheme to the $b\bar{b} \to h$ process. This was important because it tests whether the collinear scheme is universal. The collinear limit is universal, but the collinear scheme as defined in [9] is not transparently universal. If this calculation produces a different counterterm than the Drell-Yan calculation did, we know the collinear scheme is not universal.

This calcuation will be completed treating the bottom quark as massless, with the exception of the bottom-Higgs coupling, which is proportional to the bottom quark mass (m_b).

2.1 Leading Order

At leading order there is a single diagram, shown in figure 2.1. the cross section for this process is

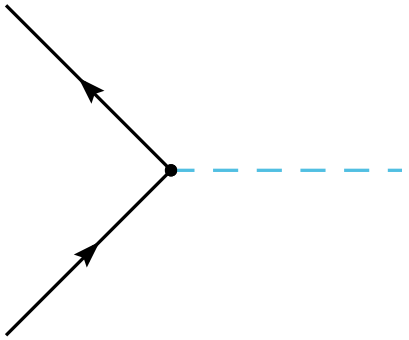

Figure 2.1: $b\bar{b} \to H$ at LO

$$\sigma = \frac{\pi}{6S}\frac{{m_b}^2}{v^2}\left\{b \otimes \bar{b}\right\}(z_0) = \sigma_{LO}\left\{b \otimes \bar{b}\right\}(z_0) \tag{2.1}$$

where I use the standard convolution notation:

$$(f_1 \otimes f_2)(x) \equiv \int_0^1 dx_1 \int_0^1 dx_2\, \delta(x_1 x_2 - x) f_1(x_1) f_2(x_2) \tag{2.2}$$

2.2 Initial Gluon Corrections

The initial gluon corrections to this process are shown in figure 2.2 the cross section for this process is

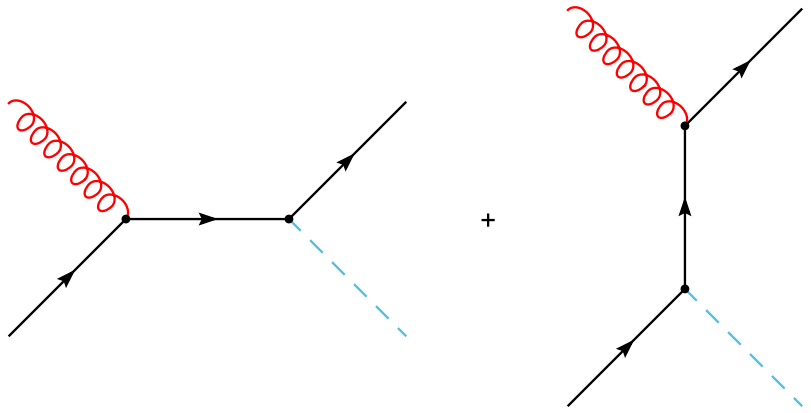

Figure 2.2: Initial gluon corrections to $b\bar{b} \to H$.

$$\sigma = \frac{\pi}{6S}\frac{{m_b}^2}{v^2}\frac{\alpha_s}{2\pi}\int_{m_H^2}^{S}\frac{ds}{s^2}\{g\otimes b\}\left(\frac{s}{S}\right)\int_{-\infty}^{0}dt\int_{-\infty}^{0}du\,\delta(s+t+u-m_H^2)\frac{1}{2}\left[\frac{s}{-t}+\frac{-t}{s}-2-\frac{2m_H^2u}{st}\right] \quad (2.3)$$

the collinear divergence is clearly visible in the divergence of $\frac{1}{-t}$ as $t \to 0$. Taking the terms that diverge as $t \to 0$ as collinear and the others as noncollinear, the cross section consists of a collinear part and a non-collinear part. Changing variables to $z = \frac{Q^2}{s}$, gives

$$\sigma^{col} = \frac{\pi}{6S}\frac{{m_b}^2}{v^2}\frac{\alpha_s}{2\pi}\int_{z_0}^{1}\frac{dz}{z}\{g\otimes b\}\left(\frac{z_0}{z}\right)\int_{-s(1-z)}^{0}\frac{dt}{-t}P_{qg}(z) \quad (2.4)$$

$$\sigma^{non} = \frac{\pi}{6S}\frac{{m_b}^2}{v^2}\frac{\alpha_s}{2\pi}\int_{z_0}^{1}\frac{dz}{z}\{g\otimes b\}\left(\frac{z_0}{z}\right)\int_{-s(1-z)}^{0}dt\,\frac{z}{2m_H^2}\left[-\frac{tz}{m_H^2}-2(1-z)\right] \quad (2.5)$$

We construct a 'collinear plot' of these two cross sections to examine the collinear behavior by taking a derivative of each of these cross sections with respect to t, then multiplying by $-t$. This will cause the limit $t \to 0$ to be finite. Plotting this against $\frac{\sqrt{-t}}{m_H}$ gives figure 2.3. The collinear divergence is manifest in the infinite area of the collinear term as the plot extends towards the left.

At this point we want to construct the collinear scheme counterterm and use the collinear plot to determine what the scale μ should be. The counterterm is constructed by keeping the residue of the t pole in the collinear part of the cross section, and multiplying this residue by $\int_{-\mu^2}^{0}\frac{dt}{-t}$. Graphically this corresponds to looking at the height of the plateau plot in the $t \to 0$ limit, then subtracting that value all the way up to

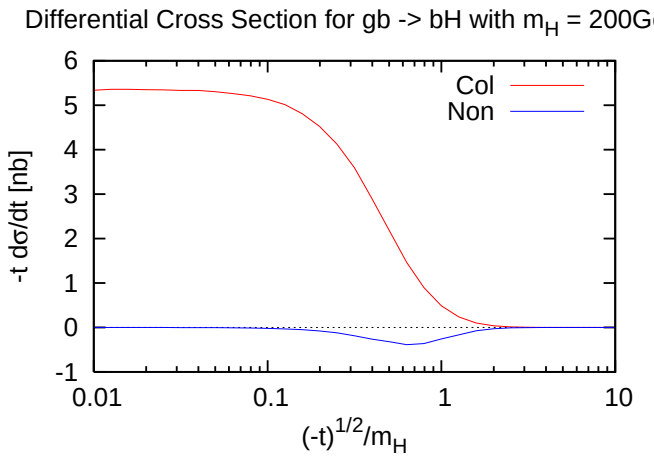

Figure 2.3: Collinear plot for initial gluon corrections of $b\bar{b} \to H$ at the LHC with $m_H = 200$ GeV. This, and all following plots use the CTEQ6 Leading Order PDFs.

the cutoff at $t = -\mu^2$. The counterterm, then, will look like a step function and will be

$$\bar{\sigma} = \lim_{t\to 0}\left[-t\frac{d\sigma}{dt}\right]\int_{-\mu^2}^{0}\frac{dt}{-t} \tag{2.6}$$

$$= \frac{\pi}{6S}\frac{{m_b}^2}{v^2}\frac{\alpha_s}{2\pi}\int_{z_0}^{1}\frac{dz}{z}\left\{g\otimes b\right\}\left(\frac{z_0}{z}\right)P_{qg}(z)\int_{-\mu^2}^{0}\frac{dt}{-t} \tag{2.7}$$

subtracting this counterterm gives the factorized cross section:

$$\sigma^{\text{fac}} = \frac{\pi}{6S}\frac{{m_b}^2}{v^2}\frac{\alpha_s}{2\pi}\int_{z_0}^{1}\frac{dz}{z}\left\{g\otimes b\right\}\left(\frac{z_0}{z}\right)\left[\int_{-s(1-z)}^{-\mu^2}\frac{dt}{-t}P_{qg}(z)+\int_{-s(1-z)}^{0}dt\,\frac{z}{2m_H^2}\left[-\frac{tz}{m_H^2}-2(1-z)\right]\right]$$

$$= \frac{\pi}{6S}\frac{{m_b}^2}{v^2}\frac{\alpha_s}{2\pi}\int_{z_0}^{1}\frac{dz}{z}\left\{g\otimes b\right\}\left(\frac{z_0}{z}\right)\left[P_{qg}(z)\log\frac{m_H^2(1-z)}{\mu^2 z}-\frac{3}{4}(1-z)^2\right] \tag{2.8}$$

plotting this cross section along side the leading order cross section gives figure 2.9.

2.2.1 Choosing the Factorization Scale

A method for choosing a scale μ is completes the calculation in the collinear scheme. A reasonable criteria for choosing a scale is to choose the scale μ so that the area of the collinear part of the cross section equals the area of the counterterm. With this choice, all of the collinear physics is subtracted into the parton distribution functions. Using the symmetry of the plateau plot this will be very close to the value that the collinear curve drops to half of its limiting value. This happens at $\mu = 0.44 m_H$. Notice the correction to the cross section is very small at this choice of factorization scale.

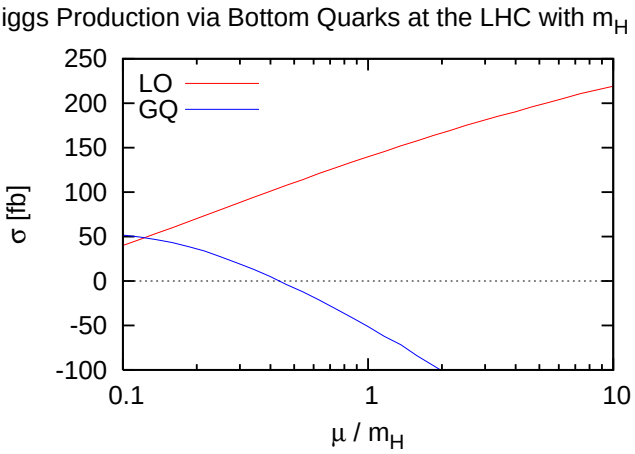

Figure 2.4: A plot of the $bg \to bH$ cross section versus the leading order cross section as a function of factorization scale. The initial gluon correction is small (less than 1%) near the factorization scale chosen using the collinear plot.

2.2.2 The PDF Counterterm

In order to compute the PDF counterterm explicitly, one must work in dimensional regularization.[1] Completing the calculation in dimensional regularization yields the same final cross section and the quark pdf counterterm:

$$\delta b(z) = -\frac{\alpha_s}{2\pi}\int_x^1 \frac{dz}{z} g\left(\frac{x}{z}\right)\left[\left(\frac{1}{\epsilon} - \gamma_E + \log\frac{4\pi\mu_D^2}{\mu^2(1-z)}\right) P_{qg}(z) - z(1-z)\right] \tag{2.9}$$

this is identical to the counterterm that we found in the Drell Yan computation, which is both expected and a good thing.

2.3 Radiated and Virtual Gluons

The same approach will not work with radiated and virtual gluon corrections to $b\bar{b} \to H$, because the story is more complex this time. The problem is that it is only the combination of the radiated and virtual corrections that are infrared and gauge-invariant, so we must consider the virtual diagrams in our calculation of the collinear counterterm. Furthermore there is a vertex renormalization that we will have to perform in this calculation, so the whole calculation will be performed using dimensional regularization.

[1] As opposed to writing it in terms of a divergent integral, which is possible in 4 dimensions, but not particularly useful for calculating numerical PDF values.

2.3.1 Radiated Gluons

The radiated gluon corrections are shown in figure 2.5. This yields:

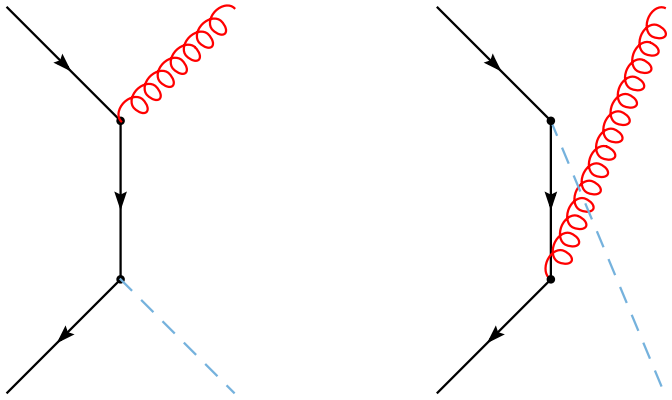

Figure 2.5: Radiated gluon corrections to $b\bar{b} \to H$.

$$\begin{aligned}\sigma_R &= \frac{\pi}{6S}\frac{{m_b}^2}{v^2}\mu_D^{2\epsilon}\frac{(4\pi\mu_D^2)^\epsilon}{\Gamma(1-\epsilon)}\frac{\alpha_s}{2\pi}\frac{2}{3}\int_{m_H^2}^{S}\frac{ds}{s^2}\left\{b\otimes\bar{b}\right\}\left(\frac{s}{S}\right) \\ &\quad \int_{-\infty}^{0}dt\int_{-\infty}^{0}du\,\delta(s+t+u-m_H^2)\left(\frac{s}{tu}\right)^\epsilon\left[(1-\epsilon)\left(\frac{t}{u}+\frac{u}{t}+2\right)+\frac{2sm_H^2}{tu}\right] \end{aligned} \tag{2.10}$$

a quick examination of the divergences reveals that there are collinear divergences both at $t = 0$ and $u = 0$. When $t = u = 0$, there is an infrared divergence as well. This is clear because the delta function forces $s = m_H^2$ when both t and u are zero.[2]

2.3.2 Virtual Gluons

There are two virtual gluon corrections, a vertex correction and the wavefunction renormalization diagram, shown in figures 2.6 and 2.7, respectively.

The wavefunction renormalization diagram in dimensional regularization is zero, because there is no scale for the loop integral to be proportional to. This happens because an collinear divergence cancels against an ultraviolet divergence, so we know that this graph contains collinear physics.

The vertex correction shifts the coupling to the Higgs by a constant value: $m_b^2 \to m_b^2(1+\Gamma)$ where

$$\Gamma = -2\imath g_s^2\mu_D^{2\epsilon}C_F\int_0^1 dx\int_0^1 dy\int_0^1 dz\,\delta(x+y+z-1)\int\frac{d^dk}{(2\pi)^d}\frac{dk^2-m_H^2(dxy+2z)}{[k^2+xym_H^2]^3} \tag{2.11}$$

[2]Additionally, we can use the identity $\frac{1}{tu} = \frac{1}{s-m_H^2}\left(\frac{1}{-t}+\frac{1}{-u}\right)$ This makes clear that this is an overlapping collinear and infrared divergence.

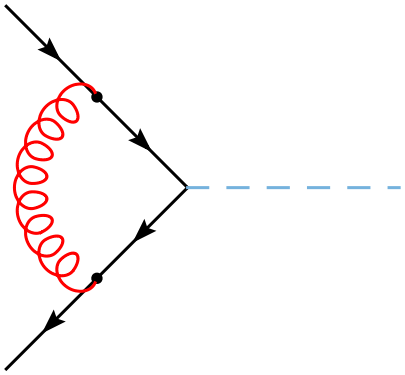

Figure 2.6: Vertex correction to $b\bar{b} \to H$.

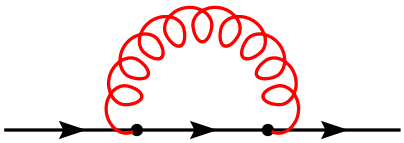

Figure 2.7: Self energy diagram correcting the external legs. This diagram has two effects: the first is a wavefunction renormalization on the bottom quark field, the second is a renormalization of the Higgs coupling because this diagram also renormalizes the bottom mass.

where x, y, and z are Feynman parameters. Performing the loop integral over k yields

$$\Gamma = \frac{\alpha}{2\pi} C_F \left(\frac{4\pi\mu_D^2}{-m_H^2}\right)^\epsilon \frac{\Gamma(1+\epsilon)}{2} \int_0^1 dx \int_0^1 dy \int_0^1 dz\, \delta(x+y+z-1) \left(\frac{1}{xy}\right)^\epsilon \left[\frac{d(d-2)}{\epsilon} - \frac{2z}{xy}\right] \tag{2.12}$$

we need to be able to combine the wavefunction renormalization term with this term. To facilitate that, we multiply the expression for the wavefunction renormalization graph by $\frac{(p_2+l)^2}{(p_2+l)^2}$ if p_1 is the branch we're renormalizing, and l is the unshifted loop momentum.[3] Then the denominator structure is the same in both diagrams, and thus the Feynman parameters will come out the same. This produces

$$\Sigma'(0) \quad = \quad -4ig_s^2\mu_D^{2\epsilon} C_F(1-\epsilon) \int_0^1 dx \int_0^1 dy \int_0^1 dz\, \delta(x+y+z-1) \int \frac{d^dk}{(2\pi)^d} \frac{\frac{2y}{d}k^2 - (1-y)(k^2 + y(1-x)m_H^2)}{[k^2 + xym_H^2]^3} \tag{2.13}$$

Once again, integrating over the loop momentum:

$$\begin{aligned}\Sigma'(0) \quad = \quad & \frac{\alpha_s}{2\pi} C_F(1-\epsilon)\Gamma(1+\epsilon) \left(\frac{4\pi\mu_D^2}{-m_H^2}\right)^\epsilon \int_0^1 dx \int_0^1 dy \int_0^1 dz\, \delta(x+y+z-1) \\ & \left(\frac{1}{xy}\right)^\epsilon \left[\frac{d}{2\epsilon}\left(\frac{2y}{d} - (1-y)\right) - \frac{(1-x)(1-y)}{x}\right]\end{aligned} \tag{2.14}$$

[3]Of course we know this diagram shouldn't know about p_2, so anything that looks like it depends on p_2 must integrate to zero.

combining these two corrections together:

$$\begin{aligned}\sigma_{LO} &\rightarrow \sigma_{LO}\left(1+\Gamma+\frac{1}{2}\Sigma'(0)_{p_1}+\frac{1}{2}\Sigma'(0)_{p_2}\right)\\ &= \sigma_{LO}\Bigg(1+\frac{\alpha_s}{2\pi}\frac{C_F}{2}\Gamma(1+\epsilon)(1-\epsilon)\left(\frac{4\pi\mu_D^2}{m_H^2}\right)^{\epsilon}\int dx\,dy\,dz\,\delta(x+y+z-1)\left(\frac{1}{xy}\right)^{\epsilon}\\ &\quad \mathrm{Re}[(-1)^{\epsilon}]\left(\frac{2d}{\epsilon}-\frac{2z}{(1-\epsilon)xy}+\frac{1-z}{\epsilon}-\frac{d}{2\epsilon}(1+z)-\left(\frac{1}{x}+\frac{1}{y}\right)(z+xy)\right)\Bigg)\end{aligned} \tag{2.15}$$

2.3.3 Feynmandelstam

To combine the virtual and radiative corrections and construct the counterterm, we need to extract the collinear part of the virtual term. Notice the similarity of the region of integration of the phase space:

$$\int_{m_H^2}^{S} ds\int_{-\infty}^{0} dt\int_{-\infty}^{0} du\,\delta(s+t+u-m_H^2) \tag{2.16}$$

and the region of integration of Feynman parameters:

$$\int_0^1 dx\int_0^1 dy\int_0^1 dz\,\delta(x+y+z-1) \tag{2.17}$$

both integrals are over a triangular region. Notice that with the following mapping[4]

$$x\rightarrow -\frac{u}{s}\quad y\rightarrow -\frac{t}{s}\quad z\rightarrow \frac{m_H^2}{s} \tag{2.18}$$

the region of integration of the Feynmandelstam is mapped to

$$\int_0^1 dx\int_0^1 dy\int_0^1 dz\,\delta(x+y+z-1)\rightarrow \int_{m_H^2}^{\infty}\frac{ds}{s^2}\frac{m_H^2}{s}\int_{-\infty}^{0} dt\int_{-\infty}^{0} du\,\delta(s+t+u-m_H^2) \tag{2.19}$$

and the virtual correction can be written

$$\begin{aligned}\sigma_V &= \sigma_{LO}\frac{\alpha_s}{2\pi}\frac{C_F}{2}\Gamma(1+\epsilon)(1-\epsilon)\left(\frac{4\pi\mu_D^2}{m_H^2}\right)^{\epsilon}\int_{m_H^2}^{\infty}\frac{ds}{s^2}\frac{m_H^2}{s}\int_{-\infty}^{0} dt\int_{-\infty}^{0} du\,\delta(s+t+u-m_H^2)\left(\frac{s^2}{tu}\right)^{\epsilon}\\ &\quad \mathrm{Re}[(-1)^{\epsilon}]\left(\frac{2d}{\epsilon}-\frac{2sm_H^2}{(1-\epsilon)tu}+\frac{1-\frac{m_H^2}{s}}{\epsilon}-\frac{d}{2\epsilon}\left(1+\frac{m_H^2}{s}\right)-\left(\frac{s}{-t}+\frac{s}{-u}\right)\left(\frac{m_H^2}{s}+\frac{tu}{s^2}\right)\right)\end{aligned} \tag{2.20}$$

Equation 2.19 is the fundamental idea to the Feynmandelstam approach to the collinear scheme; by choosing an appropriate mapping, we can map the virtual corrections to the same integral space as the

[4]Called by my collaborator and the inventor, Tom McElmurry, the Feynmandelstam mapping.

radiative corrections. From there we can just take the collinear limit ($t \to 0$ or $u \to 0$) and construct the counterterm just as we did in the initial gluon case.

2.3.4 Constructing the Counterterm

Combining the radiative cross section and the virtual cross section produces

$$\begin{aligned}\sigma_{R+V} &= \sigma_{LO}\frac{\alpha_s}{2\pi}C_F\mu_D^{2\epsilon}\frac{(4\pi\mu_D^2)^\epsilon}{\Gamma(1-\epsilon)}\int_{m_H^2}^{\infty}\frac{ds}{s^2}\int_{-\infty}^{0}dt\int_{-\infty}^{0}du\,\delta(s+t+u-m_H^2)\\ &\left[\theta(S-s)\left\{b\otimes\bar{b}\right\}\left(\frac{s}{S}\right)\left[(1-\epsilon)\left(\frac{t}{u}+\frac{u}{t}+2\right)+\frac{2sm_H^2}{tu}\right]\right.\\ &+\left\{b\otimes\bar{b}\right\}\left(\frac{m_H^2}{S}\right)\Gamma(1-\epsilon)\Gamma(1+\epsilon)\mathrm{Re}[(-1)^\epsilon]\left(\frac{m_H^2}{s}\right)^{1-\epsilon}\left(\frac{2d}{\epsilon}-\frac{2sm_H^2}{(1-\epsilon)tu}+\frac{1-\frac{m_H^2}{s}}{\epsilon}\right.\\ &\left.\left.-\frac{d}{2\epsilon}\left(1+\frac{m_H^2}{s}\right)-\left(\frac{s}{-t}+\frac{s}{-u}\right)\left(\frac{m_H^2}{s}+\frac{tu}{s^2}\right)\right)\right]\end{aligned} \tag{2.21}$$

Consider the infrared behavior: the infrared pole should cancel between the radiative and virtual terms. This happens in the $s \to m_H^2$, or $t, u \to 0$ limit. The $\frac{1}{tu}$ terms in the integrand are:

$$\left\{b\otimes\bar{b}\right\}\left(\frac{s}{S}\right)\left[\frac{2sm_H^2}{tu}\right]+\left\{b\otimes\bar{b}\right\}\left(\frac{m_H^2}{S}\right)\Gamma(1-\epsilon)\Gamma(1+\epsilon)\mathrm{Re}[(-1)^\epsilon]\left(\frac{m_H^2}{s}\right)^{1-\epsilon}\left(-\frac{2sm_H^2}{(1-\epsilon)tu}\right) \tag{2.22}$$

keeping just the $O(\epsilon^0)$ term and taking the $s \to m_H^2$ limit,

$$\left\{b\otimes\bar{b}\right\}\left(\frac{m_H^2}{S}\right)\left[\frac{2m_H^4}{tu}\right]-\left\{b\otimes\bar{b}\right\}\left(\frac{m_H^2}{S}\right)\frac{2m_H^4}{tu}=0 \tag{2.23}$$

we see the infrared cancellation between these two terms manifestly. Next we turn to constructing the counterterm by taking the collinear limit, just as we did in the initial gluon case.[5] For this cross section the counterterm is

$$-t\frac{d\sigma_{R+V}}{dt}=\sigma_{LO}\frac{\alpha_s}{2\pi}C_F\int_{m_H^2-t}^{\infty}\frac{ds}{s}\left[\theta(S-s)\{b\otimes\bar{b}\}\left(\frac{s}{S}\right)\frac{s^2+m_H^4}{s(s-m_H^2)}-\{b\otimes\bar{b}\}\left(\frac{m_H^2}{S}\right)\frac{m_H^4}{s}\frac{3s-m_H^2}{s-m_H^2}\right] \tag{2.24}$$

this is plotted in figure 2.8. The factorization scale obtained from this plot is $\mu = 0.61 m_H$.

From here the calculation proceeds exactly the same as the initial gluon correction calculation did. Performing the integrals over phase space and changing variables from s to z:

$$\sigma_{R+V} = \sigma_{LO}\mu_D^{2\epsilon}\frac{\alpha_s}{2\pi}\left(\frac{4\pi\mu_D^2}{m_H^2}\right)^\epsilon\frac{C_F}{\Gamma(1-\epsilon)}\int_{z_0}^{1}\frac{dz}{z}\{b\otimes\bar{b}\}\left(\frac{z_0}{z}\right)\left[-\frac{2}{\epsilon}\frac{1+z^2}{(1-z)_+}\right.$$

[5] We construct the counterterm in 4 dimensions. We just follow the same proceedure as before, then take the limit $d \to 4$.

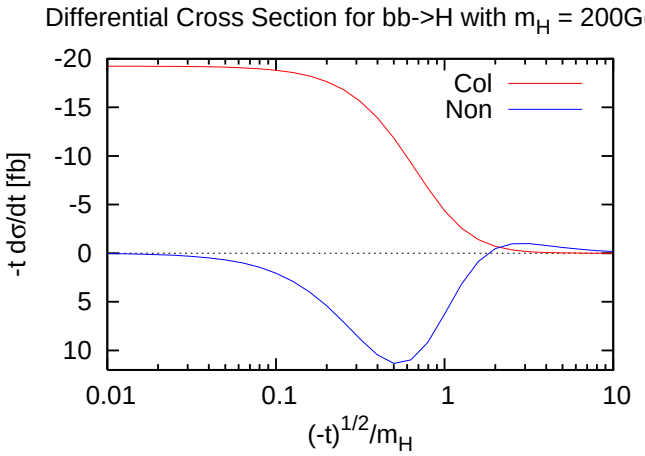

Figure 2.8: Plot of the collinear and noncollinear parts of the real and virtual corrections cross section at the LHC. μ_R (to be discussed later) is set to m_H. Notice the correction is opposite in sign to the correction due to the initial gluons.

$$+4(1+z^2)\left(\frac{\log 1-z}{1-z}\right) - 2\frac{1+z^2}{1-z}\log z + 2(1-z) + \delta(1-z)\left(\frac{2\pi^2}{3}-2\right)\Bigg] \tag{2.25}$$

there are collinear poles that arise in both the $t \to 0$ and $u \to 0$ limits, so we must subtract two copies of the collinear counterterm:

$$\begin{aligned}\bar{\sigma}_{R+V} &= \sigma_{LO}\mu_D^{2\epsilon}\frac{\alpha_s}{2\pi}\left(\frac{4\pi\mu_D^2}{\mu^2}\right)^{\epsilon}\frac{C_F}{\Gamma(1-\epsilon)}\int_{z_0}^1\frac{dz}{z}\{b\otimes\bar{b}\}\left(\frac{z_0}{z}\right)\Bigg[-\frac{2}{\epsilon}\left(\frac{1+z^2}{1-z}\right)_+ \\ &\quad +2(1+z^2)\left(\frac{\log 1-z}{1-z}\right)+2(1-z)+\delta(1-z)\left(2\pi^2-7\right)\Bigg]\end{aligned} \tag{2.26}$$

additionally one must add back in a counter-counterterm. The calculation has double-subtracted the point $t = u = 0$, because this point is included in the counterterms for both the t and u poles. The counter-counterterm is

$$\bar{\bar{\sigma}}_{R+V} = \lim_{t,u\to 0}\left[(tu)^{1+\epsilon}\frac{d^2\sigma_{R+V}}{dtdu}\right]\int_{-\mu^2}^0\frac{dt}{(-t)^{1+\epsilon}}\int_{-\mu^2}^0\frac{du}{(-u)^{1+\epsilon}} \tag{2.27}$$

$$= \sigma_{LO}\mu_D^{2\epsilon}\frac{\alpha_s}{2\pi}\left(\frac{4\pi\mu_D^2}{\mu^2}\right)^{\epsilon}\frac{C_F}{\Gamma(1-\epsilon)}\int_{z_0}^1\frac{dz}{z}\{b\otimes\bar{b}\}\left(\frac{z_0}{z}\right)\left[\frac{2\pi^2}{3}\delta(1-z)\right] \tag{2.28}$$

Assembling all of this together, the factorized cross section is:

$$\begin{aligned}\sigma^{\text{fac}}_{R+V} &= \sigma_{LO}\mu_D^{2\epsilon}\frac{\alpha_s}{2\pi}\left(\frac{4\pi\mu_D^2}{m_H^2}\right)^{\epsilon}\frac{C_F}{\Gamma(1-\epsilon)}\int_{z_0}^1\frac{dz}{z}\{b\otimes\bar{b}\}\left(\frac{z_0}{z}\right)\Bigg[2\left(\frac{1+z^2}{1-z}\right)_+\log\frac{m_H^2}{\mu^2} \\ &\quad +2(1+z^2)\left(\frac{\log 1-z}{1-z}\right)_+ - 2\frac{1+z^2}{1-z}\log z + \left(5-\frac{2\pi^2}{3}+\frac{3}{\epsilon}\right)\delta(1-z)\Bigg]\end{aligned} \tag{2.29}$$

Notice that after subtracting the collinear counterterm we still have a divergence in the $\delta(1-z)$ term. This is because there is a mass renormalization that occurs because of the quark self-energy diagram that hast not been dealt with yet. The mass shift that arises from the self-energy diagram is $m_b \to m_b + \delta m_b$, where

$$\delta m_b = m_b \frac{\alpha_s}{2\pi} \frac{C_F}{2} \Gamma(1+\epsilon) \left(\frac{4\pi\mu_D^2}{m_H^2} \right)^{\epsilon} \left[\frac{3}{\epsilon} + 4 \right] \tag{2.30}$$

to deal with this one must renormalize the mass. This is accomplished by reinterpreting the shifted mass as a mass that depends on the renormalization scale plus a counterterm ($m_b + \delta m_b = m_b(\mu_R) + \delta m_R$). Taking the mass counterterm to be the $\overline{\text{MS}}$ counterterm, which says to just take the leading divergence, plus a γ_E and $\log \frac{4\pi\mu_D^2}{\mu_R^2}$ produces:

$$\delta m_R = m_b \frac{\alpha_s}{2\pi} \frac{C_F}{2\Gamma(1-\epsilon)} \left(\frac{4\pi m u_D^2}{\mu_R^2} \right)^{\epsilon} \frac{3}{\epsilon} \tag{2.31}$$

using this mass renormalization produces the factorized, renormalized cross section. The 4 dimensional limit of this cross section is well defined:

$$\begin{aligned} \sigma_{R+V}^{\text{fac, R}} \quad = \quad & \frac{\pi}{6S} \left(\frac{m(\mu_R)}{v} \right)^2 \frac{\alpha_s}{2\pi} \int_{z_0}^1 \frac{dz}{z} \{b \otimes \bar{b}\} \left(\frac{z_0}{z} \right) \left[2P_{qq}(z) \log \frac{m_H^2}{\mu^2} \right. \\ & \left. -\frac{8}{3}(1+z^2) \left(\frac{\log 1-z}{1-z} \right)_+ + \frac{8}{3} \frac{1+z^2}{1-z} \log z + \left(\frac{20}{3} - \frac{8\pi^2}{9} + 4 \log \frac{\mu_R^2}{m_H^2} \right) \delta(1-z) \right] \end{aligned} \tag{2.32}$$

this cross section is plotted alongside the leading order cross section in figure 2.9.

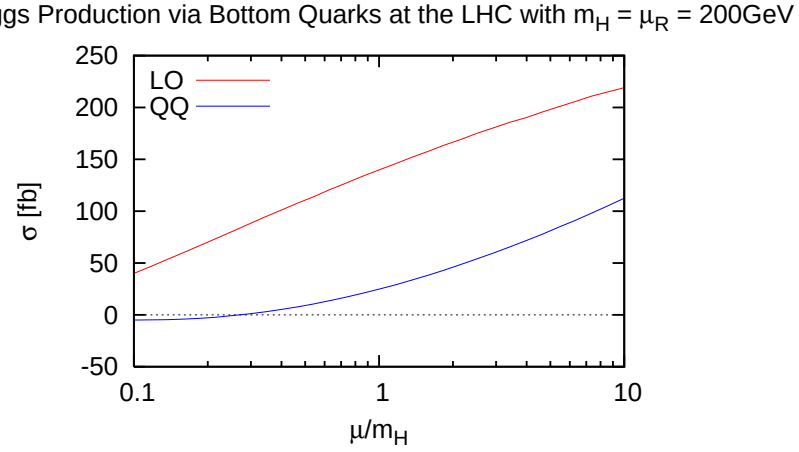

Figure 2.9: Plot of the real and virtual gluon corrections to $b\bar{b} \to H$ for a range of factorization scales. The renormalization scale here has been chosen to be $\mu_R = m_H$. Once again the correction at the specified factorization scale is small. This time on the order of 9%.

2.3.5 PDF Counterterm

The collinear conterterm correction of the quark PDF is

$$\begin{aligned}\delta b(x) &= -\frac{\alpha_s}{2\pi}\int_x^1 \frac{dz}{z} b\left(\frac{x}{z}\right)\left[\left(\frac{1}{\epsilon}-\gamma_E+\log\frac{4\pi\mu_D^2}{\mu^2}\right)P_{qq}(z)-\frac{4}{3}(1+z^2)\left(\frac{\log 1-z}{1-z}\right)_+\right.\\ &\left.-\frac{4}{3}(1-z)-\left(\frac{8\pi^2}{9}-\frac{14}{3}\right)\delta(1-z)\right] \qquad (2.33)\end{aligned}$$

This is also the same PDF counterterm we found for the quarks in Drell Yan. This is good, both the PDF counterterms we found in the $b\bar{b}\to H$ process match the ones we found in Drell Yan. This seems to indicate that there is a good chance that the PDF counterterms are universal.

Chapter 3

Gluon Fusion

Next we implemented the collinear scheme on the $gg \to h$ process. This allowed us to determine what the gluon PDF counterterms are, providing a complete definition of the collinear scheme. The procedure for this process looks very similar to the cases of Drell-Yan and Bottom Quark fusion.

This calculation is done in the effective theory approximation, where the top quark loop is integrated out and reduced to an effective ggH vertex. This approach produces the following Feynman rules:

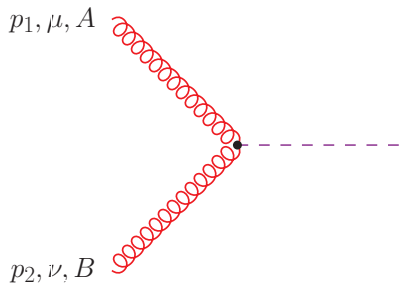

Figure 3.1: Graph for the ggH vertex. The Feynman rule for this graph is $\imath A \delta^{AB} H^{\mu\nu}(p_1, p_2)$

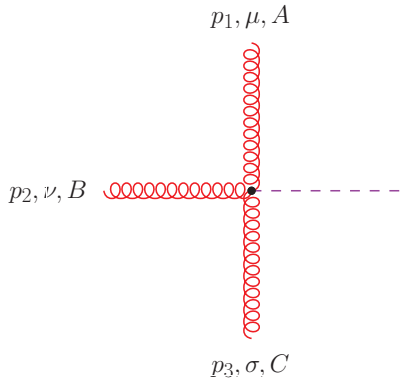

Figure 3.2: Graph for the $gggH$ vertex. The Feynman rule for this graph is $-A g_s f^{ABC} V^{\mu\nu\sigma}(p_1, p_2, p_3)$

where

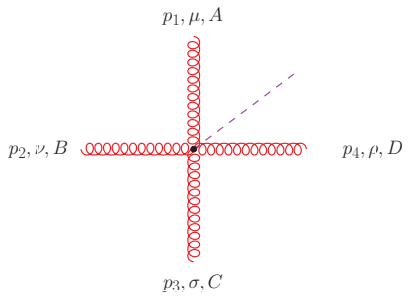

Figure 3.3: Graph for the $gggH$ vertex. The Feynman rule for this graph is $-\imath A g_s^2 X^{ABCD}_{\mu\nu\sigma\rho}$

$$A = \frac{\alpha_s}{3\pi v}\left(1+\frac{\alpha_s}{2\pi}\frac{11}{2}\right) \tag{3.1}$$

$$H^{\mu\nu}(p_1,p_2) = g^{\mu\nu}p_1\cdot p_2 - p_2^\mu p_1^\nu \tag{3.2}$$

$$V^{\mu\nu\sigma}(p_1,p_2,p_3) = (p_1-p_2)^\sigma g^{\mu\nu} + (p_2-p_3)^\mu g^{\nu\sigma} + (p_3-p_1)^\nu g^{\sigma\mu} \tag{3.3}$$

$$\begin{aligned} X^{\mu\nu\sigma\rho}_{ABCD} &= f_{ABE}f_{CDE}(g^{\mu\rho}g^{\nu\sigma}-g^{\mu\sigma}g^{\nu\rho}) + f_{ACE}f_{BDE}(g^{\mu\nu}g^{\rho\sigma}-g^{\mu\sigma}g^{\nu\rho}) \\ &\quad + f_{ADE}f_{BCE}(g^{\mu\nu}g^{\rho\sigma}-g^{\mu\rho}g^{\nu\sigma}) \end{aligned} \tag{3.4}$$

3.1 Leading Order

At leading order, the Feynman diagram is just figure 3.1. Using this diagram and the corresponding Feynman rule, the cross section is[1]

$$\sigma = \frac{\alpha_s^2}{576\pi v^2}\frac{m_H^2}{s}(1+\epsilon+\epsilon^2)\mu^{2\epsilon}\delta(1-z) = \sigma_{LO}\delta(1-z) \tag{3.5}$$

notice how a factor of z is included in the definition of σ_{LO}.

3.2 Quark Anti-Quark Initial State

One of the corrections at NLO is finite and can be calculated directly in 4 dimensions. This correction comes from a $q\bar{q}$ initial state and is shown in figure 3.4 this diagram produces a matrix element

$$\overline{|\mathcal{M}|^2} = \frac{4}{81}\frac{\alpha_s^3}{\pi v^2}\frac{u^2+t^2-\epsilon(u+t)^2}{s} \tag{3.6}$$

[1]Keeping of course just the leading behavior in α_s.

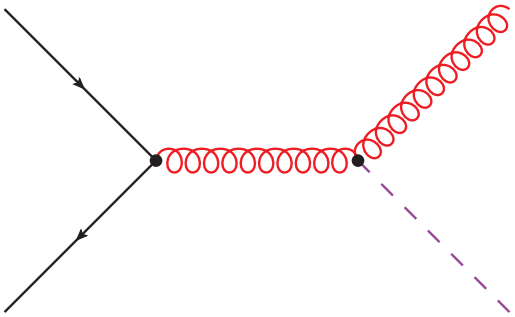

Figure 3.4: $q\bar{q}$ initial state correction to $gg \to H$. This diagram has no divergences and can be calculated directly in four dimensions.

which when integrated over phase space produces

$$\sigma_{q\bar{q}} = \sigma_{LO} \frac{\alpha_s}{2\pi} \frac{64}{27} \frac{(1-z)^3}{z} \tag{3.7}$$

3.3 Quark Gluon Initial State

The next correction to the cross section is the crossed diagram from figure 3.4. This diagram is shown in figure 3.5. The matrix element for the diagram in figure 3.5 is:

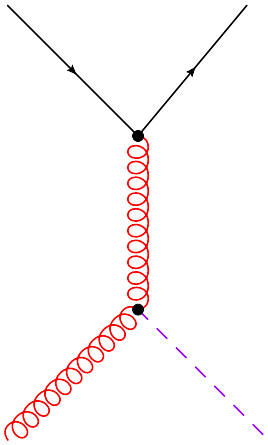

Figure 3.5: qg initial state correction to $gg \to H$. This diagram has a t channel collinear divergence.

$$\overline{|\mathcal{M}|^2} = \frac{1}{54(1-\epsilon)} \frac{\alpha_s^3}{\pi v^2} \frac{s^2 + u^2 - \epsilon(s+u)^2}{-t} \tag{3.8}$$

when integrated over the d dimensional phase space

$$\Phi_2 = \frac{1}{8\pi s}\frac{(4\pi\mu_D^2)^\epsilon}{\Gamma(1-\epsilon)}\int_{-s(1-z)}^{0} dt \left(\frac{s}{tu}\right)^\epsilon \tag{3.9}$$

this yields the cross section:

$$\sigma_{qg} = \frac{\alpha_s^2}{576\pi v^2} z \frac{\alpha_s}{2\pi} C_F \left(\frac{4\pi\mu_D^2}{m_H^2}\right)^\epsilon \frac{\Gamma(1-\epsilon)}{\Gamma(1-2\epsilon)} \left(\frac{1+(1-z)^2}{z}\left[-\frac{1}{\epsilon} + \log\frac{(1-z)^2}{z}\right] + \frac{(1-z)(3z-7)}{2z}\right) \tag{3.10}$$

Because the collinear divergence is the only divergence in this diagram, we can work with the collinear scheme explicitly in four dimensions.[2] Considering the collinear limit we have $u = Q^2 - s - t \to -s(1-z)$, and so we see

$$\overline{|\mathcal{M}|^2} \lim_{t\to 0} = \frac{1}{54(1-\epsilon)}\frac{\alpha_s^3}{\pi v^2} s^2 \frac{1+(1-z)^2}{-t} \tag{3.11}$$

this gives a collinear plot, which is plotted in figure 3.6

$$-t\frac{d\sigma}{dt} = \int_0^{\frac{m_H^2}{m_H^2 - t}} \frac{dz}{z}\{g\otimes q\}\left(\frac{z_0}{z}\right)\frac{\alpha_s^2}{576\pi v^2} z \frac{\alpha_s}{2\pi} C_F \frac{1+(1-z)^2}{z} \tag{3.12}$$

and the collinear counterterm is

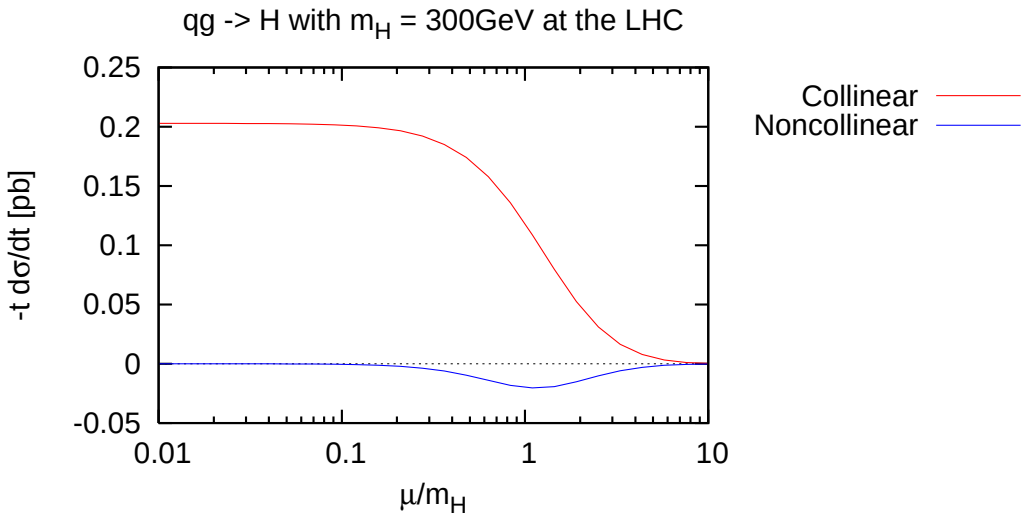

Figure 3.6: Collinear plot of the initial quark correction to $gg \to H$ at the LHC with $m_H = 200$ GeV. This, and all following plots in this section are made using the CTEQ5 $\overline{\text{MS}}$ set of PDFs. This is representative of a large range of m_H, where we have $\mu \approx m_H$

[2]Performing the calculation both ways, we see this gives the same result.

$$\begin{aligned}\bar{\sigma} &= \frac{1}{2s}\frac{1}{8\pi s}\int_{-\mu}^{0} dt \frac{1}{54}\frac{\alpha_s^3}{\pi v^2} s^2 \frac{1+(1-z)^2}{-t} \\ &= \frac{\alpha_s^2}{576\pi v^2} z \frac{\alpha_s}{2\pi} P_{gq}(z) \int_{-\mu}^{0} \frac{dt}{-t} \end{aligned} \tag{3.13}$$

which has the same form as the counterterm for quark-gluon splitting that we found in the Drell-Yan and bottom quark fusion calculations. Calculating the regulated cross section then,

$$\sigma_{qg} - \bar{\sigma} = \frac{1}{16\pi s^2}\frac{\alpha_s^3}{54\pi v^2}\left[\int_{-s(1-z)}^{0} dt \frac{s^2+u^2}{-t} - s^2(1+(1-z)^2)\int_{-\mu^2}^{0}\frac{dt}{-t}\right] \tag{3.14}$$

$$= \frac{\alpha_s^2}{576\pi v^2}\frac{1}{s^2}\frac{\alpha_s}{2\pi}C_F\left[\int_{-s(1-z)}^{0} dt \frac{s^2+(s(1-z)+t)^2}{-t} - s^2(1+(1-z)^2)\int_{-\mu^2}^{0}\frac{dt}{-t}\right] \tag{3.15}$$

$$= \frac{\alpha_s^2}{576\pi v^2}\frac{1}{s^2}\frac{\alpha_s}{2\pi}C_F\left[-\int_{-s(1-z)}^{0} dt(t+2s(1-z)) + s^2(1+(1-z)^2)\int_{-s(1-z)}^{-\mu^2}\frac{dt}{-t}\right] \tag{3.16}$$

$$= \frac{\alpha_s^2}{576\pi v^2} z \frac{\alpha_s}{2\pi}C_F\left[-\frac{3}{2}\frac{(1-z)^2}{z} + \frac{(1+(1-z)^2)}{z}\log\frac{m_H^2(1-z)}{\mu^2 z}\right] \tag{3.17}$$

$$= \frac{\alpha_s^2}{576\pi v^2} z \frac{\alpha_s}{2\pi}\left[P_{gq}(z)\log\frac{m_H^2(1-z)}{\mu^2 z} - 2\frac{(1-z)^2}{z}\right] \tag{3.18}$$

3.3.1 The PDF Counterterm

Performing the calcuation in d dimensions yields the PDF counterterm:

$$\delta g(x) = -\frac{\alpha_s}{2\pi}\int_x^1 \frac{dz}{z} q\left(\frac{x}{z}\right)\left[\left(\frac{1}{\epsilon} - \gamma_E + \log\frac{4\pi\mu_D^2}{\mu^2(1-z)}\right)P_{gq}(z) - z\right] \tag{3.19}$$

3.4 Gluon Gluon Initial State

There are both radiative and virtual corrections to the gluon gluon initial state corrections. We will follow the same method here as we did with $bb \to H$, first we will look at the collinear component of the radiative corrections, and using the Feynmandelstam mapping combine the radiative and virtual corrections into an infrared-safe collinear cross section.

3.4.1 Radiative Corrections

There are s channel, t channel, u channel, and contact diagrams that contribute at this order with a gluon gluon initial state. These diagrams are shown in figure 3.7. these diagrams together give a matrix element:

$$\overline{|\mathcal{M}|^2} = \frac{1}{24(1-\epsilon)^2}\frac{\alpha_s^3}{\pi v^2}\frac{(s^4+t^4+u^4+m_H^8)(1-2\epsilon)+\frac{\epsilon}{2}(s^2+t^2+u^2+m_H^4)^2}{stu} \tag{3.20}$$

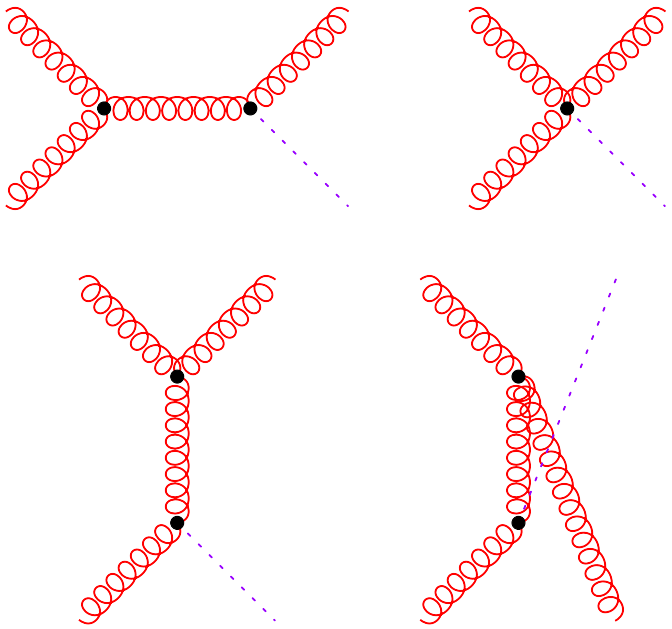

Figure 3.7: Initial gluon gluon corrections to $gg \to H$.

3.4.2 Virtual Corrections

Again there are both vertex corrections and wavefunction renormalization graphs in the virtual correction. One must again use some algebra to bring all the diagrams into the same denominator structure so they can be combined and used in the Feynmandelstam mapping.

Vertex Corrections

The vertex correction graphs are shown in figure 3.8. Consider first the triangle diagram[3]

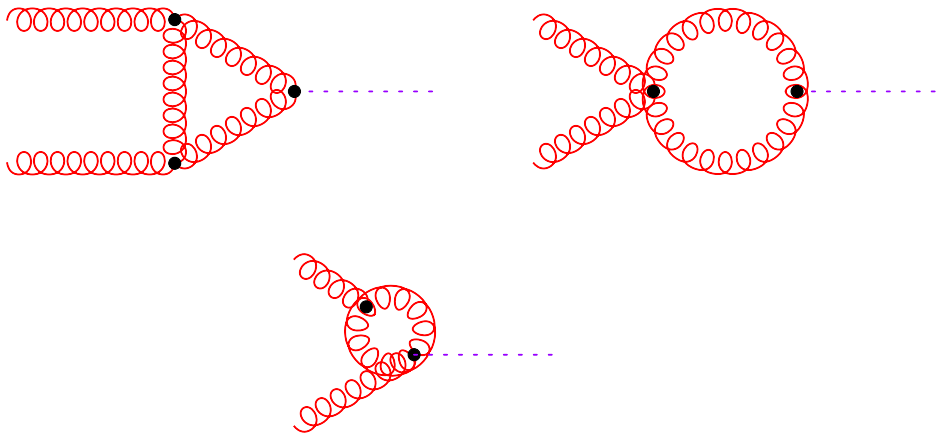

Figure 3.8: Vertex corrections to $gg \to H$. We refer to the top-left diagram as the triangle diagram, the top-right as the four-point diagram, and the bottom diagram as the bubble diagram. There is also a second bubble diagram, where the bottom incoming gluon splits into a loop instead of the top.

$$\imath\mathcal{M}^{\mu\nu}_{triangle} = g_s^2\delta^{AB}AC_A\int\frac{d^dl}{(2\pi)^d}\frac{num}{l^2(p_1-l)^2(p_2+l)^2} \tag{3.21}$$

$$\begin{aligned} num = &-\Big[g^{\mu\nu}\big(l^4-3l^2(l\cdot p_1-l\cdot p_2+3p_1\cdot p_2)+2(3p_1\cdot p_2(l\cdot p_1-l\cdot p_2)+2(p_1\cdot p_2)^2 \\ &+(l\cdot p_1)^2+(l\cdot p_2)^2)\big)+l^\mu l^\nu((4d-5)l^2-2(2d-3)(l\cdot p_1-l\cdot p_2)-4(d-4)p_1\cdot p_2) \\ &l^\mu p_1^\nu(l^2-2(l\cdot p_1 3l\cdot p_2)) \\ &-p_2^\mu l^\nu(l^2+6l\cdot p_1+2l\cdot p_2)-p_2^\mu p_1^\nu(-9l^2+6(l\cdot p_1-l\cdot p_2)+4p_1\cdot p_2)\Big] \end{aligned} \tag{3.22}$$

Shifting the denominator using Feynman parameters:

$$\frac{1}{l^2(p_1-l)^2(p_2+l)^2} = \int_0^1 dx\int_0^{1-x}dy\frac{2}{((1-x-y)l^2+x(p_1-l)^2+y(p_2+l)^2)^3} \tag{3.23}$$

$$= \int_0^1 dx\int_0^{1-x}dy\frac{2}{(k^2+2xyp_1\cdot p_2)^3} \tag{3.24}$$

where $k=l+yp_2-xp_1$. Shifting the numerator produces a very long expression, but one can use two facts to simplify it considerably. First, the terms odd in k will integrate to zero, so we can drop those outright. Secondly the incoming gluons are on shell so we can use $\epsilon_\mu(p_1)p_1^\mu=0$, and likewise for the other gluon. This means that the only tensors we will have in the final numerator are $g^{\mu\nu}$ and $p_2^\mu p_1^\nu$.[4]

$$\imath\mathcal{M}^{\mu\nu}_{triangle} = g_s^2\delta^{AB}AC_A\int\frac{d^dk}{(2\pi)^d}\int_0^1 dx\int_0^{1-x}dy\frac{num_{triangle}}{(k^2+2xyp_1\cdot p_2)^3} \tag{3.25}$$

$$\begin{aligned} num_{triangle} = &\frac{2}{d}\Big(g^{\mu\nu}\big[5(d-1)k^4+(d(-12xy+7(x+y)-13)+2(xy+8))k^2p_1\cdot p_2 \\ &+2d(2x^2y^2-3xy(x+y)+x^2+y^2-3(x+y)+2)(p_1\cdot p_2)^2\big] \\ &+p_2^\mu p_1^\nu\big[(d(4xyd^2+d(11xy-3(x+y)-9))-20xy+8(x+y)+12)k^2 \\ &+2d\big((5-4d)x^2y^2+2(d-2)xy(x+y)+(11-2d)xy+x^2+y^2 \\ &-3(x+y)+2\big)p_1\cdot p_2\big]\Big) \end{aligned} \tag{3.26}$$

Next we consider the four point vertex diagram. The matrix element is

$$\imath\mathcal{M}^{\mu\nu} = g_s^2\delta^{AB}AC_A\int\frac{d^dl}{(2\pi)^d}\frac{num}{(p_1-l)^2(p_2+l)^2} \tag{3.27}$$

[3] I'll use the notation $\mathcal{M}=\mathcal{M}^{\mu\nu}\epsilon^A_\mu(p_1)\epsilon^B_\nu(p_2)$ to make the expressions shorter.

[4] This includes performing simplifications of terms like $k^\mu p_1^\nu k\cdot p_2$, which we can rewrite as $p_2^\mu p_1^\nu\frac{k^2}{d}$.

where after performing the same tensor simplifications we have

$$num = g^{\mu\nu}(2d-4)(l^2 + l\cdot p_1 - l\cdot p_2 - p_1\cdot p_2) + 2l^\mu l^\nu + l^\mu p_1^\nu - p_2^\mu l^\nu - p_2^\mu p_1^\nu \tag{3.28}$$

now, to combine all the virtual corrections together, we want them all to have the same denominators so they have the same Feynman parameter structure. Notice this diagram has a different denominator than the triangle diagrams. By multiplying on top and bottom by l^2, we can force the diagram to have the same denominator as the triangle diagram:

$$\imath\mathcal{M}^{\mu\nu} = g_s^2\delta^{AB}AC_A\int\frac{d^dl}{(2\pi)^d}\frac{num_{four-point}}{l^2(p_1-l)^2(p_2+l)^2} \tag{3.29}$$

Where $num_{four-point} = l^2 num$. Now we can perform the same denominator shift as in the previous diagram. We shift the numerator and perform simplify

$$\imath\mathcal{M}^{\mu\nu}_{four-point} = g_s^2\delta^{AB}AC_A\int\frac{d^dk}{(2\pi)^d}\int_0^1 dx\int_0^{1-x}dy\frac{num_{four-point}}{(k^2+2xyp_1\cdot p_2)^3} \tag{3.30}$$

$$\begin{aligned} num_{four-point} = \frac{2}{d}\Bigg[2g^{\mu\nu}\Bigg((d-1)^2k^4 + ((14-4d^2)xy - (4-d^2)(x+y) + d(2-d))k^2p_1\cdot p_2 \\ + 2d(d-2)xy(2xy-x-y+1)(p_1\cdot p_2)^2\Bigg) + p_2^\mu p_1^\nu\Bigg((-(8+2d)xy \\ + (2+d)(x+y) - d)k^2 + 2dxy(2xy-x-y+1)p_1\cdot p_2)\Bigg)\Bigg] \end{aligned} \tag{3.31}$$

Finally, there is the bubble diagram. One must again use the same technique of multiplying by one in a modified factor to get the denominator to have the same form as the triangle diagram. The matrix element is:

$$\imath\mathcal{M}^{\mu\nu}_{bubble} = g_s^2\delta^{AB}AC_A\int\frac{d^dl}{(2\pi)^d}\frac{num}{l^2(p_1-l)^2} \tag{3.32}$$

$$num = g^{\mu\nu}(-2l^2 + 2l\cdot p_2 + p_1\cdot p_2 + 2l^\mu l^\nu - 2p_2^\mu l^\nu + l^\mu p_1^\nu - p_2^\mu p_1^\nu) \tag{3.33}$$

after multiplying by $\frac{(p_2+l)^2}{(p_2+l)^2}$ and simplifying

$$\imath\mathcal{M}^{\mu\nu}_{bubble} = g_s^2\delta^{AB}AC_A\int\frac{d^dk}{(2\pi)^d}\frac{num_{bubble}}{(k^2+2xyp_1\cdot p_2)^3} \tag{3.34}$$

$$\begin{aligned} num_{bubble} = \frac{2}{d}\Bigg[g^{\mu\nu}\Bigg(2(d-1)k^4 + ((12+8d)xy - 2dx + d)k^2p_1\cdot p_2 + 2dx(1-y)(4xy+2x+1)(p_1\cdot p_2)^2\Bigg) \\ + p_2^\mu p_1^\nu\Bigg(((8+2d)xy + 2dx + (2+d)y + d - 2)k^2 + 2dx(1+2x)(1-y^2)p_1\cdot p_2\Bigg)\Bigg] \end{aligned} \tag{3.35}$$

the other bubble diagram that comes off the bottom gluon leg gives the same factor with $x \leftrightarrow y$. Putting all of these together and performing the loop integral, for the vertex correction yields:

$$\begin{aligned}
\imath\mathcal{M}^{\mu\nu}_{VC} &= \delta^{AB} A \frac{\imath g_s^2}{16\pi^2} \left(-\frac{4\pi\mu_D^2}{2p_1\cdot p_2}\right)^{\epsilon} \Gamma(1+\epsilon) C_A \int_0^1 dx \int_0^{1-x} dy \left(\frac{1}{xy}\right)^{\epsilon} F_{VC} \qquad (3.36)\\
F_{VC} &= \frac{g^{\mu\nu} p_1\cdot p_2}{2xy}\Bigg[\left(-\frac{48}{\epsilon} + (96-32\epsilon) + \frac{8}{1-\epsilon}\right) x^2y^2 - \left(\frac{12}{\epsilon} + 4 - 8\epsilon\right)(x^2y + xy^2)\\
&\quad + \left(\frac{24}{\epsilon} - 24 - 8\epsilon\right) xy - 4(x^2+y^2) + 5(x+y) - 4\Bigg]\\
&\quad + \frac{p_2^\mu p_1^\nu}{2xy}\Bigg[16\left(\frac{6}{\epsilon} - 7 + 2\epsilon\right) x^2y^2 + \left(\frac{6}{\epsilon} + 8(1-\epsilon)\right)(x^2y + xy^2)\\
&\quad + 8\left(-\frac{3}{\epsilon} + 3 + \epsilon\right) xy + 4(x^2+y^2) - 5(x+y) + 4\Bigg] \qquad (3.37)
\end{aligned}$$

The total matrix element for the vertex correction is

$$\imath\mathcal{M}^{\mu\nu} = \imath A\delta^{AB}\left(g^{\mu\nu} p_1\cdot p_2 - p_2^\mu p_1^\nu + \frac{\alpha_s}{4\pi} C_A \Gamma(1+\epsilon)\left(-\frac{4\pi\mu_D^2}{m_H^2}\right)^{\epsilon} \int_0^1 dx \int_0^{1-x} dy \left(\frac{1}{xy}\right)^{\epsilon} F_{VC}\right) \qquad (3.38)$$

squaring and summing over spins & colors yields:

$$\begin{aligned}
\overline{|\mathcal{M}|^2} &= \frac{A^2}{4(1-\epsilon)^2}\Bigg((d-2)(p_1\cdot p_2)^2\\
&\quad + \frac{\alpha_s}{2\pi} C_A \Gamma(1+\epsilon)\left(-\frac{4\pi\mu_D^2}{m_H^2}\right)^{\epsilon} \int_0^1 dx \int_0^{1-x} dy \left(\frac{1}{xy}\right)^{\epsilon} F_{VC}(g_{\mu\nu} p_1\cdot p_2 - p_{2\mu} p_{1\nu})\Bigg)
\end{aligned}$$

performing the tensor contractions:

$$\begin{aligned}
g^{\mu\nu} p_1\cdot p_2 (g_{\mu\nu} p_1\cdot p_2 - p_{2\mu} p_{1\nu}) &= (d-1)(p_1\cdot p_2)^2 \qquad (3.39)\\
p_2^\mu p_1^\nu (g_{\mu\nu} p_1\cdot p_2 - p_{2\mu} p_{1\nu}) &= (p_1\cdot p_2)^2 \qquad (3.40)
\end{aligned}$$

putting all of this together

$$\begin{aligned}
\hat{\sigma} &= \frac{\pi}{s}\delta(s - m_H^2)\overline{|\mathcal{M}|^2} \qquad (3.41)\\
\overline{|\mathcal{M}|^2} &= \frac{A^2(p_1\cdot p_2)^2}{2(1-\epsilon)}\left(1 + \frac{\alpha_s}{2\pi} C_A \frac{\Gamma(1+\epsilon)}{2(1-\epsilon)}\left(-\frac{4\pi\mu_D^2}{m_H^2}\right)^{\epsilon} \int_0^1 dx \int_0^{1-x} dy \left(\frac{1}{xy}\right)^{\epsilon} Integrand_{VC}\right) \qquad (3.42)\\
Integrand_{VC} &= \frac{1}{2xy}\Bigg[-\frac{8(2-\epsilon)(3-2\epsilon)(1-6\epsilon+4\epsilon^2)}{(1-\epsilon)\epsilon} x^2y^2 - \frac{2(3-2\epsilon)(5-4\epsilon^2)}{\epsilon}(x^2y + y^2x)\\
&\quad + 16\left(\frac{3}{\epsilon} - 6 + 2\epsilon + \epsilon^2\right) xy - 8(1-\epsilon)(x^2+y^2) + 10(1-\epsilon)(x+y) - 8(1-\epsilon)\Bigg]
\end{aligned}$$

(3.43)

the collinear divergences occur in the terms that have a $\frac{1}{x}$ or $\frac{1}{y}$ in the limit that x or y approaches zero. Notice that the collinear and the ultraviolet poles separate - there are no $\frac{1}{\epsilon}$ terms that go like $\frac{1}{x}$ or $\frac{1}{y}$. To complete the virtual corrections we next turn to the wavefunction renormalization diagrams:

Wavefunction Renormalization

There are four Feynman diagrams in the wavefunction renormalization corrections to $gg \to H$. There are two gluon loops, and a corresponding fermion loop and ghost loop. These are shown in figure 3.9. Consider

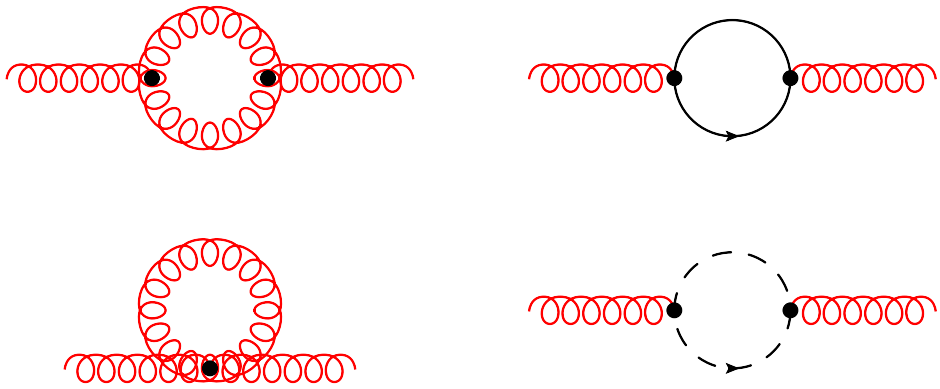

Figure 3.9: Wavefunction renormalization corrections to $gg \to H$. In short hand we call the two gluon diagrams $gluon_3$ and $gluon_4$, for the gluon verticies in them, and the fermion and ghost diagrams by those names.

first the fermion loop diagram. The matrix element is:[5]

$$\imath\Pi^{\mu\nu} = -\frac{g_s^2}{2}\delta^{AB}\int\frac{d^dl}{(2\pi)^d}\frac{\mathrm{Tr}\left[\gamma^\mu \not{l}\gamma^\nu(\not{q}+\not{l})\right]}{l^2(q+l)^2} \tag{3.44}$$

again we must combine it with the other virtual corrections, so one must force the same denominator structure as the other diagrams. We will consider the renormalization on the first leg, so we take $q = p_2$. Then I have:

$$\imath\Pi^{\mu\nu}_{fermion} = -\frac{g_s^2}{2}\delta^{AB}\int\frac{d^dl}{(2\pi)^d}\frac{\mathrm{Tr}\left[\gamma^\mu \not{l}\gamma^\nu(\not{p}_2+\not{l})\right](p_1-l)^2}{l^2(p_1-l)^2(p_2+l)^2} \tag{3.45}$$

shifting the denominator using Feynman parameters, we have to keep $p_2^2 \neq 0$:

$$\frac{1}{l^2(p_1-l)^2(p_2+l)^2} = \int_0^1 dx\int_0^1 dy\int_0^1 dz\,\delta(x+y+z-1)\frac{2}{[zl^2+x(p_1-l)^2+y(p_2+l)^2]^3} \tag{3.46}$$

[5]Using again the abreviation $\Pi = \Pi^{\mu\nu}\epsilon^A_\mu(q)\epsilon^{*B}_\nu(q)$.

$$= \int_0^1 dx \int_0^1 dy \int_0^1 dz\, \delta(x+y+z-1) \frac{2}{[(l-xp_1+yp_2)^2 + 2xyp_1\cdot p_2 + y(1-y)p_2^2]^3} \tag{3.47}$$

$$= \int_0^1 dx \int_0^1 dy \int_0^1 dz\, \delta(x+y+z-1) \frac{2}{[k^2-\Delta']^3} \tag{3.48}$$

where $\Delta' = -2xyp_1\cdot p_2 - y(1-y)p_2^2$. Next we want to shift the numerator and consider the terms that contribute to the wavefunction renormalization. Only the terms with the $g^{\mu\nu}$ metric structure will contribute to the wavefunction renormalization, so we focus on just those terms. Shifting the numerator and keeping only the terms that are even in k and have the $g^{\mu\nu}$ metric structure yields:

$$\imath\Pi^{\mu\nu}_{fermion} = g_s^2\delta^{AB}g^{\mu\nu}\int\frac{d^dk}{(2\pi)^d}\int_0^1 dx\int_0^{1-x} dy \frac{num_{fermion}}{(k^2-\Delta')^3} \tag{3.49}$$

$$\begin{aligned} num_{fermion} = 4\Bigg[&\frac{d-2}{d}k^4 + \frac{[x(-4y(d+1)+d+2)+2dy-2]p_1\cdot p_2 + y(2y(d+1)-d-2)p_2^2}{d}k^2 \\ &+ y(2x(1-x)(1-2y)(p_1\cdot p_2)^2 + y(-4xy+3x+2y-2)p_1\cdot p_2 p_2^2 - y^2(1-y)(p_2^2)^2)\Bigg] \end{aligned} \tag{3.50}$$

Next consider the $gluon_3$ diagram. The matrix element is:

$$\imath\Pi_3^{\mu\nu} = \frac{g_s^2}{2}C_A\delta^{AB}\int\frac{d^dl}{(2\pi)^d}\frac{(2d-3(2l^\mu l^\nu + l^\mu q^\nu + q^\mu l^\nu) + (d-6)q^\mu q^\nu + (2l^2+2l\cdot q+5q^2)g^{\mu\nu}}{l^2(q+l)^2} \tag{3.51}$$

once again one must perform the same simplifications as on the fermion diagram. This yields:

$$\imath\Pi_3^{\mu\nu} = g_s^2\delta^{AB}g^{\mu\nu}\int\frac{d^dk}{(2\pi)^d}\int_0^1 dx\int_0^{1-x} dy\frac{num_3}{(k^2-\Delta')^3} \tag{3.52}$$

$$\begin{aligned} num_3 = C_A\Bigg[&\frac{6(d-1)}{d}k^4 + \frac{2(x(d+2)-2y(d(4x-3)+x+1)-2)p_1\cdot p_2 + (d(8y^2-2y+5)-6y^2)p_2^2}{d}k^2 \\ &+ y\left(2(1-x)p_1\cdot p_2 + yp_2^2\right)(2x(1-2y)p_1\cdot p_2 + (-2y(1-y)+5)p_2^2)\Bigg] \end{aligned} \tag{3.53}$$

Next consider the $gluon_4$ diagram. This gives the matrix element:

$$\imath\Pi_4^{\mu\nu} = -g_s^2C_A\delta^{AB}(d-1)g^{\mu\nu}\int\frac{d^dl}{(2\pi)^2}\frac{1}{l^2} \tag{3.54}$$

to make this the same form as the other diagrams we have to multiply by $\frac{(p_1-l)^2(p_2+l)^2}{(p_1-l)^2(p_2+l)^2}$. After shifting the numerator and keeping only the even terms in k this gives:

$$\begin{aligned} \imath\Pi_4^{\mu\nu} &= g_s^2\delta^{AB}g^{\mu\nu}\int\frac{d^dk}{(2\pi)^2}\int_0^1 dx\int_0^{1-x}dy\frac{num_4}{(k^2-\Delta')^3} && (3.55)\\ num_4 &= -2C_A(d-1)\Bigg[k^4+\frac{2\left[((x+y-2xy)(d+2)-2)p_1\cdot p_2-y(1-y)(d+2)p_2^2\right]}{d}k^2 \\ &\quad + y\left(4x(1-x)(1-y)(p_1\cdot p_2)^2+2y(-2xy+3x+y-2)p_1\cdot p_2p_2^2+y^2(y-2)(p_2^2)^2\right)\Bigg] && (3.56)\end{aligned}$$

Finally consider the ghost diagram. This diagram has matrix element

$$\imath\Pi_{ghost}^{\mu\nu} = -g_s^2C_A\delta^{AB}\int\frac{d^dl}{(2\pi)^d}\frac{(l+q)^\mu l^\nu}{l^2(l+q)^2} \tag{3.57}$$

once again performing the same simplifications yields

$$\begin{aligned} \imath\Pi_{ghost}^{\mu\nu} &= g_s^2\delta^{AB}g^{\mu\nu}\int\frac{d^dk}{(2\pi)^d}\int_0^1 dx\int_0^{1-x}dy\frac{num_{ghost}}{(k^2-\Delta')3} && (3.58)\\ num_{ghost} &= -\frac{2C_A}{d}\left[k^4+y(2(1-x)p_1\cdot p_2+yp_2^2)\right] && (3.59)\end{aligned}$$

We need to assemble all of this into the correction to the cross section. Because $\Pi^{\mu\nu}$ corrects the gluon propagator, for some function $\Pi(q^2)$ we can write

$$\imath\Pi^{\mu\nu} = \imath(q^2g^{\mu\nu}-q^\mu q^\nu)\delta^{AB}\Pi(q^2) \tag{3.60}$$

in this case (using Peskin and Schroder's notation here)

$$\begin{aligned} Z_3 &= \frac{1}{1-\Pi(0)} && (3.61)\\ g_s &\to g_s\sqrt{Z_3}\approx g_s\left(1+\frac{1}{2}\Pi(0)\right) && (3.62)\\ \alpha_s &\to \alpha_s(1+\Pi(0)) && (3.63)\\ \sigma_{LO} &\to \sigma_{LO}\left(1+2\Pi(0)\right) && (3.64)\end{aligned}$$

Adding together the diagrams with the appropriate symmetry factors and including n_f copies of the fermion diagram for the different fermions

$$\imath\Pi^{\mu\nu} = g_s^2\delta^{AB}g^{\mu\nu}\int\frac{d^dk}{(2\pi)^d}\int_0^1 dx\int_0^{1-x}dy\frac{n_f num_{fermion}+\frac{1}{2}(num_3+num_4)+num_{ghost}}{(k^2-\Delta')^3} \tag{3.65}$$

this makes clear that

$$\Pi(p_2^2) = \frac{g_s^2}{\imath p_2^2}\int\frac{d^dk}{(2\pi)^d}\int_0^1 dx\int_0^{1-x}dy\frac{n_f num_{fermion}+\frac{1}{2}(num_3+num_4)+num_{ghost}}{(k^2-\Delta')^3} \tag{3.66}$$

adding the same expression on the other leg is the same as adding the same term with $x \leftrightarrow y$. Combining these two terms and integrating over k gives

$$\Pi(0) = \frac{g_s^2}{(4\pi)^{2-\epsilon}}C_A\Gamma(1+\epsilon)\left(-\frac{4\pi\mu_D^2}{2p_1\cdot p_2}\right)^\epsilon\delta^{AB}\int_0^1 dx\int_0^{1-x}\left(\frac{1}{xy}\right)^\epsilon Integrand_{WR} \tag{3.67}$$

$$\begin{aligned} Integrand_{WR} &= \frac{1}{\epsilon}\left[\frac{20-25(x+y)+32(x^2+y^2)}{4}+\frac{n_f}{C_A}\left(16(x^2+y^2)-12(x+y)\right)\right] \\ &+\frac{1}{4}\Bigg(5y(9-10y)+5x(9-10x)-24-9\left(\frac{y(1-y)}{x}+\frac{x(1-x)}{y}\right) \\ &\quad +5\left(\frac{1}{x}+\frac{1}{y}\right)\Bigg)+\frac{n_f}{C_A}\left(y(23-24y)+x(23-24x)-4-\frac{4y(1-y)}{x}-\frac{4x(1-x)}{y}\right) \\ &-\epsilon\Bigg[\frac{(1-x)(1-8x)(1-2y)}{4y}+\frac{(1-y)(1-8y)(1-2x)}{4x} \\ &\quad +\frac{n_f}{C_A}\left(\frac{(1-x)(1-4x)(1-2y)}{y}+\frac{(1-y)(1-4y)(1-2x)}{x}\right)\Bigg] \end{aligned} \tag{3.68}$$

now to combine this with the real correction, we need to perform the same Feynmandelstam mapping that we did in the $b\bar{b}\to H$ calculation. Performing that mapping and only keeping the limiting terms as $t\to 0$ gives

$$\begin{aligned} \sigma_{virt} &= \frac{\alpha_s^2}{576\pi v^2(1-\epsilon)}\frac{m_H^2}{S}\left\{g\otimes g\right\}\left(\frac{m_H^2}{S}\right)\frac{\alpha_s}{2\pi}C_A\Gamma(1+\epsilon)\left(-\frac{4\pi\mu_D^2}{m_H^2}\right)^\epsilon \\ &\times\int_{m_H^2}^\infty\frac{ds}{s^2}\int_{-\infty}^0 dt\int_{-\infty}^0 du\,\delta(s+t+u-m_H^2)\frac{m_H^2}{s}\Bigg[-\frac{2s^2}{s-m_H^2}\left(\frac{1}{-t}\right) \\ &\quad +\left(7-\frac{9\epsilon}{2}-\frac{n_F}{C_A}(4-5\epsilon)\right)\frac{s-m_H^2}{-t}\Bigg] \end{aligned}$$

combining this with the real term in the collinear limit (and multiplying by two, for t and u channel divergences), the collinear plot expression is:

$$-t\frac{d\sigma}{dt} = \frac{a_s^2}{576\pi v^2}\frac{m_H^2}{S}\frac{\alpha_s}{2\pi}C_A 2\int_0^{\frac{m_H^2}{m_H^2-t}}\frac{dz}{z}\left[\theta(z-z_0)\{g\otimes g\}\left(\frac{z_0}{z}\right)\frac{2(1-z+z^2)^2}{z(1-z)}\right.$$
$$\left. -\{g\otimes g\}(z_0)z\left(\frac{2}{1-z}-1+z(-3+2z)+2\frac{n_F}{C_A}\right)\right] \tag{3.69}$$

notice that in the collinear limit, $t \to 0$, so this produces

$$-t\frac{d\sigma}{dt} = \frac{a_s^2}{576\pi v^2}\frac{m_H^2}{S}\frac{\alpha_s}{2\pi}C_A 2\int_0^1\frac{dz}{z}\{g\otimes g\}\left(\frac{z_0}{z}\right)P_{gg}(z) \tag{3.70}$$

which is plotted in figure 3.10. If we construct the counterterm as before we get

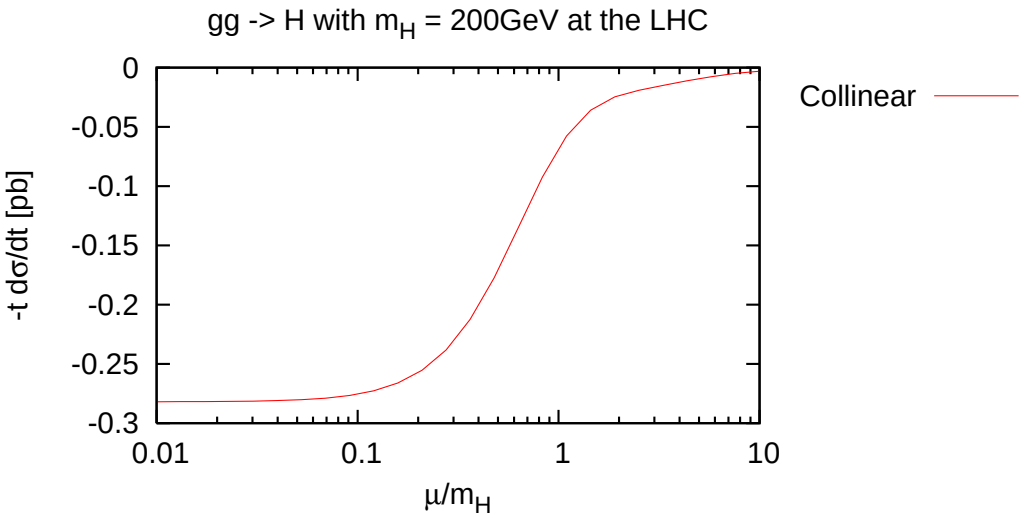

Figure 3.10: Collinear plot of the radiated and virtual gluon correction to $gg \to H$ at the LHC with $m_H = 300$ GeV. This is representative of a large range of m_H, where we have $\mu \approx m_H/2$

$$\bar{\sigma} = \frac{\alpha_s^2}{576\pi v^2(1-\epsilon)}\frac{m_H^2}{S}\frac{\alpha_s}{2\pi}\frac{C_A}{\Gamma(1-\epsilon)}\left(\frac{4\pi\mu_D^2}{\mu^2}\right)^\epsilon$$
$$\int_{z_0}^1\frac{dz}{z}\{g\otimes g\}\left(\frac{z_0}{z}\right)\left[-\frac{2}{\epsilon}P_{gg}(z)+4\frac{(1-z+z^2)^2}{z}\left(\frac{\log 1-z}{1-z}\right)_+ +\delta(1-z)\left(-\frac{67}{9}+\frac{10n_F}{9C_A}+2\pi^2\right)\right] \tag{3.71}$$

the countercounterterm is

$$\bar{\bar{\sigma}} = \frac{\alpha_s^2}{576\pi v^2(1-\epsilon)}\frac{m_H^2}{S}\frac{\alpha_s}{2\pi}\frac{C_A}{\Gamma(1-\epsilon)}\left(\frac{4\pi\mu_D^2}{\mu^2}\right)^\epsilon\left(\frac{m_H^2}{\mu^2}\right)^\epsilon\frac{2\pi^2}{3}\{g\otimes g\}(z_0) \tag{3.72}$$

so what one should subtract from the cross section is:

$$\begin{aligned}\bar{\sigma} - \frac{1}{2}\bar{\bar{\sigma}} &= \frac{\alpha_s^2}{576\pi v^2(1-\epsilon)}\frac{m_H^2}{S}\frac{\alpha_s}{2\pi}\frac{C_A}{\Gamma(1-\epsilon)}\left(\frac{4\pi\mu_D^2}{\mu^2}\right)^{\epsilon} \\ &\int_{z_0}^1 \frac{dz}{z}\{g\otimes g\}\left(\frac{z_0}{z}\right)\left[-\frac{2}{\epsilon}P_{gg}(z) + 4\frac{(1-z+z^2)^2}{z}\left(\frac{\log 1-z}{1-z}\right)_+ + \delta(1-z)\left(-\frac{67}{9}+\frac{10n_F}{9C_A}+\frac{4\pi^2}{3}\right)\right]\end{aligned} \tag{3.73}$$

which means the PDF counterterm is:

$$\begin{aligned}\delta g(x) &= -\frac{\alpha_s}{2\pi}\int_x^1 \frac{dz}{z} q\left(\frac{x}{z}\right)\left[\left(\frac{1}{\epsilon} - \gamma_E + \log\frac{4\pi\mu_D^2}{\mu^2(1-z)}\right)P_{gg}(z) + 2\frac{(1-z+z^2)^2}{z}\left(\frac{\log 1-z}{1-z}\right)_+ \right. \\ &\left. + \delta(1-z)\left(-\frac{67}{18}+\frac{5n_F}{9C_A}+\frac{2\pi^2}{3}\right)\right]\end{aligned} \tag{3.74}$$

using this PDF counterterm, the cross section for real and virtual emission combined is:

$$\begin{aligned}\sigma_{R+V} &= \sigma_{LO}\frac{\alpha_s}{2\pi}\left(\frac{4\pi\mu_D^2}{m_H^2}\right)^{\epsilon}\frac{1}{\Gamma(1-\epsilon)}\int_{z_0}^1\frac{dz}{z}\{g\otimes g\}\left(\frac{z_0}{z}\right) \\ &\left[2P_{gg}(z)\log\frac{m_H^2}{\mu^2} - \frac{11}{3}C_A\frac{(1-z)^3}{z} + 4C_A\frac{(1-z+z^2)^2}{z}\left(\frac{\log 1-z}{1-z}\right)_+ \right. \\ &\left. - 4C_A\frac{(1-z+z^2)^2}{z(1-z)}\log z + \left(\frac{2}{\epsilon}b_0 + \frac{100}{3} - \frac{10n_F}{9} - 2\pi^2\right)\delta(1-z)\right]\end{aligned} \tag{3.75}$$

there is still a divergence in the $\delta(1-z)$ term because we have to renormalize the ultraviolet divergence from the vertex corrections. I'll do this using the $\overline{\text{MS}}$ counterterm. This yields a finite 4 dimensional cross section:

$$\begin{aligned}\sigma_{gg} &= \sigma_{LO}\frac{\alpha_s}{2\pi}\int_{z_0}^1\frac{dz}{z}\{g\otimes g\}\left(\frac{z_0}{z}\right) \\ &\left[2P_{gg}(z)\log\frac{m_H^2}{\mu^2} - \frac{11}{3}C_A\frac{(1-z)^3}{z} + 4C_A\frac{(1-z+z^2)^2}{z}\left(\frac{\log 1-z}{1-z}\right)_+ \right. \\ &\left. - 4C_A\frac{(1-z+z^2)^2}{z(1-z)}\log z + \left(2b_0\log\frac{\mu_{UV}^2}{m_H^2} + \frac{100}{3} - \frac{10n_F}{9} - 2\pi^2\right)\delta(1-z)\right]\end{aligned} \tag{3.76}$$

3.5 Results

The results from this calculation are shown in figure 3.11. Notice how the qg initial state is very small near the factorization scale of $\mu \approx m_H$, and the gg initial state is small near $\mu \approx m_H/2$, as we found in the collinear plots. Notice as well how small the correction is near $\mu \approx 3m_H/4$. In the $\overline{\text{MS}}$ factorization scheme

the correction is quite large, often 100% over a range of scales. The same plot with a Higgs mass of 100

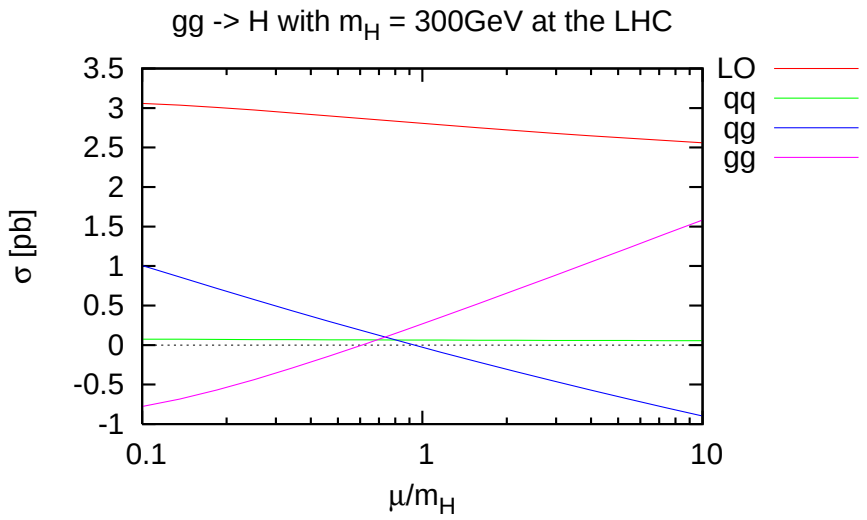

Figure 3.11: Plot of the LO and NLO contributions to $gg \to H$. Curves are labelled by initial state.

GeV is shown in figure 3.12. Similarly a 500 GeV Higgs mass is used in figure 3.13. Notice for the $m_H = 100$ GeV Higgs how the gg initial state never vanishes completely. This is a different from what we found in Drell-Yan and $b\bar{b} \to H$. Figure 3.14 shows the gg initial state collinear plot with $m_H = 100$ GeV.

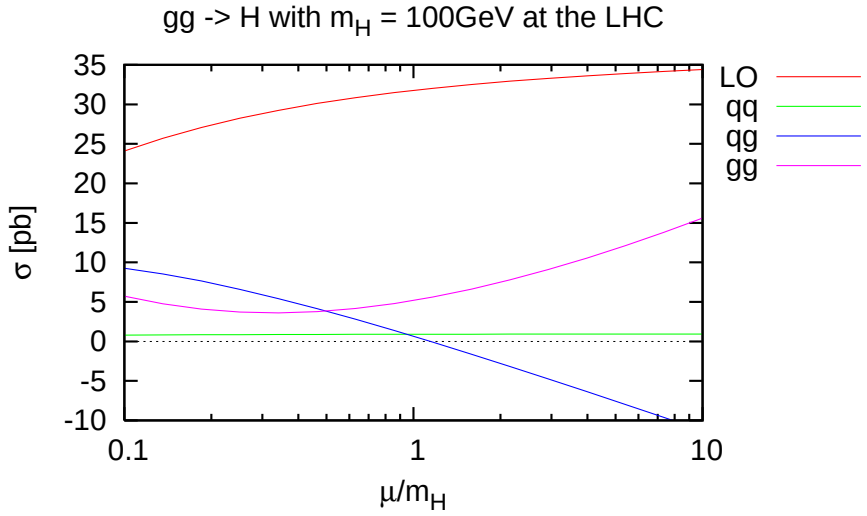

Figure 3.12: Plot of the LO and NLO contributions to $gg \to H$. Curves are labelled by initial state.

That being said, the collinear scheme works quite well for $gg \to H$, much better than, for example the $\overline{\text{MS}}$ factorization scheme.[6] This suggests that perhaps the large corrections to $gg \to H$ in the $\overline{\text{MS}}$ factorization scheme have more to do with factorization than with QCD in general. This is very interesting, and something

[6]Plots of this calculation in the $\overline{\text{MS}}$ factorization scheme are presented later in figures 6.14 and 6.16.

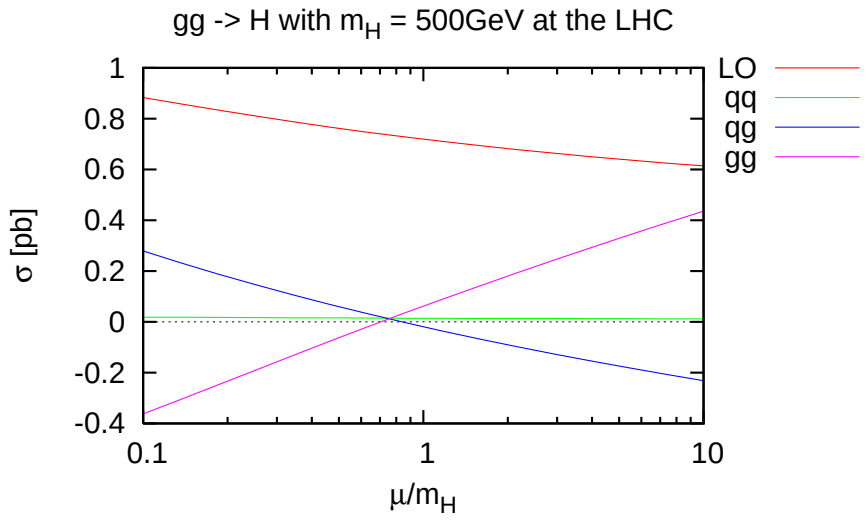

Figure 3.13: Plot of the LO and NLO contributions to $gg \to H$. Curves are labelled by initial state.

we will return to more in later discussion, but first we must turn to the issue of gauge invariance.

Before that discussion though, there is one clue that this method of choosing the factorization scale may run into some problems. Notice that in figure 3.12 the gg term never reaches zero. The collinear plot for this choice of kinematics is shown in figure 3.14. Notice the strange shape. This occurs because of a competition between the plus-distribution term, which produces a negative signed contribution, and the rest of the $\delta(1-z)$ term, which produces a positive signed contribution. For small enough values of m_H^2, the collinear plot exhibits this strange shape.

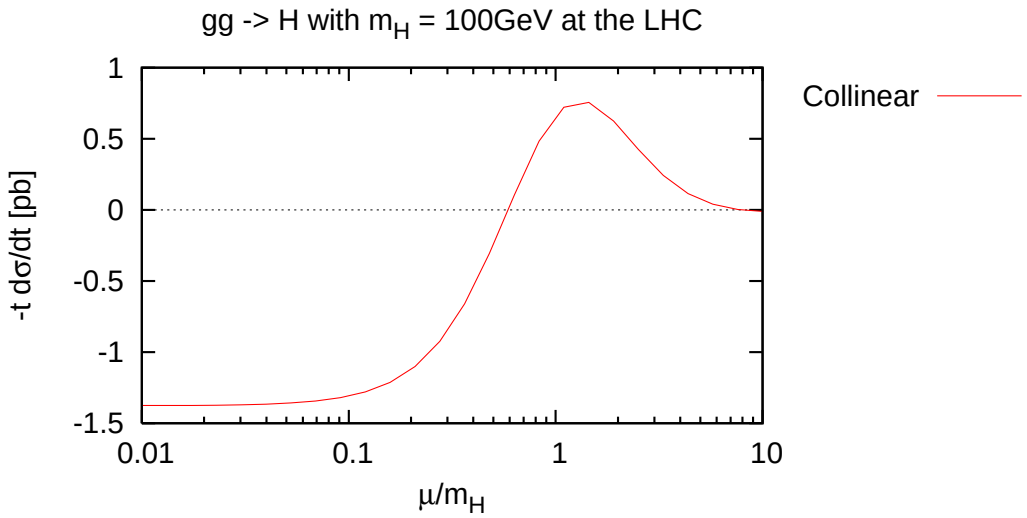

Figure 3.14: Collinear plot of the gg initial state corrections to $gg \to H$ for $m_H = 100$ GeV.

Chapter 4

The Death of Feynmandelstam

The departure of my work from my predecessor's began with the discovery that the collinear scheme as was previously suggested is not gauge-invariant. From this point the collinear scheme as we knew it had to be rebuilt to deal with virtual corrections in a different way.

4.1 Drell-Yan

We will consider the gauge-invariance of the collinear scheme applied to the order α_s corrections of Drell-Yan. In Drell-Yan, there are two separate cross sections that are gauge invariant and infrared safe. The first is initial gluon corrections. These are gauge-invariant and infrared safe on their own. The second cross section combines the radiated gluon corrections combined with the virtual corrections. These two terms are separately gauge invariant and only together infrared safe.

The purpose of the Feynmandelstam process is to isolate the collinear physics in the virtual corrections and combine it with the collinear physics in the radiative corrections to create an infrared safe collinear counterterm. We know this process does work to create and infrared safe counterterm, but we have not looked at the gauge invariance of this approach.

The radiative corrections are trivally gauge invariant. When we construct the counterterm we use the matrix element, which we know is gauge invariant. The virtual correction is more complex. The vertex correction in a general R_ξ gauge is:

$$\Gamma^\rho = \imath g_s^2 \mu_D^{2\epsilon} C_F \int \frac{d^d l}{(2\pi)^d} \frac{\gamma^\mu (\not{p}_2 - \not{l}) \gamma^\rho (\not{p}_1 + \not{l}) \gamma^\nu}{l^2 (p_1 + l)^2 (p_2 - l)^2} \left(g_{\mu\nu} - (1 - \xi) \frac{l_\mu l_\nu}{l^2} \right) \tag{4.1}$$

we consider just the second term, since all the gauge dependence is contained in that term.

4.1.1 The Vertex Correction

Recall that the vertex correction has external quarks that are on shell, so we can simplify using the Dirac equation:

$$\begin{aligned} \bar{v}(p_2)\not{p}_2 = 0 \\ \not{p}_1 u(p_1) = 0 \end{aligned} \tag{4.2}$$

so one can insert these terms for free on either side of this equation.

$$\begin{aligned} \Gamma^\rho &= -\imath g_s^2 \mu_D^{2\epsilon} C_F \int \frac{d^d l}{(2\pi)^d} \frac{\not{l}(\not{p}_2 - \not{l})\gamma^\rho(\not{p}_1 + \not{l})\not{l}}{l^4(p_1+l)^2(p_2-l)^2} \\ F_1 &= \imath g_s^2 \mu_D^{2\epsilon} C_F \int \frac{d^d l}{(2\pi)^d} \frac{(p_1+l)^2(p_2-l)^2}{l^4(p_1+l)^2(p_2-l)^2} \end{aligned}$$

now one can clearly just cancel the top and bottom of this integrand, but we want to use the Feynmandelstam process, so we won't do that. Using Feynman parameters then we can simplify the integrand:

$$\begin{aligned} \frac{1}{l^4(p_1+l)^2(p_2-l)^2} &= \int_0^1 dx \int_0^{1-x} dy \int_0^{1-x-y} dz \frac{6}{[(1-x-y-z)l^2 + zl^2 + x(p_1+l)^2 + y(p_2-l)^2]^4} \\ &= \int_0^1 dx \int_0^{1-x} dy \int_0^{1-x-y} dz \frac{6}{[(1-x-y)l^2 + x(l^2+2l\cdot p_1) + y(l^2 - 2l\cdot p_2)]^4} \\ &= \int_0^1 dx \int_0^{1-x} dy \frac{6(1-x-y)}{[l^2 + 2l\cdot(xp_1 - yp_2)]^4} \\ &= \int_0^1 dx \int_0^{1-x} dy \frac{6(1-x-y)}{[(l+xp_1-yp_2)^2 - (xp_1-yp_2)^2]^4} \\ &= \int_0^1 dx \int_0^{1-x} dy \frac{6(1-x-y)}{[(l+xp_1-yp_2)^2 + xyQ^2]^4} \\ &= \int_0^1 dx \int_0^{1-x} dy \frac{6(1-x-y)}{(k^2+xyQ^2)^4} \end{aligned}$$

shifting the numerator:

$$\begin{aligned} (p_1+l)^2(p_2-l)^2 &= (p_1 + (k - xp_1 + yp_2))^2(p_2 - (k - xp_1 + yp_2))^2 \\ &= (k + (1-x)p_1 + yp_2))^2(k - xp_1 - (1-y)p_2)^2 \\ &= (k^2 + 2k\cdot((1-x)p_1 + yp_2) + (1-x)yQ^2)(k^2 - 2k\cdot(xp_1 + (1-y)p_2) + x(1-y)Q^2) \end{aligned} \tag{4.3}$$

keeping just the even terms in k the gauge dependent part of the vertex correction is

$$\begin{aligned}
F_1 &= 6\imath g_s^2 \mu_D^{2\epsilon} C_F \int \frac{d^d k}{(2\pi)^d} \int_0^1 dx \int_0^{1-x} dy (1-x-y) \\
&\quad \frac{(k^2+(1-x)yQ^2)(k^2+x(1-y)Q^2) - 4k\cdot((1-x)p_1+yp_2)k\cdot(xp_1+(1-y)p_2)}{(k^2+xyQ^2)^4} \\
&= 6\imath g_s^2 \mu_D^{2\epsilon} C_F \int \frac{d^d k}{(2\pi)^d} \int_0^1 dx \int_0^{1-x} dy (1-x-y) \\
&\quad \frac{(k^4+(x(1-y)+(1-x)y)k^2Q^2 + xy(1-x)(1-y)Q^4) - \frac{4}{d}(xy+(1-x)(1-y))k^2Q^2}{(k^2+xyQ^2)^4} \\
&= 6\imath g_s^2 \mu_D^{2\epsilon} C_F \int \frac{d^d k}{(2\pi)^d} \int_0^1 dx \int_0^{1-x} dy (1-x-y) \\
&\quad \frac{k^4 + k^2Q^2(x(1-y)+(1-x)y - \frac{4}{d}(xy+(1-x)(1-y))) + xy(1-x)(1-y)Q^4}{(k^2+xyQ^2)^4}
\end{aligned} \tag{4.4}$$

using these loop integrals:

$$\begin{aligned}
\int \frac{d^{4-2\epsilon}k}{(2\pi)^{4-2\epsilon}} \frac{1}{(k+xyQ^2)^4} &= \frac{\imath}{(4\pi)^{2-\epsilon}} \Gamma[1+\epsilon] \left(\frac{1}{-xyQ^2}\right)^\epsilon \frac{1+\epsilon}{6(xyQ^2)^2} \\
\int \frac{d^{4-2\epsilon}k}{(2\pi)^{4-2\epsilon}} \frac{k^2}{(k+xyQ^2)^4} &= \frac{\imath}{(4\pi)^{2-\epsilon}} \Gamma[1+\epsilon] \left(\frac{1}{-xyQ^2}\right)^\epsilon \frac{2-\epsilon}{6xyQ^2} \\
\int \frac{d^{4-2\epsilon}k}{(2\pi)^{4-2\epsilon}} \frac{k^4}{(k+xyQ^2)^4} &= \frac{\imath}{(4\pi)^{2-\epsilon}} \Gamma[1+\epsilon] \left(\frac{1}{-xyQ^2}\right)^\epsilon \frac{(3-\epsilon)(2-\epsilon)}{6\epsilon}
\end{aligned}$$

integrating over the loop momentum:

$$\begin{aligned}
F_1 &= -\frac{6g_s^2 C_F}{(4\pi)^2} \left(\frac{4\pi\mu_D^2}{-Q^2}\right)^\epsilon \Gamma[1+\epsilon] \int_0^1 dx \int_0^{1-x} dy \left(\frac{1}{xy}\right)^\epsilon (1-x-y) \\
&\quad \left[\frac{(3-\epsilon)(2-\epsilon)}{6\epsilon} + \frac{2-\epsilon}{6xyQ^2} Q^2(x(1-y)+(1-x)y - \frac{4}{d}(xy+(1-x)(1-y))) \right. \\
&\quad \left. + \frac{1+\epsilon}{6(xyQ^2)^2} xy(1-x)(1-y)Q^4\right] \\
&= -\frac{\alpha_s C_F}{4\pi} \left(\frac{4\pi\mu_D^2}{-Q^2}\right)^\epsilon \Gamma[1+\epsilon] \int_0^1 dx \int_0^{1-x} dy \left(\frac{1}{xy}\right)^\epsilon (1-x-y) \\
&\quad \left[\frac{(3-\epsilon)(2-\epsilon)}{\epsilon} + \frac{2-\epsilon}{xy}(x(1-y)+(1-x)y - \frac{4}{4-2\epsilon}(xy+(1-x)(1-y))) + \frac{1+\epsilon}{xy}(1-x)(1-y)\right]
\end{aligned} \tag{4.5}$$

we are interested in the terms that are collinear in the Feynmandelstam scheme, which correspond to the $\frac{1}{x}$ and $\frac{1}{y}$ terms in this integrand. These are:

$$F_1^{\rm col} = -\frac{\alpha_s C_F}{4\pi} \left(\frac{4\pi\mu_D^2}{-Q^2}\right)^\epsilon \Gamma[1+\epsilon] \int_0^1 dx \int_0^{1-x} dy \left(\frac{1}{xy}\right)^\epsilon \left[\frac{\epsilon}{xy} + (2-3\epsilon)\left(\frac{1}{x}+\frac{1}{y}\right) - 2(1-\epsilon)\left(\frac{x}{y}+\frac{y}{x}\right)\right]$$

(4.6)

4.1.2 Wavefunction Renormalization

The other virtual diagram with collinear divergences is the wavefunction renormalization graph. We know that in dimensional regularization this diagram is zero because there is no momentum scale for the loop integral to be proportional to. This happens because an ultraviolet divergence cancels against a collinear divergence.

The matrix element for this graph is

$$\Sigma(\not{p}_1) = -\imath g_s^2 \mu_D^{2\epsilon} C_F \int \frac{d^d l}{(2\pi)^d} \frac{\gamma^\mu (\not{p}_1 + \not{l}) \gamma^\nu}{l^2 (p_1 + l)^2} \left(g_{\mu\nu} - (1-\xi) \frac{l_\mu l_\nu}{l^2} \right) \tag{4.7}$$

we wish to focus only on the gauge-dependent part, which is

$$\Sigma(\not{p}_1) = \imath g_s^2 \mu_D^{2\epsilon} C_F \int \frac{d^d l}{(2\pi)^d} \frac{\not{l}(\not{p}_1 + \not{l})\not{l}}{l^2 (p_1 + l)^2} \tag{4.8}$$

now what one must to do is take the $\not{p}_1$ term of this equation and then set $\not{p}_1 = 0$. In this process we need to be careful because before we take the $\not{p}_1$ term we have to keep p_1^2 off-shell. However, because

$$\frac{d}{d\not{p}_1} [p_1^2]_{\not{p}_1 \to 0} = \frac{d}{d\not{p}_1} [\not{p}_1 \not{p}_1]_{\not{p}_1 \to 0} = [2\not{p}_1]_{\not{p}_1 \to 0} = 0 \tag{4.9}$$

one can neglect p_1^2 terms, which otherwise would arise in the numerator and denominator. Furthermore, because we want to apply the Feynmandelstam map to this graph, we multiply the numerator and denominator by a factor of $(p_2 - l)^2$ so this has the same denominator form as the vertex correction graph:

$$\Sigma(\not{p}_1) = \imath g_s^2 \mu_D^{2\epsilon} C_F \int \frac{d^d l}{(2\pi)^d} \frac{\not{l}(\not{p}_1 + \not{l})\not{l}(p_2 - l)^2}{l^2 (p_1 + l)^2 (p_2 - l)^2} = \imath g_s^2 \mu_D^{2\epsilon} C_F \int \frac{d^d l}{(2\pi)^d} \frac{(\not{l}(l^2 + 2l \cdot p_1) - \not{p}_1 l^2)(p_2 - l)^2}{l^2 (p_1 + l)^2 (p_2 - l)^2} \tag{4.10}$$

now let's think about where terms like $\not{p}_1$ will come from. We will perform the same shift of loop momentum that we did with the vertex correction graph, so we will make the replacement $l = k - xp_1 + yp_2$. Clearly then the obvious terms will come from already slashed explicit $\not{p}_1$ and $\not{l}$ terms. There is one more source of $\not{p}_1$ terms though, consider a term that is proportional to $\not{k}\, k \cdot p_1$. When performing the loop integral over k this will be nonzero only for symmetric terms in k, and the replacement $k_\mu k_\nu \to \frac{g_{\mu\nu}}{d} k^2$ is made. This

replacement will cause $\not{k}\, k\cdot p_1 \to \frac{k^2}{d}\not{p}_1$. Using all of this one can find the $\not{p}_1$ term:

$$\begin{aligned}
\frac{d\not{l}}{d\not{p}_1} &= \frac{d}{d\not{p}_1}[\not{k} - x\not{p}_1 + y\not{p}_2] = -x \\
\frac{d}{d\not{p}_1}[(\not{l}(l^2+2l\cdot p_1) - \not{p}_1 l^2)(p_2-l)^2] &= -l^2(p_2-l)^2 - x(l^2+2l\cdot p_1)(p_2-l)^2 \\
&\quad + \frac{k^2}{d}\frac{d\not{l}}{d\not{k}}\frac{d}{dk\cdot p_1}[(l^2+2l\cdot p_1)(p_2-l)^2] \qquad (4.11)
\end{aligned}$$

shifting the loop momentum and keeping only terms even in k:

$$\begin{aligned}
-l^2(p_2-l)^2 &= -(k-xp_1+yp_2)^2(k-xp_1+(1-y)p_2)^2 \\
&= -(k^2 - xyQ^2 + 2k\cdot(yp_2-xp_1))(k^2+x(1-y)Q^2 - 2k\cdot(xp_1+(1-y)p_2)) \\
&= -(k^2-xyQ^2)(k^2+x(1-y)Q^2) + \frac{4k^2}{d}(yp_2-xp_1)\cdot(xp_1+(1-y)p_2) \\
&= -(k^4 + k^2Q^2(x(1-y)-xy) - x^2y(1-y)Q^4) - \frac{2k^2Q^2}{d}(xy - x(1-y)) \\
&= -k^4 - k^2Q^2x(1-2y)\left(1+\frac{2}{d}\right) + x^2y(1-y)Q^4 \qquad (4.12) \\
(l^2+2l\cdot p_1)(p_2-l)^2 &= (l+p_1)^2(l-p_2)^2 \\
&= (k+(1-x)p_1+yp_2)^2(k-xp_1-(1-y)p_2)^2 \\
&= (k^2+(1-x)yQ^2)(k^2+x(1-y)Q^2) \\
&\qquad - 4k\cdot((1-x)p_1+yp_2)k\cdot(xp_1+(1-y)p_2) \\
&= k^4 + k^2Q^2((1-x)y + y(1-x)) + xy(1-x)(1-y)Q^4 \\
&\qquad - \frac{2k^2Q^2}{d}(xy + (1-x)(1-y)) \\
&= k^4 + k^2Q^2\left((1-x)y + y(1-x) - \frac{2}{d}(xy+(1-x)(1-y))\right) \\
&\qquad + xy(1-x)(1-y)Q^4
\end{aligned} \qquad (4.13)$$

the last term is slightly more complex:

$$\begin{aligned}
\frac{d\not{l}}{d\not{k}}\frac{d}{dk\cdot p_1}[(l^2+2l\cdot p_1)(p_2-l)^2] &= \frac{d}{dk\cdot p_1}[(l^2+2l\cdot p_1)](p_2-l)^2 + (l^2+2l\cdot p_1)\frac{d}{dk\cdot p_1}[(p_2-l)^2] \\
&= (l-p_2)^2\frac{d}{dk\cdot p_1}[(l+p_1)^2] + (l+p_1)^2\frac{d}{dk\cdot p_1}[l^2] \\
&= 2(1-x)(k-xp_1-(1-y)p_2)^2 - 2x(k+(1-x)p_1+yp_2)^2 \\
&= 2(1-x)(k^2+x(1-y)Q^2) - 2x(k^2+y(1-x)Q^2)
\end{aligned}$$

$$= \quad 2k^2(1-2x) + 2Q^2x(1-x)(1-2y) \tag{4.14}$$

putting all of this together, along with the Feynman reduced denominator the gauge-dependent wavefunction renormalization term is

$$\begin{aligned}
\Sigma'(0) &= \imath g_s^2 \mu_D^{2\epsilon} C_F \int \frac{d^dk}{(2\pi)^d} \int_0^1 dx \int_0^{1-x} dy \frac{6(1-x-y)}{[k^2+xyQ^2]^4} \\
&\quad \left[-k^4 - k^2Q^2x(1-2y)\left(1+\frac{2}{d}\right) + x^2y(1-y)Q^4 \right. \\
&\quad -x\left(k^4 + k^2Q^2\left((1-x)y + y(1-x) - \frac{2}{d}(xy + (1-x)(1-y))\right) + xy(1-x)(1-y)Q^4\right) \\
&\quad \left. + \frac{2k^2}{d}(k^2(1-2x) + Q^2x(1-x)(1-2y)) \right] \\
&= \imath g_s^2 \mu_D^{2\epsilon} C_F \int \frac{d^dk}{(2\pi)^d} \int_0^1 dx \int_0^{1-x} dy \frac{6(1-x-y)}{[k^2+xyQ^2]^4} \left[k^4\left(\frac{2}{d}(1-2x) - (1+x)\right) \right. \\
&\quad \left. + k^2Q^2\left(-x(1-y+x(1-2y)) + \frac{2}{d}x(1-y-2x(1-2y))\right) + Q^4x^3y(1-y) \right]
\end{aligned} \tag{4.15}$$

integrating over loop momentum using the integrals listed in the previous section produces

$$\begin{aligned}
\Sigma'(0) &= -\frac{g_s^2}{(4\pi)^2}\left(\frac{4\pi\mu_D^2}{-Q^2}\right)^\epsilon C_F\Gamma[1+\epsilon] \int_0^1 dx \int_0^{1-x} dy \left(\frac{1}{xy}\right)^\epsilon (1-x-y) \\
&\quad \left[\left(\frac{2}{d}(1-2x) - (1+x)\right)\frac{(3-\epsilon)(2-\epsilon)}{\epsilon} \right. \\
&\quad \left. + \left(-(1-y+x(1-2y)) + \frac{2}{d}(1-y-2x(1-2y))\right)\frac{2-\epsilon}{y} + \frac{x}{y}(1-y)(1+\epsilon) \right]
\end{aligned} \tag{4.16}$$

The collinear terms are:

$$\Sigma'^{\text{col}}(0) = -\frac{\alpha_s C_F}{4\pi}\left(\frac{4\pi\mu_D^2}{-Q^2}\right)^\epsilon \Gamma[1+\epsilon] \int_0^1 dx \int_0^{1-x} dy \left[-(1-\epsilon)\frac{1}{y} - (2-\epsilon)\frac{x}{y} + (3-2\epsilon)\frac{x^2}{y} \right] \tag{4.17}$$

4.1.3 Collinear Virtual Corrections

The total virtual correction multiplies the leading order cross section by a factor

$$\sigma_V = \sigma_{LO}\left(F_1 + \frac{1}{2}\Sigma'(0) + \frac{1}{2}\Sigma'(0)_{x\leftrightarrow y}\right) \tag{4.18}$$

The relevant question is whether the collinear scheme counterterm is gauge invariant. To construct the collinear scheme counterterm we combine the real and virtual corrections using the Feynmandelstam map:

$$\begin{aligned} x &= -\frac{u}{s} \\ y &= -\frac{t}{s} \\ z &= \frac{Q^2}{s} \\ \int_0^1 dx \int_0^1 dy \int_0^1 dz\, \delta(x+y+z-1) &= \int_{Q^2}^\infty \frac{ds}{s^2}\frac{Q^2}{s} \int_{-\infty}^0 dt \int_{-\infty}^0 du\, \delta(s+t+u-Q^2) \end{aligned} \tag{4.19}$$

using this mapping we can write the virtual and radiated combined into one integral and construct the counterterm as usual:

$$\bar{\sigma} = \lim_{t\to 0}\left[(-t)^{1+\epsilon}\frac{d\sigma}{dt}\right]\int_{-\mu^2}^0 \frac{dt}{(-t)^{1+\epsilon}} \tag{4.20}$$

Combining the collinear terms that we found for the two different virtual corrections we have

$$\begin{aligned} F_1 + \frac{1}{2}\Sigma'(0) + \frac{1}{2}\Sigma'(0)_{x\leftrightarrow y} &= -\frac{\alpha_s C_F}{4\pi}\left(\frac{4\pi\mu_D^2}{-Q^2}\right)^\epsilon \Gamma[1+\epsilon]\int_0^1 dx \int_0^{1-x} dy \left(\frac{1}{xy}\right)^\epsilon \\ &\quad \left[\frac{\epsilon}{xy} + \frac{1}{2}(3-5\epsilon)\left(\frac{1}{x}+\frac{1}{y}\right) - \frac{1}{2}(6-5\epsilon)\left(\frac{x}{y}+\frac{y}{x}\right) + \frac{1}{2}(3-2\epsilon)\left(\frac{x^2}{y}+\frac{y^2}{x}\right)\right] \\ &= -\frac{\alpha_s C_F}{4\pi}\left(\frac{4\pi\mu_D^2}{-Q^2}\right)^\epsilon \Gamma[1+\epsilon]\int_0^1 dx \int_0^1 dy \int_0^1 dz\delta(x+y+z-1)\left(\frac{1}{xy}\right)^\epsilon \\ &\quad \left[\frac{\epsilon}{xy} + \frac{1}{2}(3-5\epsilon)\left(\frac{1}{x}+\frac{1}{y}\right) - \frac{1}{2}(6-5\epsilon)\left(\frac{x}{y}+\frac{y}{x}\right) + \frac{1}{2}(3-2\epsilon)\left(\frac{x^2}{y}+\frac{y^2}{x}\right)\right] \end{aligned} \tag{4.21}$$

performing the Feynmandelstam mapping this is

$$\begin{aligned} \sigma_V^{\rm col} &= -\sigma_{LO}\frac{\alpha_s C_F}{2\pi}\left(\frac{4\pi\mu_D^2}{-Q^2}\right)^\epsilon \Gamma[1+\epsilon]\int_{Q^2}^\infty \frac{ds}{s^2}\frac{Q^2}{s}\int_{-\infty}^0 dt\int_{-\infty}^0 du\,\delta(s+t+u-Q^2)\left(\frac{s^2}{tu}\right)^\epsilon \\ &\quad \left[\epsilon\frac{s^2}{tu} + \frac{1}{2}(3-5\epsilon)\left(\frac{s}{-t}+\frac{s}{-u}\right) - \frac{1}{2}(6-5\epsilon)\left(\frac{t}{u}+\frac{u}{t}\right) - \frac{1}{2}(3-2\epsilon)\left(\frac{t^2}{su}+\frac{u^2}{st}\right)\right] \end{aligned} \tag{4.22}$$

constructing the counterterm will involve

$$\begin{aligned} \lim_{t\to 0}\left[(-t)^{1+\epsilon}\frac{d\sigma_V}{dt}\right] &= -\sigma_{LO}\frac{\alpha_s C_F}{2\pi}\left(\frac{4\pi\mu_D^2}{-Q^2}\right)^\epsilon \Gamma[1+\epsilon]\int_{Q^2}^\infty \frac{ds}{s^2}\frac{Q^2}{s}\int_{-\infty}^0 du\,\delta(s+u-Q^2)\left(\frac{s^2}{-u}\right)^\epsilon \\ &\quad \left[\epsilon\frac{s^2}{-u} + \frac{1}{2}(3-5\epsilon)s + \frac{1}{2}(6-5\epsilon)u + \frac{1}{2}(3-2\epsilon)\frac{u^2}{s}\right] \\ &= -\sigma_{LO}\frac{\alpha_s C_F}{2\pi}\left(\frac{4\pi\mu_D^2}{-Q^2}\right)^\epsilon \Gamma[1+\epsilon]\int_{Q^2}^\infty \frac{ds}{s}\frac{Q^2}{s}\left(\frac{s^2}{s-Q^2}\right)^\epsilon \end{aligned}$$

$$
\begin{aligned}
&\left[\epsilon\frac{s}{s-Q^2}+\frac{1}{2}(3-5\epsilon)-\frac{1}{2}(6-5\epsilon)\frac{s-Q^2}{s}+\frac{1}{2}(3-2\epsilon)\frac{(s-Q^2)^2}{s^2}\right]\\
= &-\sigma_{LO}\frac{\alpha_s C_F}{2\pi}\left(\frac{4\pi\mu_D^2}{-Q^2}\right)^{\epsilon}\Gamma[1+\epsilon]\int_0^1\frac{dz}{z}z\left(\frac{Q^2}{z(1-z)}\right)^{\epsilon}\\
&\left[\frac{\epsilon}{1-z}+\frac{1}{2}(3-5\epsilon)-\frac{1}{2}(6-5\epsilon)(1-z)+\frac{1}{2}(3-2\epsilon)(1-z)^2\right]\\
= &-\sigma_{LO}\frac{\alpha_s C_F}{2\pi}\left(-4\pi\mu_D^2\right)^{\epsilon}\Gamma[1+\epsilon]\int_0^1 dz z^{-\epsilon}(1-z)^{-\epsilon}\\
&\left[\frac{\epsilon}{1-z}+\frac{1}{2}(3-5\epsilon)-\frac{1}{2}(6-5\epsilon)(1-z)+\frac{1}{2}(3-2\epsilon)(1-z)^2\right]\\
= &-\sigma_{LO}\frac{\alpha_s C_F}{2\pi}\left(-4\pi\mu_D^2\right)^{\epsilon}\Gamma[1+\epsilon]\frac{\Gamma^2[1-\epsilon]}{\Gamma[1-2\epsilon]}\\
&\left[\frac{\epsilon}{-\epsilon}+\frac{3-5\epsilon}{2(1-2\epsilon)}-\frac{6-5\epsilon}{4(1-2\epsilon)}+\frac{1}{2}(3-2\epsilon)\frac{2-\epsilon}{2(1-2\epsilon)(3-2\epsilon)}\right]\\
= &-\sigma_{LO}\frac{\alpha_s C_F}{2\pi}\left(-4\pi\mu_D^2\right)^{\epsilon}\Gamma[1+\epsilon]\frac{\Gamma^2[1-\epsilon]}{\Gamma[1-2\epsilon]}\\
&\left[-1+\frac{3-5\epsilon}{2(1-2\epsilon)}-\frac{6-5\epsilon}{4(1-2\epsilon)}+\frac{2-\epsilon}{4(1-2\epsilon)}\right]\\
= &\ \sigma_{LO}\frac{\alpha_s C_F}{2\pi}\left(-4\pi\mu_D^2\right)^{\epsilon}\Gamma[1+\epsilon]\left(\frac{1}{2}+\frac{\epsilon}{2}\right)+O(\epsilon)
\end{aligned}
\tag{4.23}
$$

the gauge dependent part of the counterterm is:

$$
\begin{aligned}
\bar{\sigma} &= \sigma_{LO}\frac{\alpha_s C_F}{2\pi}\left(-4\pi\mu_D^2\right)^{\epsilon}\Gamma[1+\epsilon]\left(\frac{1}{2}+\frac{\epsilon}{2}\right)\int_{-\mu^2}^0\frac{dt}{(-t)^{1+\epsilon}}\\
&= -\sigma_{LO}\frac{\alpha_s C_F}{2\pi}\left(\frac{4\pi\mu_D^2}{-\mu^2}\right)^{\epsilon}\Gamma[1+\epsilon]\left(\frac{1}{2\epsilon}+\frac{1}{2}\right)
\end{aligned}
\tag{4.24}
$$

This is clearly not good. Not only is the counterterm not gauge invariant, but the gauge dependent term is actually divergent. We have not yet considered the counter-counterterm though. The counter-counterterm takes into account the double subtracting of the IR pole at $t = u = 0$. Because we have double subtracted this pole we have to add back in the counter-counterterm:

$$
\bar{\bar{\sigma}} = \lim_{t,u\to 0}\left[(tu)^{1+\epsilon}\frac{d^2\sigma}{dtdu}\right]\int_{-\mu^2}^0\frac{dt}{(-t)^{1+\epsilon}}\int_{-\mu^2}^0\frac{du}{(-u)^{1+\epsilon}}
\tag{4.25}
$$

this term is:

$$
\begin{aligned}
\bar{\bar{\sigma}} &= -\sigma_{LO}\frac{\alpha_s C_F}{2\pi}\left(\frac{4\pi\mu_D^2}{-Q^2}\right)^{\epsilon}\frac{\mu^{-4\epsilon}}{\epsilon^2}\Gamma[1+\epsilon]\int_{Q^2}^{\infty}\frac{ds}{s^2}\frac{Q^2}{s}\,\delta(s-Q^2)\left(s^2\right)^{\epsilon}\left[\epsilon s^2\right]\\
&= -\sigma_{LO}\frac{\alpha_s C_F}{2\pi}\left(\frac{4\pi\mu_D^2}{-\mu^2}\right)^{\epsilon}\left(\frac{Q^2}{\mu^2}\right)^{\epsilon}\frac{1}{\epsilon}\Gamma[1+\epsilon]\\
&= -\sigma_{LO}\frac{\alpha_s C_F}{2\pi}\left(\frac{4\pi\mu_D^2}{-\mu^2}\right)^{\epsilon}\Gamma[1+\epsilon]\left(\frac{1}{\epsilon}+\log\frac{Q^2}{\mu^2}\right)
\end{aligned}
\tag{4.26}
$$

combining the counterterm with the counter-counterterm eliminates the gauge-dependent divergence:

$$\bar{\sigma} - \frac{1}{2}\bar{\bar{\sigma}} = -\sigma_{LO}\frac{\alpha_s}{2\pi}C_F\frac{1}{2}\left(1 - \log\frac{Q^2}{\mu^2}\right) \tag{4.27}$$

however we still see that there is a finite gauge-dependent term left. We thus conclude that the Feynmandelstam method of combining the virtual and radiative corrections to regulate collinear divergences in the collinear scheme is not gauge-invariant.

4.2 A General Argument

The general problem with the Feynmandelstam approach, as well as other approaches that use the same methodology, but with perhaps a different set of variables to define what is collinear physics, is that while the integrals that appear in the radiative corrections have the same form as the integrals that appear in the virtual corrections, they correspond to different physical entities. The radiative cross section takes the form

$$\sigma_R \propto \int \frac{ds}{s^2}\int dt \int du\,\delta(s+t+u-Q^2)\,\overline{|\mathcal{M}_R|^2} \tag{4.28}$$

so looking at an object like $\frac{d\sigma}{dt}$ still involves a full matrix element. Since we know that $\mathcal{M}_R$ is gauge invariant, then clearly the differential cross section will be as well. For virtual corrections it is a different story. As we saw above, the virtual correction has the form

$$\sigma_V \propto 2\mathrm{Re}\left[\mathcal{M}^*_{born}\mathcal{M}_V\right] = \int dx \int dy \int dz\,\delta(x+y+z-1)\,I \tag{4.29}$$

where I is the loop integrand. These integrals look similar, but physically they enter at different levels; the integrals in the radiative corrections are integrals over a physical object: $\mathcal{M}_R$ is a physical observable. The integrals in the virtual are within a physical object - in other words $\frac{d\sigma}{dx} \propto \frac{d\mathcal{M}_V}{dx}$, which is not a physical observable. It is because Feynmandelstam used this non-physical object that it runs into problems with gauge invariance. Any scheme that tries to peer inside the virtual matrix element to identify and extract the collinear physics is going to have this same problem because only the integrated matrix element is gauge invariant. Thus we must find a different way of dealing with the virtual corrections. In a sense we're back to the drawing board here. This does give us a chance to look at things back from the beginning though, which will lead to some interesting conclusions. This is the subject of the next chapter.

Chapter 5

A Generalized Collinear Scheme

At this point we went back to the drawing board. This seemed like a good opportunity to examine our goals and the collinear scheme in a little more detail. One of the most important attributes we want our scheme to have is universality; anything we propose to use is not very useful if we have to redo the whole calculation for each process. To that end, let me examine a general scattering problem: a process with an initial quark and a final state that has invariant mass Q. This is shown in figure 5.1.

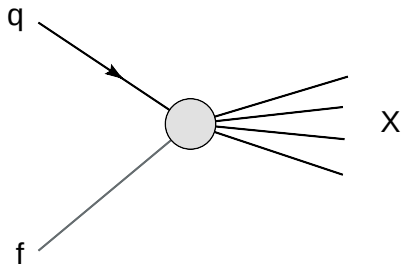

Figure 5.1: Generalized $qf \to X$ process. The only information we have is that one of the initial states is a quark, and that the final state has invariant mass Q.

If we now consider the possible collinear corrections to this process, it is clear that there are two diagrams. In one diagram an initial gluon splits into a quark-antiquark pair, of which the quark then scatters, and the other is that an initial quark radiates a gluon and then scatters. These are shown in figures 5.2 and 5.3, respectively.

Of the two of these diagrams, the one shown in figure 5.2 will be much easier to deal with. This is because at leading order we do not need to consider virtual corrections. Examining this diagram will be the subject of the first half of this chapter. After that we will examine virtual corrections and extend the results to include the diagram shown in figure 5.3.

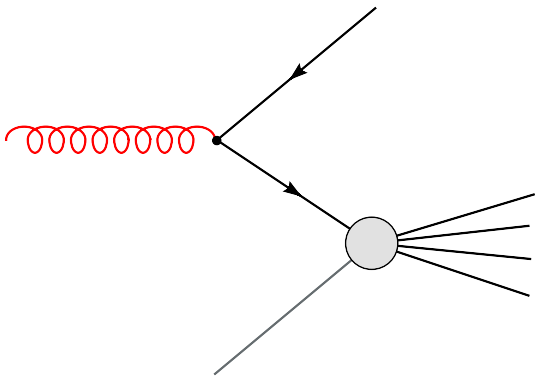

Figure 5.2: Initial gluon correction to a generalized $qf \to X$ process.

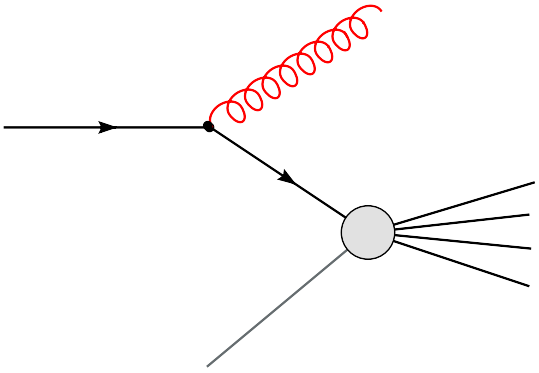

Figure 5.3: Initial gluon correction to a generalize $qf \to X$ process.

5.1 The Cross Section

One can ask how matrix element in figure 5.2 relates to the matrix element in figure 5.1. In general the two will be very different. We do know, however, that in the collinear limit, the matrix element factorizes [8]. Specifically if we label the four-momentum of the incoming gluon k, the four-momentum of the outgoing antiquark p, and the four-momentum of the scattering quark q

$$\overline{|\mathcal{M}_{gf\to\bar{q}X}|^2} = \frac{2g_s^2\mu_D^{2\epsilon}p_\perp^2}{z(1-z)} P_{gq}^d(z) \left(\frac{1}{q^2}\right)^2 \overline{|\mathcal{M}_{qf\to X}|} \tag{5.1}$$

where z is the fraction of momentum that the initial gluon passes to the quark that scatters, $p_\perp$ is the perpendicular component of the momentum the quark carries, and $\frac{1}{q^2}$ is the propagator of the t-channel quark. $P_{gq}^d(z)$ is the d-dimensional DGLAP splitting function.

Given that we know the collinear form of the matrix element, it makes sense to ask if we can calculate what the collinear form of the cross section is. If we write the antiquark final momentum as p, we can

calculate the cross section:

$$\begin{aligned}
\sigma_{gf\to\bar{q}X} &= \frac{1}{2s}\int \frac{d^{d-1}p}{(2\pi)^{d-1}}\frac{1}{2p^0}\{g\otimes f\}\left(\frac{1}{q^2}\right)^2 d\Pi_X \overline{|\mathcal{M}_{gf\to\bar{q}X}|^2} && (5.2)\\
&= \int \frac{d^{d-1}p}{(2\pi)^{d-1}}\frac{1}{2p^0}\{g\otimes f\}\frac{2g_s^2\mu_D^{2\epsilon}p_\perp^2}{z(1-z)}P_{gq}^d(z)\left(\frac{1}{q^2}\right)^2\frac{1}{2s}d\Pi_X\overline{|\mathcal{M}_{qf\to X}|} && (5.3)\\
&= g_s^2\mu_D^{2\epsilon}\int\frac{d^{d-1}p}{(2\pi)^d}\frac{1}{p^0}\{g\otimes f\}\frac{p_\perp^2}{z(1-z)}P_{gq}^d(z)\left(\frac{1}{q^2}\right)^2\sigma_{qf\to X} && (5.4)
\end{aligned}$$

now notice that if the gluon has initial momentum k, then $p^0=(1-z)k^0\equiv(1-z)k$. Furthermore

$$d^{d-1}p = dp^3d^{d-2}p_\perp = dzkd\,|p_\perp|\,|p_\perp|^{d-3}\,d^{d-3}\Omega = \frac{k}{d-2}dzd\,|p_\perp|^{d-2}\,d^{d-3}\Omega = \frac{k}{d-2}dzd\,|p_\perp|^{d-2}\,\frac{2\pi^{\frac{d-2}{2}}}{\Gamma\left(\frac{d-2}{2}\right)} \tag{5.5}$$

so

$$\sigma_{gf\to\bar{q}X} = \frac{g_s^2\mu_D^{2\epsilon}}{2^{d-2}\pi^{d/2}\Gamma\left(\frac{d-2}{2}\right)}\frac{1}{d-2}\int dzd\,|p_\perp|^{d-2}\,\{g\otimes f\}\frac{1}{1-z}\frac{p_\perp^2}{z(1-z)}P_{gq}^d(z)\left(\frac{1}{q^2}\right)^2\sigma_{qf\to X} \tag{5.6}$$

now, in the collinear limit the 4-momenta should be

$$\begin{aligned}
k &= (k,0,0,k)\\
p &= ((1-z)k,0,0,(1-z)k)\\
q &= (zk,0,0,zk) && (5.7)
\end{aligned}$$

if we now add a component $p_\perp$ to p and q, but keep it such that $p^2=0$, up to $O(p_\perp^4)$, which we know we must have since the external antiquark is on shell, we must modify it such that

$$\begin{aligned}
p &= \left((1-z)k,p_\perp,0,(1-z)k-\frac{p_\perp^2}{2(1-z)k}\right) && (5.8)\\
p^2 &= (1-z)^2k^2-p_\perp^2-(1-z)^2k^2+p_\perp^2+O(p_\perp^4)=0 && (5.9)
\end{aligned}$$

then

$$\begin{aligned}
q &= \left(zk,-p_\perp,0,zk+\frac{p_\perp^2}{2(1-z)k}\right) && (5.10)\\
q^2 &= z^2k^2-p_\perp^2-z^2k^2-2zk\frac{p_\perp^2}{2(1-z)k}+O(p_\perp^4)=-\frac{p_\perp^2}{1-z}+O(p_\perp^4) && (5.11)
\end{aligned}$$

and so

$$\sigma_{gf\to\bar{q}X} = \frac{g_s^2\mu_D^{2\epsilon}}{2^{d-2}\pi^{d/2}\Gamma\left(\frac{d-2}{2}\right)}\frac{1}{d-2}\frac{d-2}{2}\int dz d\left|p_\perp\right|^{d-2}\{g\otimes f\}\frac{1}{1-z}\frac{p_\perp^2}{z(1-z)}P_{gq}^d(z)\frac{(1-z)^2}{p_\perp^4}\sigma_{qf\to X} \tag{5.12}$$

$$= \frac{g_s^2\mu_D^{2\epsilon}}{2^{d-1}\pi^{d/2}\Gamma\left(\frac{d-2}{2}\right)}\int\frac{dz}{z}\frac{d\left|p_\perp\right|^{d-2}}{p_\perp^2}\{g\otimes f\}P_{gq}^d(z)\sigma_{qf\to X} \tag{5.13}$$

changing integration variables:

$$d\left|p_\perp\right|^{d-2} = \frac{d-2}{2}(p_\perp^2)^{\frac{d-4}{2}}dp_\perp^2 \tag{5.14}$$

$$\sigma_{gf\to\bar{q}X} = \frac{g_s^2\mu_D^{2\epsilon}}{2^{d-1}\pi^{d/2}\Gamma\left(\frac{d-2}{2}\right)}\frac{1}{d-2}\int\frac{dz}{z}\frac{d\left|p_\perp\right|^{d-2}}{p_\perp^2}\{g\otimes f\}P_{gq}^d(z)\sigma_{qf\to X} \tag{5.15}$$

$$= \frac{\alpha_s}{2\pi}\frac{(4\pi\mu_D^2)^\epsilon}{\Gamma(1-\epsilon)}\int\frac{dz}{z}\frac{dp_\perp 2}{(p_\perp^2)^{1+\epsilon}}\{g\otimes f\}P_{gq}^d(z)\sigma_{qf\to X} \tag{5.16}$$

let me now change kinematic variables. $p_\perp$ is a fine variable for identifying the collinear divergence because it does go to zero in the collinear limit, but it has a problem; it is not independent of z. That is the upper limit of $p_\perp$ is going to depend on how much momentum gets transmitted to the scattering quark from the incoming gluon. Let us choose a different variable, v:

$$v = -\frac{t}{s(1-z)} = \frac{p_\perp^2}{s(1-z)^2} \tag{5.17}$$

which satisfies $v = \frac{1}{2}(1-\cos\theta)$, where θ is the angle of separation between the incoming gluon and outgoing antiquark, so it ranges from 0 to 1 and goes to zero in the collinear limit. This variable has the advantage of being untangled from z, so the integral form of our expression will be an integral over two independent variables, the center of mass energy, and the angle. Using this substitution,

$$\sigma_{gf\to\bar{q}X} = \frac{\alpha_s}{2\pi}\frac{(4\pi\mu_D^2)^\epsilon}{\Gamma(1-\epsilon)}\int\frac{dz}{z}s^{-\epsilon}(1-z)^{-2\epsilon}\frac{dv}{v^{1+\epsilon}}\{g\otimes f\}P_{gq}^d(z)\sigma_{qf\to X}(z) \tag{5.18}$$

furthermore, the invariant mass of X is Q, so labelling the incoming momentum of the other parton f:

$$Q^2 = (q+f)^2 = 2q\cdot f = 2zk\cdot f = sz \tag{5.19}$$

and so we see that $z = \frac{Q^2}{s}$, giving

$$\sigma_{gf\to\bar{q}X} = \frac{\alpha_s}{2\pi}\left(\frac{4\pi\mu_D^2}{Q^2}\right)^\epsilon\frac{1}{\Gamma(1-\epsilon)}\int\frac{dz}{z}z^\epsilon(1-z)^{-2\epsilon}\frac{dv}{v^{1+\epsilon}}\{g\otimes f\}P_{gq}^d(z)\sigma_{qf\to X}(z) \tag{5.20}$$

5.2 The Generalized Collinear Scheme

Notice that starting with the factorization of the matrix element, we was able to determine the collinear limit of the cross section. This limit is universal, and depends only on the fact that we scattered a quark, and the kinematics of the process. The kinematics enter at the final step, where I calculate that $z = \frac{Q^2}{s}$. If we considered a case where, for example, the initial state had a finite mass, or a negative mass squared,[1] there would be a different relationship between the fraction of the momentum that the quark carries to scatter and s and Q^2. Because this expression is universal, we take this to define a universal counterterm.

If one were to calculate the cross section from scratch, we know that one would find the expression above, plus a part that doesn't contain any collinear divergences. Furthermore, because we know the matrix element is a rational function of v and z, we know the form of the above expression will be the same form as the cross section. Finally we know that in the total cross section the limits of integration will be from z_0 up to 1 in the z integral, and from 0 to 1 in the v integral. Putting all of this together, we know one can write the total cross section as:

$$\sigma_{gf\to\bar{q}X} = \frac{\alpha_s}{2\pi}\left(\frac{4\pi\mu_D^2}{Q^2}\right)^{\epsilon}\frac{1}{\Gamma(1-\epsilon)}\int_{z_0}^1\frac{dz}{z}z^{\epsilon}(1-z)^{-2\epsilon}\{g\otimes f\}P_{gq}^d(z)\int_0^1\frac{dv}{v^{1+\epsilon}}\sigma_{qf\to X} + \text{finite} \tag{5.21}$$

If we want to construct a counterterm and find the factorization scale as we did in the previously defined collinear scheme, we must use the v variable instead of the t variable. Notice, however, that with the choice of the v variable, all the dependence on v is contained within the integral. The collinear plot, then will be rather boring - it will stay at a constant height that extends from $v = 0$ to $v = 1$, then it will drop to zero. Defining my counterterm by subtracting off the collinear limit up to a cutoff v_{cut}, then the cross section counterterm will be:

$$\bar{\sigma}_{gf\to\bar{q}X} = \frac{\alpha_s}{2\pi}\left(\frac{4\pi\mu_D^2}{Q^2}\right)^{\epsilon}\frac{1}{\Gamma(1-\epsilon)}\int_{z_0}^1\frac{dz}{z}z^{\epsilon}(1-z)^{-2\epsilon}\{g\otimes f\}P_{gq}^d(z)\int_0^{v_{cut}}\frac{dv}{v^{1+\epsilon}}\sigma_{qf\to X} \tag{5.22}$$

rewriting this as a gluon PDF counterterm for the quark PDF:

$$\begin{aligned}
\delta q(x) &= \frac{\alpha_s}{2\pi}\left(\frac{4\pi\mu_D^2}{Q^2}\right)^{\epsilon}\frac{1}{\Gamma(1-\epsilon)}\int_x^1\frac{dz}{z}g\left(\frac{x}{z}\right)z^{\epsilon}(1-z)^{-2\epsilon}P_{gq}^d(z)\int_0^{v_{cut}}\frac{dv}{v^{1+\epsilon}} &(5.23)\\
&= -\frac{\alpha_s}{2\pi}\left(\frac{4\pi\mu_D^2}{v_{cut}Q^2}\right)^{\epsilon}\frac{1}{\Gamma(1-\epsilon)}\frac{1}{\epsilon}\int_x^1\frac{dz}{z}g\left(\frac{x}{z}\right)z^{\epsilon}(1-z)^{-2\epsilon}P_{gq}^d(z) &(5.24)\\
&= -\frac{\alpha_s}{2\pi}\left(\frac{4\pi\mu_D^2}{v_{cut}Q^2}\right)^{\epsilon}\frac{1}{\Gamma(1-\epsilon)}\int_x^1\frac{dz}{z}g\left(\frac{x}{z}\right)\left[\frac{1}{\epsilon}P_{gq}(z) - T_R(z^2+(1-z)^2)\log\frac{(1-z)^2}{z} - 2T_Rz(1-z)\right]
\end{aligned}$$

[1] As in deep inelastic scattering.

(5.25)

now we ask the question, what should we do with v_{cut}? Well if we turn to the DGLAP equations, we find that in order for this counterterm to satisfy DGLAP, we must have $v_{cut} \propto \mu^2$. Because the only other momentum scale around is Q, and we know that v_{cut} is a scalar, we conclude that one must take $v_{cut} = \frac{\mu^2}{Q^2} f(z)$. However as was discussed earlier, v is an ideal variable because it fully unentangles from z; this is why we chose v. This choice is undone if we choose to reinsert dependence on z into our v_{cut} so we take $v_{cut} = \frac{\mu^2}{Q^2}$, and we have

$$\delta q(x) = -\frac{\alpha_s}{2\pi}\left(\frac{4\pi\mu_D^2}{\mu^2}\right)^{\epsilon}\frac{1}{\Gamma(1-\epsilon)}\int_x^1 \frac{dz}{z} g\left(\frac{x}{z}\right)\left[\frac{1}{\epsilon}P_{gq}(z) - T_R(z^2+(1-z)^2)\log\frac{(1-z)^2}{z} - 2T_R z(1-z)\right] \tag{5.26}$$

this counterterm defines (part) of the collinear scheme. Now notice something interesting here.

$$\delta q^{\overline{\text{MS}}}(x) = -\frac{\alpha_s}{2\pi}\left(\frac{4\pi\mu_D^2}{\mu^2}\right)^{\epsilon}\frac{1}{\Gamma(1-\epsilon)}\int_x^1 \frac{dz}{z} g\left(\frac{x}{z}\right)\frac{1}{\epsilon}P_{gq}(z) \tag{5.27}$$

is the counterterm for the $\overline{\text{MS}}$ factorization scheme. The $\log 4\pi$ and γ_E terms come out of expanding the coefficient that sits in front of the integral. Where do the extra terms we find in the collinear scheme come from? There are two sources. The logarithmic term comes from phase space. The polynomial term comes from the extra term in $P_{gq}^d(z)$ that is not in $P_{gq}(z)$. One way to interpret the generalized collinear scheme then, is that it takes consistently the d-dimensionality of the calculation. Rather than just subtracting the pole, the collinear scheme subtracts the pole and the terms that arise from phase space and extra polarization indicies that occur in d dimensions.

5.3 Choosing the Scale

Next we turn to the issue of choosing the scale. Our scheme is well defined, but without a way to choose the scale we haven't gained anything. As discussed earlier, if we choose to use a collinear plot to determine what the scale should be, we will always choose $v_{cut} = 1$, which corresponds to $\mu = Q$.

Recall earlier the discussion the form of the cross section will have. By taking $v_{cut} = 1$, we actually subtract all of the universal term that we know must be there from looking at the collinear limit. Essentially in taking $\mu = Q$ then, the collinear scheme begins by looking in the collinear limit to establish the universal form of the cross section. Then by using some knowledge of the algebraic form of the matrix element, we can subtract off the entire universal term back into the PDF. The collinear limit is the anchor point, and

using it we can determine the form of the universal term that must be there, and that is what we subtract back into the PDFs.[2]

This is good news; this generalized collinear scheme has the advantage of having a scale that we don't have to do any work to obtain. This is useful is because we don't want to have to use the NLO cross section to choose the factorization scale. The situation we have in mind is where we only have a LO cross section, and we want to learn how to get the most out of our low-order calculation. This generalized collinear scheme allows us to determine what the scale should be for the LO calculation without examining the NLO calculation at all.

5.4 The Other PDF Counterterms

At this point we are well on the way to the completed generalized collinear scheme. We've found one of the counterterms, and we've found the way to choose the scale. To complete the generalized collinear factorization scheme, we need to find the other PDF counterterms. Following the calculation through with the diagram in figure 5.3, we find

$$\delta q(x) = -\frac{\alpha_s}{2\pi}\left(\frac{4\pi\mu_D^2}{\mu^2}\right)^{\epsilon}\frac{1}{\Gamma(1-\epsilon)}\frac{1}{\epsilon}\int_x^1 \frac{dz}{z} q\left(\frac{x}{z}\right) z^{\epsilon}(1-z)^{-2\epsilon}\tilde{P}_{qq}^d(z) \tag{5.28}$$

where

$$\tilde{P}_{qq}^d(z) = C_F\left(\frac{1+z^2}{1-z} - \epsilon(1-z)\right) \tag{5.29}$$

Notice the similarity between this counterterm and equation 5.24. The reason we get $\tilde{P}_{qq}(z)$ is because we've not included the virtual corrections. The virtual corrections add another term at $z = 1$, which regulates the soft divergence found in $\tilde{P}_{qq}(z)$. We will consider virtual corrections and regulating the soft divergence in the PDF counterterms in the next section.

If we repeat the same calculation using an initial gluon instead of an initial quark, we find the other two counterterms:

$$\delta g(x) = -\frac{\alpha_s}{2\pi}\left(\frac{4\pi\mu_D^2}{\mu^2}\right)^{\epsilon}\frac{1}{\Gamma(1-\epsilon)}\frac{1}{\epsilon}\int_x^1 \frac{dz}{z} q\left(\frac{x}{z}\right) z^{\epsilon}(1-z)^{-2\epsilon}P_{gq}^d(z) \tag{5.30}$$

$$\delta g(x) = -\frac{\alpha_s}{2\pi}\left(\frac{4\pi\mu_D^2}{\mu^2}\right)^{\epsilon}\frac{1}{\Gamma(1-\epsilon)}\frac{1}{\epsilon}\int_x^1 \frac{dz}{z} g\left(\frac{x}{z}\right) z^{\epsilon}(1-z)^{-2\epsilon}\tilde{P}_{gg}^d(z) \tag{5.31}$$

[2]Indeed, $v = 1$ is anti-collinear limit, so in taking $v_{cut} = 1$, we've left the collinear limit far behind.

where

$$\tilde{P}^d_{gg}(z) = 2C_A \frac{(1-z+z^2)^2}{z(1-z)} \tag{5.32}$$

Again we see that in one counterterm there is an unregulated soft divergence that requires me to consider the virtual contribution more clearly. If I expand out equation 5.30, I find

$$\delta g(x) = -\frac{\alpha_s}{2\pi}\left(\frac{4\pi\mu_D^2}{\mu^2}\right)^{\epsilon} \frac{1}{\Gamma(1-\epsilon)}\frac{1}{\epsilon}\int_x^1 \frac{dz}{z} q\left(\frac{x}{z}\right)\left[\frac{1}{\epsilon}P_{gq}(z) - C_F\frac{1+(1-z)^2}{z}\log\frac{(1-z)^2}{z} - C_F z\right] \tag{5.33}$$

To complete the generalized collinear scheme, we next have to consider the virtual corrections and regulating the soft divergence in the other two PDF counterterms.

5.5 Virtual Corrections

In order to complete the generalized collinear scheme, we need to deduce the appropriate regularization of the soft divergence in the final two PDF counterterms. We still want to keep the analysis fully general, so we will have to be clever with how we do this.[3]

5.5.1 Sum Rules

First let us consider the sum rules that are used to deduce the $z = 1$ component of the DGLAP splitting functions. Conservation of quark number, quark momentum, and gluon momentum, respectively, produce three sum rules the DGLAP kernels have to satisfy:

$$\int_0^1 dz\, P_{qq}(z) = 0 \tag{5.34}$$

$$\int_0^1 dz\, z[P_{qq}(z) + P_{gq}(z)] = 0 \tag{5.35}$$

$$\int_0^1 dz\, z[2n_f P_{qg}(z) + P_{gg}(z)] = 0 \tag{5.36}$$

the first two equations determine the $\delta(1-z)$ term in $P_{qq}(z)$, and the last equation determines the $\delta(1-z)$ term in $P_{gg}(z)$:

$$P_{qq}(z) = C_F\left(\frac{1+z^2}{1-z}\right)_+ \tag{5.37}$$

$$P_{gg}(z) = 2C_A\frac{(1-z+z^2)^2}{z(1-z)_+} + \left(\frac{11}{6}C_A - \frac{2n_f T_F}{3}\right)\delta(1-z) \tag{5.38}$$

[3]It is this author's opinion that a fully general analysis is isomorphic to proving the factorization of collinear divergences for a general perturbative QCD cross section. This proof does not exist, so I will have to make some assumptions.

This, however, is not enough information to determine our PDF counterterms. This is because the $(1-z)^{-2\epsilon}$ that arises from phase space will produce a $\log(1-z)$ term that also must be regulated. The sum rules do not give us a handle for regulating this logarithmic term. For this reason one must consider the virtual corrections more explicitly.

5.5.2 Point-Like Verticies

In general there will be both wavefunction renormalization and vertex correction virtual diagrams. For a diagram with generic incoming partons though, there will always be a triangle-type diagram as shown in figure 5.4.

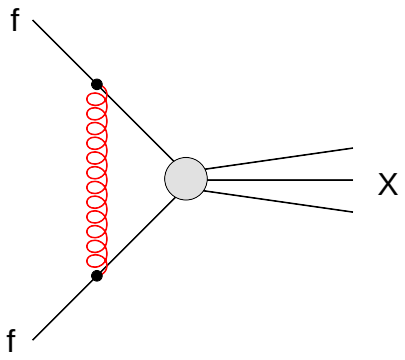

Figure 5.4: One of many possible virtual diagrams that will exist as corrections to the generalized process. Notice that this diagram exists whether the initial partons are both quarks or both gluons.

The denominator structure of this diagram will be

$$\frac{1}{l^2}\frac{1}{(p_1-l)^2}\frac{1}{(p_2+l)^2} \tag{5.39}$$

In general other diagrams (for example wavefunction renormalization) may not have this same denominator structure, but multiplying by unity in a clever form can bring them to have this same denominator structure. We saw this in the $b\bar{b} \to H$ and $gg \to H$ calculations considered in chapters 2 and 3 already.

Let me now consider what we can learn from this. Combining the denominator using Feynman parameters will result in:

$$\frac{1}{l^2(p_1-l)^2(p_2+l)^2} = \int_0^1 dx \int_0^1 dy \int_0^1 dz\, \delta(x+y+z-1)\frac{2}{[zl^2+x(p_1-l)^2+y(p_2+l)^2]^3} \tag{5.40}$$

$$= \int_0^1 dx \int_0^1 dy \int_0^1 dz\, \delta(x+y+z-1)\frac{2}{[(l-xp_1=yp_2)^2+2xyp_1\cdot p_2]^3} \tag{5.41}$$

$$= \int_0^1 dx \int_0^1 dy \int_0^1 dz\, \delta(x+y+z-1)\frac{2}{[k^2+xyQ^2]^3} \tag{5.42}$$

(5.43)

this is only the total expression if the vertex is point-like. If the generalized vertex contains any propagators in itself, for example, this will introduce more Feynman parameters and result in a more complex expression. If the cross section that we are calculating is infrared safe though, the difference in total cross section can only be a finite term. We then choose to take the point-like vertex as a benchmark case to define what we know the singularity structure of the virtual correction must be and what to subtract to regulate my PDF counterterms.

When calculating the vertex correction the numerator of the expression will be a polynomial in k^2, with coefficients that are rational functions of the Feynman parameters. One can write in general then (using F as a generic function of the arguments),

$$\sigma_{virt} = -\sigma_{LO} g_s^2 \mu_D^{2\epsilon} \int_0^1 dx \int_0^1 dy \int_0^1 dz\, \delta(x+y+z-1) \frac{2}{[k^2+xyQ^2]^3} F(k^2, x, y, z, Q^2, d) \tag{5.44}$$

Notice the following though, from dimensional analysis one can deduce that (with some different function F)

$$\begin{aligned} \int \frac{d^d k\, k^m}{[k^2-\Delta]^n} &= \frac{1}{(4\pi)^{d/2}} \left(\frac{1}{\Delta}\right)^{n-\frac{d}{2}-\frac{m}{2}} \Gamma\left(n-\frac{d}{2}-\frac{m}{2}\right) F(n,m,D) &(5.45)\\ &= \frac{1}{16\pi^2} \left(\frac{4\pi}{\Delta}\right)^{\epsilon} \left(\frac{1}{\Delta}\right)^{n-\frac{m}{2}-2} \Gamma\left(n-\frac{d}{2}-\frac{m}{2}\right) F(n,m,D) &(5.46) \end{aligned}$$

we can then write (for some dimensionless function G)

$$\sigma_{virt} = -\sigma_{LO} \frac{\alpha_s}{2\pi} \mathrm{Re}\left[\left(-\frac{4\pi\mu_D^2}{Q^2}\right)^{\epsilon}\right] \Gamma(1+\epsilon) \int_0^1 dx \int_0^1 dy \int_0^1 dz\, \delta(x+y+z-1) \left(\frac{1}{xy}\right)^{\epsilon} G(x,y,z,D) \tag{5.47}$$

where we have simplified and combined the gamma functions using gamma function identities. Now, from our previous discussions and examinations of the collinear divergences in the virtual diagrams, we know that the variables x and y somewhat correspond to the collinear variables t, and u. Because the calcultion up until this point has been done using z and v, we change variables to use these. Taking $v = \frac{x}{1-z}$, this results in:

$$\sigma_{virt} = -\sigma_{LO} \frac{\alpha_s}{2\pi} \left(\frac{4\pi\mu_D^2}{Q^2}\right)^{\epsilon} \mathrm{Re}\left[(-1)^{\epsilon}\right] \Gamma(1+\epsilon) \int_0^1 dz\, (1-z)^{-2\epsilon} \int_0^1 dv\, v^{-\epsilon}(1-v)^{-\epsilon} G(v,z,D) \tag{5.48}$$

we want to take equation 5.48 and deduce what to subtract for the virtual correction from it. We know that

the function $G(v,z,D)$ must be a rational function of its arguments, and we know the form of the collinear limit must be

$$\lim_{v\to 0} G(v,z,D) = \frac{1}{v} G(z,D) \tag{5.49}$$

furthermore, the sum rules discussed in sub-section 5.5.1 require[4]

$$\begin{aligned} G_{qq}(z,4) &= C_F \frac{1+z^2}{1-z} && (5.50)\\ G_{gg}(z,4) &= 2C_A \frac{1}{1-z} + \frac{11}{6} C_A - \frac{2n_f T_F}{3} && (5.51) \end{aligned}$$

because we know that in 4-dimensions that $G(z,4)$ is just the virtual term that enforces the sum rules on the DGLAP kernels, we choose to take $G(z,D) = G(z,4)$.

$$\sigma_{virt} = -\sigma_{LO} \frac{\alpha_s}{2\pi} \left(\frac{4\pi\mu_D^2}{Q^2}\right)^{\epsilon} \mathrm{Re}\left[(-1)^{\epsilon}\right] \Gamma(1+\epsilon) \int_0^1 dz\, (1-z)^{-2\epsilon} \int_0^1 \frac{dv}{v^{1+\epsilon}} G(z,D) \tag{5.52}$$

if we take the same approach we did earlier, where we subtract the integral over v up to v_{cut}, we obtain the virtual counterterm:

$$\begin{aligned} \bar{\sigma}_{virt} &= -\sigma_{LO} \frac{\alpha_s}{2\pi} \left(\frac{4\pi\mu_D^2}{Q^2}\right)^{\epsilon} \mathrm{Re}\left[(-1)^{\epsilon}\right] \Gamma(1+\epsilon) \int_0^1 dz\, (1-z)^{-2\epsilon} G(z,D) \int_0^{v_{cut}} \frac{dv}{v^{1+\epsilon}} && (5.53)\\ &= \sigma_{LO} \frac{\alpha_s}{2\pi} \left(\frac{4\pi\mu_D^2}{\mu^2}\right)^{\epsilon} \left(1 - \frac{\pi^2\epsilon^2}{3}\right) \frac{1}{\epsilon} \int_0^1 dz\, (1-z)^{-2\epsilon} G(z,D) && (5.54) \end{aligned}$$

we want to combine this with the other term, so we rewrite this expression so it has the same coefficient as the counterterm we found before:

$$\bar{\sigma}_{virt} = \sigma_{LO} \frac{\alpha_s}{2\pi} \left(\frac{4\pi\mu_D^2}{\mu^2}\right)^{\epsilon} \left(1 - \frac{\pi^2\epsilon^2}{3}\right) \frac{1}{\epsilon} \int_0^1 dz\, (1-z)^{-2\epsilon} G(z,D) \tag{5.55}$$

Combining this with the unregulated expressions gives me the final two PDF counterterms in the collinear scheme:

$$\begin{aligned} \delta q^{col}(x) &= -\frac{\alpha_s}{2\pi} \left(\frac{4\pi\mu_D^2}{\mu^2}\right)^{\epsilon} \frac{1}{\Gamma(1-\epsilon)} \int_x^1 \frac{dz}{z} q\left(\frac{x}{z}\right) \left[\frac{1}{\epsilon} P_{qq}(z) - 2C_F \left(\frac{1+z^2}{1-z} \log 1-z\right)_+ + C_F \frac{1+z^2}{1-z} \log z \right.\\ &\qquad \left. - C_F(1-z) + C_F \frac{\pi^2}{3} \delta(1-z)\right] && (5.56)\\ \delta g^{col}(x) &= -\frac{\alpha_s}{2\pi} \left(\frac{4\pi\mu_D^2}{\mu^2}\right)^{\epsilon} \frac{1}{\Gamma(1-\epsilon)} \int_x^1 \frac{dz}{z} g\left(\frac{x}{z}\right) \left[\frac{1}{\epsilon} P_{gg}(z) - 4C_A \frac{(1-z+z^2)^2}{z} \left(\frac{\log 1-z}{1-z}\right)_+ \right. \end{aligned}$$

[4]Using the notation G_{qq} for the function G in the $q \to q$ process and G_{gg} for the function G in the $g \to g$ process.

$$+ 2C_A \frac{(1-z+z^2)^2}{z(1-z)} \log z + C_A \frac{\pi^2}{3} \delta(1-z) \Bigg] \tag{5.57}$$

Notice that these counterterms have the same basic structure between the four counterterms; there is the DGLAP splitting function, then extra terms that come from the phase space which are logarithmic, and polynomial and delta function terms. In the next chapter we test this scheme and see how well it works.

Chapter 6

Results and Conclusions

6.1 Collinear Scheme PDFs

In order to be honest with my calculations, we must generate a set of collinear scheme PDFs. Generating a full set of PDFs is of course a complex and intricate subject, but there is a simple approximation one can use to find a first approximation to what the collinear scheme PDFs will be. Consider the form of the PDF counterterms in the two schemes:

$$\delta q^{col}(x) = -\frac{\alpha_s}{2\pi}\left(\frac{4\pi\mu_D^2}{\mu^2}\right)^{\epsilon}\frac{1}{\Gamma(1-\epsilon)}\int_x^1\frac{dz}{z}q\left(\frac{x}{z}\right)\left[\frac{1}{\epsilon}P_{gq}(z) - C_F\frac{1+(1-z)^2}{z}\log\frac{(1-z)^2}{z} + C_F z(1-z)\right] \tag{6.1}$$

$$\delta q^{\overline{MS}}(x) = -\frac{\alpha_s}{2\pi}\left(\frac{4\pi\mu_D^2}{\mu^2}\right)^{\epsilon}\frac{1}{\Gamma(1-\epsilon)}\int_x^1\frac{dz}{z}q\left(\frac{x}{z}\right)\frac{1}{\epsilon}P_{gq}(z) \tag{6.2}$$

I've been a little sloppy with my notation here - the $\overline{\rm MS}$ and collinear scheme PDFs have different scales. The PDFs though, do run slowly (logarithmically) with the scale, so one can approximate:

$$q^{col} = q^{LO} + \delta q^{col} = q^{LO} + \delta q^{\overline{MS}} + \delta q^{col} - \delta q^{\overline{MS}} \tag{6.3}$$

$$= q^{\overline{MS}} + \delta q^{col} - \delta q^{\overline{MS}} \tag{6.4}$$

taking into account then all the corrections to the PDFs, one can write

$$\begin{aligned} q^{col} = {} & q^{\overline{MS}} + \frac{\alpha_s}{2\pi}\int_x^1\frac{dz}{z}\left[g\left(\frac{x}{z}\right)\left(T_R(z^2+(1-z)^2)\log\frac{(1-z)^2}{z} + 2T_R z(1-z)\right)\right. \\ & \left. + q\left(\frac{x}{z}\right)\left(2C_F\left(\frac{1+z^2}{1-z}\log 1-z\right)_+ - C_F\frac{1+z^2}{1-z}\log z + C_F(1-z) - C_F\frac{\pi^2}{3}\delta(1-z)\right)\right] \end{aligned} \tag{6.5}$$

$$\begin{aligned} g^{col} = {} & g^{\overline{MS}} + \frac{\alpha_s}{2\pi}\int_x^1\frac{dz}{z}\left[q\left(\frac{x}{z}\right)\left(C_F\frac{1+(1-z)^2}{z}\log\frac{(1-z)^2}{z} + C_F z\right)\right. \\ & \left. + g\left(\frac{x}{z}\right)\left(4C_A\frac{(1-z+z^2)^2}{z}\left(\frac{\log 1-z}{1-z}\right)_+ - 2C_A\frac{(1-z+z^2)^2}{z(1-z)}\log z - C_A\frac{\pi^2}{3}\delta(1-z)\right)\right] \end{aligned}$$

(6.6)

using equations 6.6 and 6.6, we created a set of collinear scheme PDFs. For these, and all other plots in the rest of this thesis I used the CTEQ5 set of PDFs that are implemented in Mathematica. These are not the most current set of PDFs, but I am only creating a 'first order' set of PDFs anyways, so this is more of a proof of principle than a precise study. These PDFs are plotted compared with the $\overline{\text{MS}}$ PDFs in figures 6.1 through 6.6

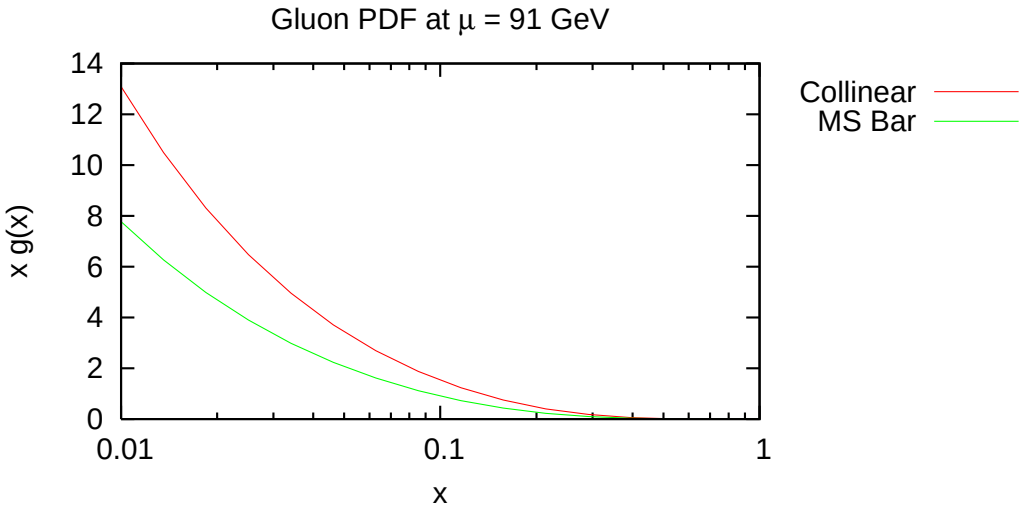

Figure 6.1: Comparison of collinear and $\overline{\text{MS}}$ gluon PDFs over a range of x with $\mu = 91$ GeV.

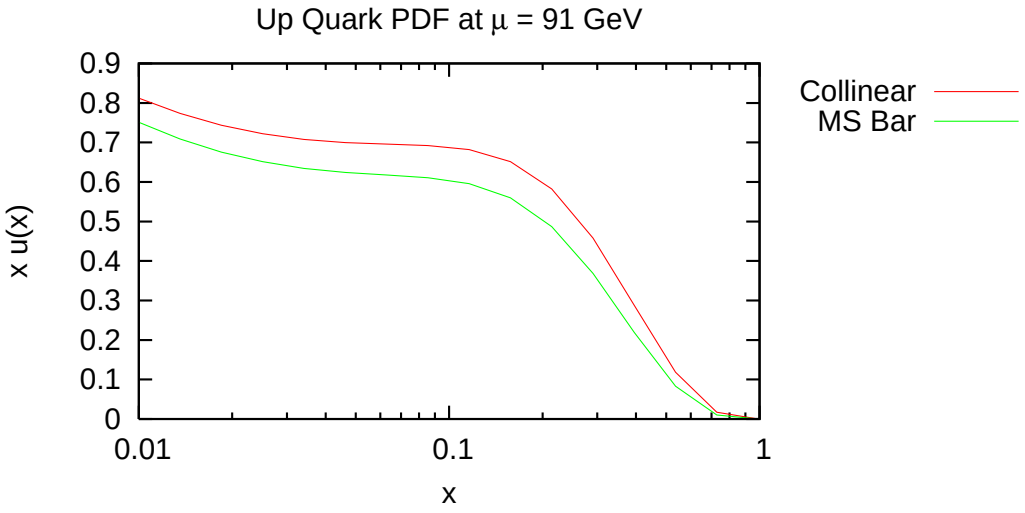

Figure 6.2: Comparison of collinear and $\overline{\text{MS}}$ up quark PDFs over a range of x with $\mu = 91$ GeV.

A ratio of the PDFs is plotted in figure 6.7. Notice that many of the PDFs get rather large corrections

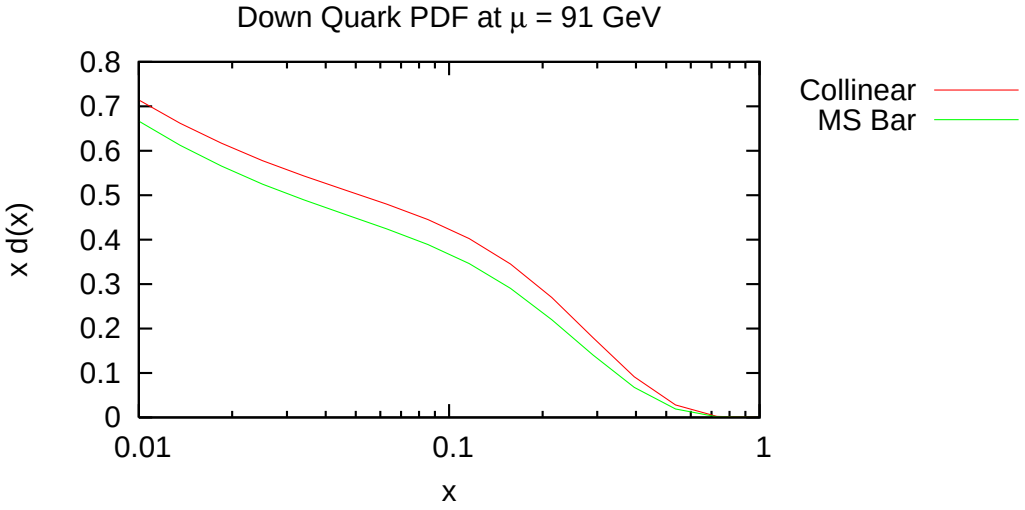

Figure 6.3: Comparison of collinear and $\overline{\text{MS}}$ down quark PDFs over a range of x with $\mu = 91$ GeV.

when compared with $\overline{\text{MS}}$. According to the interpretation of the collinear scheme then, we should expect that there will be sizeable universal corrections that are not subtracted into the PDFs in the $\overline{\text{MS}}$ factorization scheme.

Clearly the difference in PDFs will affect the way that cross sections play out. We expect the cross section should converge to the same number regardless of the scheme that we use to calculate in. Because the PDFs are larger, we generically expect a larger LO calculation in the collinear scheme, which means that generically we expect the NLO corrections to be smaller. Let me now examine the collinear scheme applied to a few different processes.

6.2 Collinear Scheme Cross Sections

Because we have explicitly demonstrated that the collinear scheme is universal and calculated the PDF counterterms, it is easy to find the NLO cross sections for various processes. All we have to do is look up the unregulated cross section at NLO and subtract the counterterm.

6.2.1 Drell-Yan

Drell-Yan production is the benchmark process in perturbative QCD, and we will consider this case first. One attractive feature of Drell-Yan is that a Ward identity protects the vertex, so we don't need to renormalize any ultraviolet divergences. This is a case where we can examine the factorization issue independent of the renormalization issue.

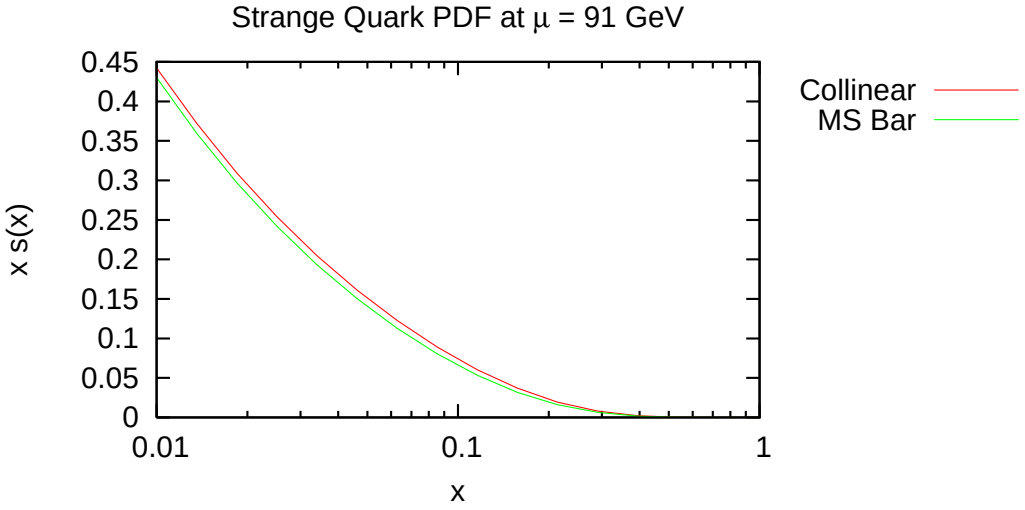

Figure 6.4: Comparison of collinear and $\overline{\text{MS}}$ strange quark PDFs over a range of x with $\mu = 91$ GeV.

Before we turn to the collinear scheme cross section, let me review the $\overline{\text{MS}}$ scheme cross section. The real Z-boson production cross section in the $\overline{\text{MS}}$ factorization scheme at the Tevatron is shown in figure 6.8. Notice the leading result is roughly scale independent at 6.15nb.[1] The total next to leading order correction is also roughly scale independent at 7.97nb, for a 30% correction. Notice as well that the correction from the gluon-quark initial state is rather small, but the gluon-gluon initial state correction is significant across the whole range of factorization scale choice.

The unregulated Drell-Yan cross section is [14]

$$\begin{aligned}\sigma_{DY} &= \frac{4\pi^2\alpha}{3S}\frac{1}{\Gamma(1-\epsilon)}\left(\frac{4\pi\mu_D^2}{Q^2}\right)^{\epsilon}\frac{\alpha_s}{2\pi}\sum_{i,j}C_{ij}\int_{z_0}^{1}\frac{dz}{z}\Bigg[\\ &\{q_i\otimes\bar{q}_j\}\left(\frac{z_0}{z}\right)\left[-\frac{2}{\epsilon}P_{qq}(z)+C_F\left(4\left(\frac{1+z^2}{1-z}\log 1-z\right)_+ - 2\frac{1+z^2}{1-z}\log z+\delta(1-z)\left(\frac{2\pi^2}{3}-1\right)\right)\right] \\ &+\{g\otimes q_i\}\left(\frac{z_0}{z}\right)\left[-\frac{1}{\epsilon}P_{qg}(z)+P_{qg}(z)\log\frac{(1-z)^2}{z}+\frac{3}{4}+\frac{1}{2}z-\frac{3}{4}z^2\right]\Bigg] \end{aligned} \tag{6.7}$$

where the C_{ij} are the electroweak coefficients, shown in table 6.1. subtracting the counterterm we get the collinear scheme cross section:

$$\begin{aligned}\sigma_{DY}^{col} &= \frac{4\pi\alpha}{3S}\frac{\alpha_s}{2\pi}\sum_{i,j}C_{ij}\int_{z_0}^{1}\frac{dz}{z}\left[\{q\otimes\bar{q}\}\left(\frac{z_0}{z}\right)\left[2P_{qq}(z)\log\frac{Q^2}{\mu^2}-C_F(1-z)\right]\right. \\ &\left.+\{g\otimes q\}\left(\frac{z_0}{z}\right)\left[P_{qg}(z)\log\frac{Q^2}{\mu^2}+\frac{1}{4}(1+2z-3z^2)\right]\right] \end{aligned} \tag{6.8}$$

[1]The scale independence is essentially a coincidence, there is no significance to this. It is good suggestive evidence that the commonly used convention of varying the scale up and down by a factor of 2 and calling that an uncertainty on the calculation is nonsense though.

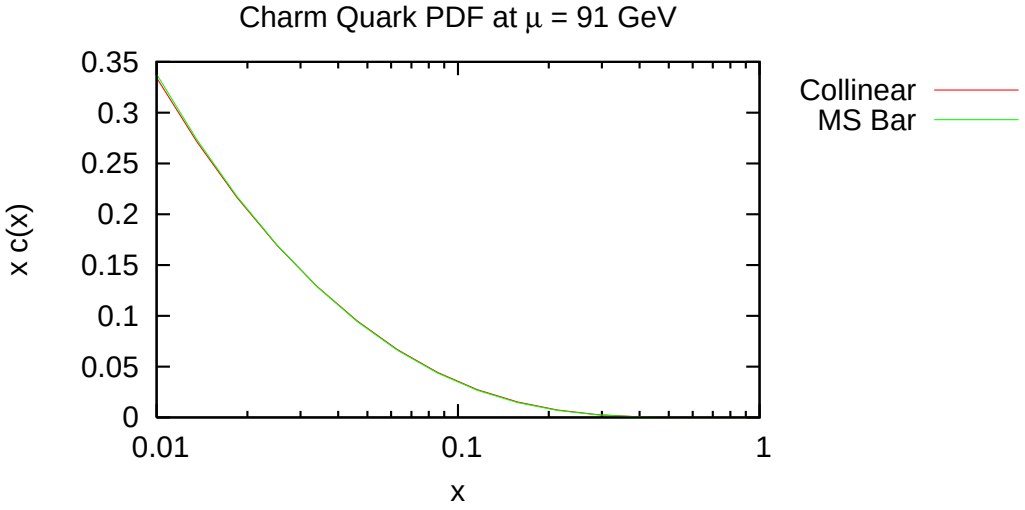

Figure 6.5: Comparison of collinear and $\overline{\text{MS}}$ charm quark PDFs over a range of x with $\mu = 91$ GeV.

$q_i\bar{q}_j \to V$	C_{ij}
$u_i\bar{u}_j \to \gamma^*$	$\frac{4}{9}\delta_{ij}$
$d_i\bar{d}_j \to \gamma^*$	$\frac{1}{9}\delta_{ij}$
$u_i\bar{d}_j \to W^+$	$\frac{1}{4\sin^2\theta_W}\left\|V_{ij}\right\|^2$
$d_i\bar{u}_j \to W^-$	$\frac{1}{4\sin^2\theta_W}\left\|V_{ji}\right\|^2$
$u_i\bar{u}_j \to Z$	$\frac{1}{8\sin^2\theta_W\cos^2\theta_W}\left(1-\frac{8}{3}\sin^2\theta_W+\frac{32}{9}\sin^4\theta_W\right)\delta_{ij}$
$d_i\bar{d}_j \to Z$	$\frac{1}{8\sin^2\theta_W\cos^2\theta_W}\left(1-\frac{4}{3}\sin^2\theta_W+\frac{8}{9}\sin^4\theta_W\right)\delta_{ij}$

Table 6.1: C_{ij} values for different modes of Drell-Yan boson production.

Notice that there are no logarithmic terms in z in the cross section. These have all been moved into the PDFs. This is because these logarithmic terms are in a sense 'related' to the collinear divergence. If there was no collinear divergence, there would be no $\frac{1}{\epsilon}$ term to produce the logarithmic terms.

The collinear scheme cross section is shown in figure 6.9. Notice that the leading order calculation has more factorization scale dependence, but this isn't a problem because we know the factorization scale should be $\mu = Q$. At this choice of scale we find that both the gluon-quark and gluon-gluon corrections are modest, and the total correction is quite small. The leading order term is 7.83nb, and the next to leading order term actaully to 7.83nb.

In this case we see the collinear scheme works quite well. The leading order term is much closer to the total cross section, and the $\overline{\text{MS}}$ and collinear factorization schemes seem to be converging towards the same answer. The collinear factorization scheme and the $\overline{\text{MS}}$ factorization scheme with $\mu = Q$ are compared for a number of different masses at the Tevatron and the LHC in table 6.2.1.

Additional plots of Drell-Yan production in the $\overline{\text{MS}}$ and collinear factorization schemes are shown in figures 6.10, 6.11, 6.12 and 6.12.

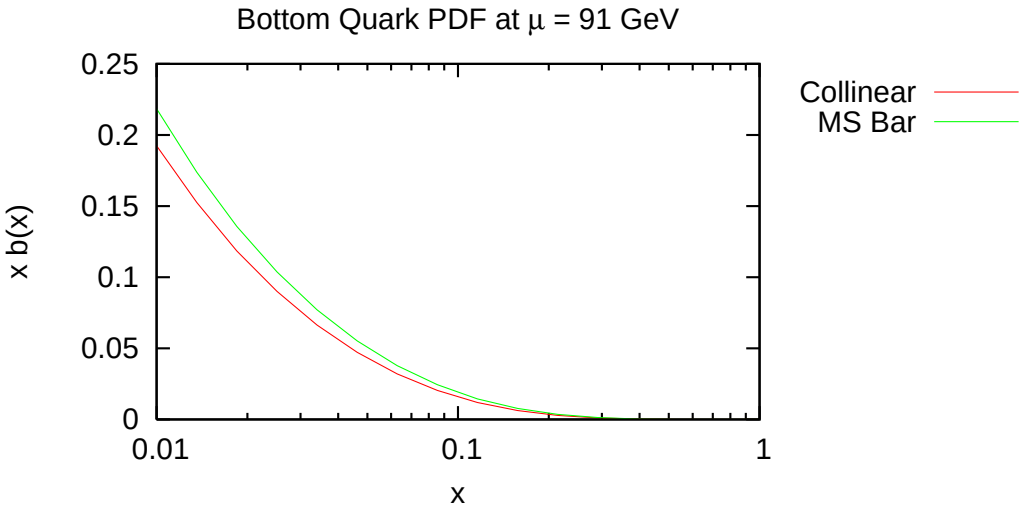

Figure 6.6: Comparison of collinear and $\overline{\text{MS}}$ bottom quark PDFs over a range of x with $\mu = 91$ GeV.

Collider	m_Z	$LO^{\overline{\text{MS}}}$	$NLO^{\overline{\text{MS}}}$	LO^{col}	NLO^{col}
Tevatron	91 GeV	6.15nb	7.97nb	7.83nb	7.83nb
Tevatron	150 GeV	1.29nb	1.66nb	1.68nb	1.65nb
Tevatron	300 GeV	120pb	156pb	162pb	158pb
LHC	200 GeV	4.70nb	5.98nb	5.42nb	5.72nb
LHC	500 GeV	221pb	275pb	264pb	268pb
LHC	2 TeV	0.679pb	0.872pb	0.884pb	0.873pb

Table 6.2: Drell-Yan Z boson production in two different factorization schemes. Notice the consistenly small NLO corrections the collinear scheme produces.

Notice that the convergence of the perturbation series improves over a range of scales at both colliders, and both schemes seem to be converging to the same value.

6.2.2 Gluon Fusion

Gluon fusion is the simplest case to consider for a gluon initiated process. Working in the effective theory where the top quark is integrated out, the $\overline{\text{MS}}$ renormalized cross section is: [4]

$$\begin{aligned}\sigma_{gg\to H} \;=\; & \frac{\alpha_s^2}{576\pi v^2(1-\epsilon)}\frac{\alpha_s}{2\pi}\left(\frac{4\pi\mu_D^2}{m_H^2}\right)^{\epsilon}\frac{1}{\Gamma(1-\epsilon)}\int_{z_0}^1 dz\Bigg[\{q\otimes\bar{q}\}\left(\frac{z_0}{z}\right)\frac{64}{27}\frac{(1-z)^3}{z} \\ & + \{g\otimes q\}\left(\frac{z_0}{z}\right)\left[-\frac{1}{\epsilon}P_{gq}(z)+P_{gq}(z)\log\frac{(1-z)^2}{z}+C_F\frac{(1-z)(3z-7)}{2z}\right]+\{g\otimes g\}\left(\frac{z_0}{z}\right)\Bigg[\\ & -\frac{2}{\epsilon}P_{gg}(z)+8C_A\frac{(1-z+z^2)^2}{z}\left(\frac{\log 1-z}{1-z}\right)_+-4C_A\frac{(1-z+z^2)^2}{z(1-z)}\log z-\frac{11}{3}C_A\frac{(1-z)^3}{z} \\ & +\left(\frac{11}{3}C_A+\frac{2\pi^2}{3}C_A-2b_0\log\frac{m_H^2}{\mu_{UV}^2}\right)\delta(1-z)\Bigg]\Bigg] \qquad (6.9)\end{aligned}$$

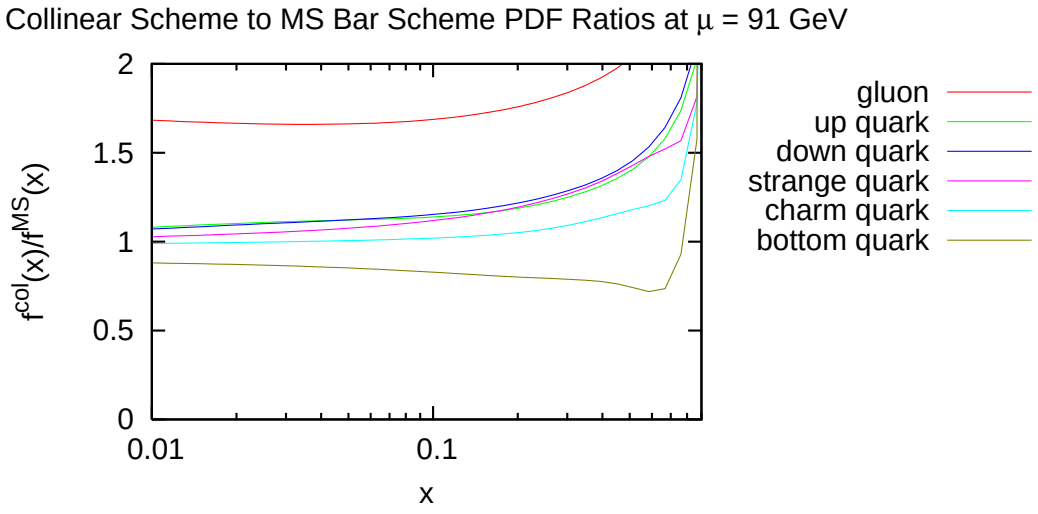

Figure 6.7: $\frac{f^{col}(x)}{f^{\overline{MS}}(x)}$ for the PDFs with $\mu = 91$ GeV. The poor behavior on the right side occurs because the PDFs drop to zero and does not affect the cross section. Notice the gluon collinear PDF consistently gets the largest corrections when compared with $\overline{\text{MS}}$, about 60%. The other collinear scheme PDFs get smaller but still sizeable corrections when comparted with the $\overline{\text{MS}}$ PDFs.

Collider	m_H	$LO^{\overline{\text{MS}}}$	$NLO^{\overline{\text{MS}}}$	LO^{col}	NLO^{col}
Tevatron	100 GeV	0.672pb	1.33pb	1.29pb	1.48pb
Tevatron	300 GeV	10.7fb	20.6fb	20.1fb	22.7fb
Tevatron	500 GeV	0.515fb	1.00fb	0.994fb	1.10fb
LHC	150 GeV	13.3pb	25.4pb	25.0pb	28.0pb
LHC	650 GeV	394fb	714fb	670fb	7.48fb
LHC	1.5 TeV	20.7fb	36.5fb	34.8fb	38.4fb

Table 6.3: $gg \to H$ with $\mu_{UV} = m_H$ and $\mu = m_H$ for the $\overline{\text{MS}}$ and collinear factorization schemes.

subtracting the collinear scheme counterterms, the collinear scheme cross section is:

$$\begin{aligned}\sigma^{col}_{gg\to H} &= \frac{\alpha_s^2}{576\pi v^2(1-\epsilon)}\frac{\alpha_s}{2\pi}\int_{z_0}^1 dz\Bigg[\{q\otimes\bar{q}\}\left(\frac{z_0}{z}\right)\frac{64}{27}\frac{(1-z)^3}{z} \\ &+ \{g\otimes q\}\left(\frac{z_0}{z}\right)\left[P_{gq}(z)\log\frac{m_H^2}{\mu^2} + C_F\left(-\frac{7}{2z}+5-\frac{5z}{2}\right)\right] + \{g\otimes g\}\left(\frac{z_0}{z}\right)\Bigg[\\ &2P_{gg}(z)\log\frac{m_H^2}{\mu^2} - \frac{11}{3}C_A\frac{(1-z)^3}{z} + \left(\frac{11}{3}C_A - 2b_0\log\frac{m_H^2}{\mu_{UV}^2}\right)\delta(1-z)\Bigg]\Bigg] \end{aligned} \tag{6.10}$$

The $\overline{\text{MS}}$ factorized cross section is plotted in figure 6.14, and the collinear scheme factorized cross section is plotted in figure 6.15. Note how much better the collinear scheme does in approximating the cross section at leading order. The leading order cross section in the collinear scheme is 1.6pb. The next to leading order cross section is 1.8nb, a 12% increase. Compare this with the $\overline{\text{MS}}$ factorization scheme, where the NLO correction is closer to 100%.

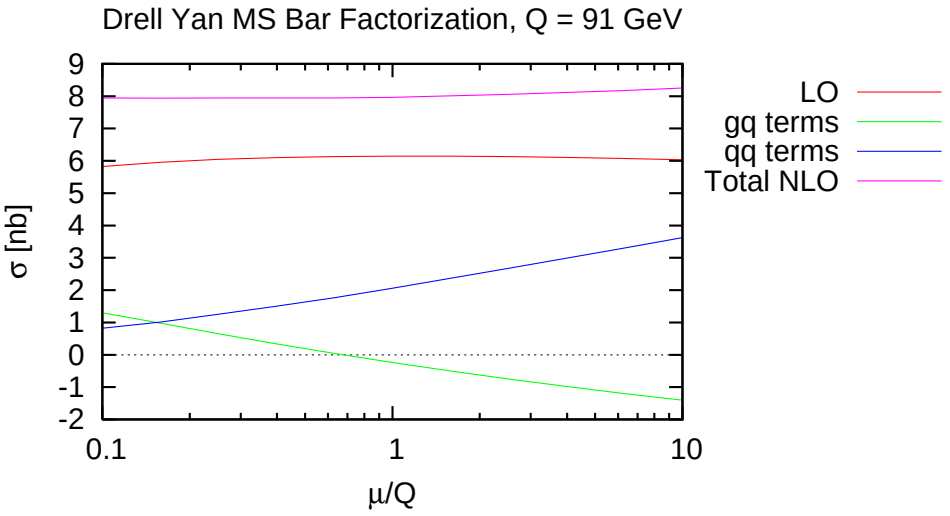

Figure 6.8: Real Z production cross section at the Tevatron calculated in the $\overline{\text{MS}}$ scheme.

The collinear scheme seems to dramatically improve the convergence of the perturbation series in this example. The corrections are now on the order of what is to be expected in a QCD calcuation, α_s. This is very encouraging.

6.2.3 Bottom Quark Fusion

The final process we will test the result on is Higgs production by bottom quark fusion. The cross unregulated cross section for Higgs production by bottom quark fusion is [5]

$$\begin{aligned}\sigma_{b\bar{b}\to H} &= \frac{\pi}{6S}\frac{m_b^2}{v^2}\mu_D^{2\epsilon}\frac{\alpha_s}{2\pi}\left(\frac{4\pi\mu_D^2}{m_H^2}\right)^{\epsilon}\frac{1}{\Gamma(1-\epsilon)}\int_{z_0}^1\frac{dz}{z} \\ &\quad\left[\{g\otimes b\}\left(\frac{z_0}{z}\right)\left[-\frac{1}{\epsilon}P_{qg}(z)+P_{qg}(z)\log\frac{(1-z)^2}{z}+\frac{1}{4}(1-z)(7z-3)\right]\right. \\ &+ \quad\{b\otimes\bar{b}\}\left(\frac{z_0}{z}\right)\left[-\frac{2}{\epsilon}P_{qq}(z)+4C_F(1+z^2)\left(\frac{\log 1-z}{1-z}\right)_+-2C_F\frac{1+z^2}{1-z}\log z+2C_F(1-z)\right. \\ &\quad\left.\left.+\,\delta(1-z)C_F\left(\frac{2\pi^2}{3}-2+3\log\frac{m_H^2}{\mu_R^2}\right)\right]\right] \qquad (6.11)\end{aligned}$$

in the collinear scheme, then the factorized cross section is

$$\begin{aligned}\sigma_{b\bar{b}\to H}^{col} &= \frac{\pi}{6S}\frac{m_b^2}{v^2}\int_{z_0}^1\frac{dz}{z}\left[\{g\otimes b\}\left(\frac{z_0}{z}\right)\left[P_{qg}(z)\log\frac{\mu^2}{m_H^2}-\frac{3}{4}(1-z)^2\right]\right. \\ &+ \quad\left.\{b\otimes\bar{b}\}\left(\frac{z_0}{z}\right)\left[2P_{qq}(z)\log\frac{m_H^2}{\mu^2}+\delta(1-z)C_F\left(5+3\log\frac{m_H^2}{\mu_{UV}^2}\right)\right]\right] \qquad (6.12)\end{aligned}$$

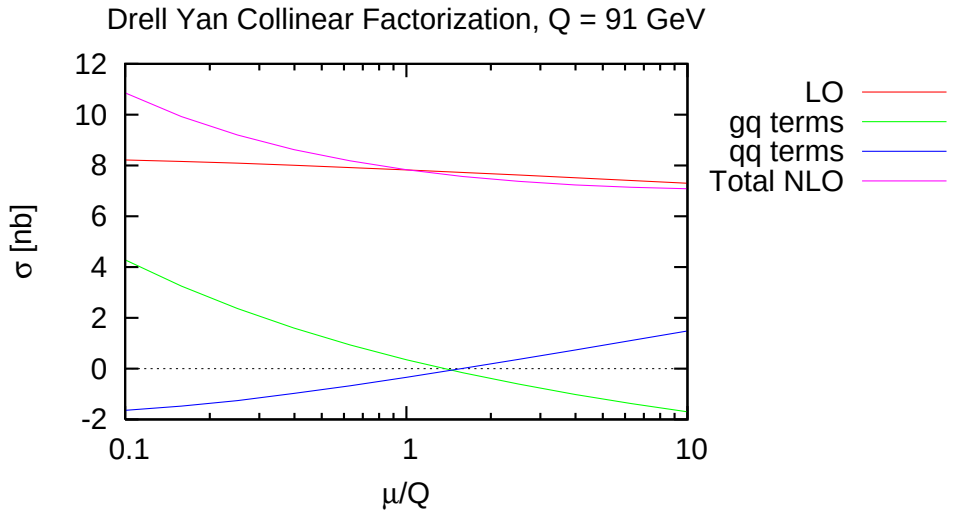

Figure 6.9: Real Z production cross section at the Tevatron calculated in the collinear scheme.

Collider	m_H	$LO^{\overline{\text{MS}}}$	$NLO^{\overline{\text{MS}}}$	LO^{col}	NLO^{col}
Tevatron	100 GeV	89.0fb	70.0fb	65.4fb	66.2pb
Tevatron	300 GeV	0.193fb	0.187fb	0.170fb	0.183fb
Tevatron	500 GeV	2.88ab	3.06ab	2.78ab	3.04ab
LHC	50 GeV	40.2pb	26.4pb	28.4pb	23.0pb
LHC	150 GeV	1.34pb	1.15pb	1.10pb	1.08pb
LHC	650 GeV	3.75fb	3.77fb	3.52fb	3.70fb

Table 6.4: $b\bar{b} \to H$ with $\mu_{UV} = m_H$ and $\mu = m_H$ for the $\overline{\text{MS}}$ and collinear factorization schemes.

The collinear scheme and $\overline{\text{MS}}$ scheme cross sections are plotted in figures 6.18, 6.19, 6.20, 6.21, 6.22, and 6.23.

In this example the $\overline{\text{MS}}$ scheme seems to do quite well over a range of kinematics. It is encouraging that the collinear factorization scheme seems to do just as well as $\overline{\text{MS}}$, and in the cases where $\overline{\text{MS}}$ sees poor convergence, the collinear scheme shows dramatic improvement over the $\overline{\text{MS}}$ scheme.[2] This is because that a large cancellation between the gb and $b\bar{b}$ initial states in the $\overline{\text{MS}}$ scheme. In the collinear scheme these two corrections are separately small, so in kinematic regions where the cancellation doesn't appear, the convergence of the perturbation series isn't affected. Note additionally that the NLO calculation at times shows less factorization scale dependence in the collinear scheme.[3]

[2]See figures 6.22 and 6.23.
[3]See figures 6.20 and 6.21

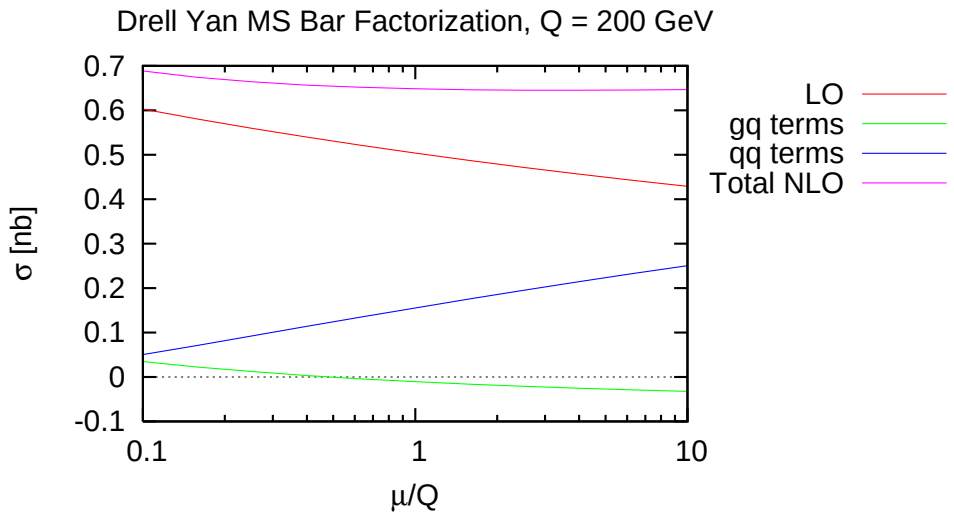

Figure 6.10: Virtual Z boson production with $Q = 200$ GeV cross section at the Tevatron calculated in the $\overline{\text{MS}}$ factorization scheme.

6.3 Conclusions

The generalized collinear scheme seems to work quite well. By analyzing the general form of the cross section that arises when the matrix element factorizes in the collinear limit, it is possible to find universal counterterms for the PDFs for radiated partons. By considering the general structure of loop corrections to point-like verticies, we can extend this definition to include the virtual corrections. This universally defined collinear scheme also provides a way to choose a scale unambiguously.

When compared with the $\overline{\text{MS}}$ factorization scheme, the collinear scheme is found to subtract additional logarithmic and polynomial terms that arise from components of phase space and spin structure that exist in $4 - 2\epsilon$ dimensions that are not present in 4 dimensions. When used to make numerical plots, it is found that these terms are numerically significant, and that using the collinear factorization scheme improves the convergence of the perturbation series, at times dramatically. For all three cases examined, the collinear factorization scheme appears to be a much better choice than the $\overline{\text{MS}}$ factorization scheme.[4] The generalized collinear scheme is manifestly universal, gauge-invariant, and leads to dramatic improvement of the convergence of the perturbation series.

[4]These examples were chosen because they are representative of all the possible spin scenarios. In Drell-Yan, we have two spin $\frac{1}{2}$ fermions producing a spin 1 boson. In Higgs production by bottom quark fusion, we have two spin $\frac{1}{2}$ particles producing a spin 0 boson, and in Higgs production by gluon fusion, we have two spin 1 bosons producing a spin 0 boson.

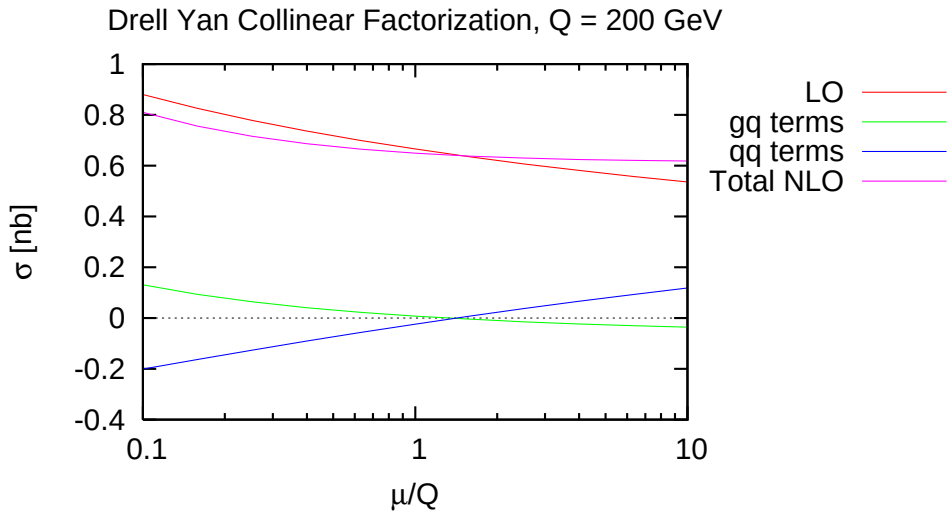

Figure 6.11: Virtual Z boson production with $Q = 200$ GeV cross section at the Tevatron calculated in the collinear factorization scheme.

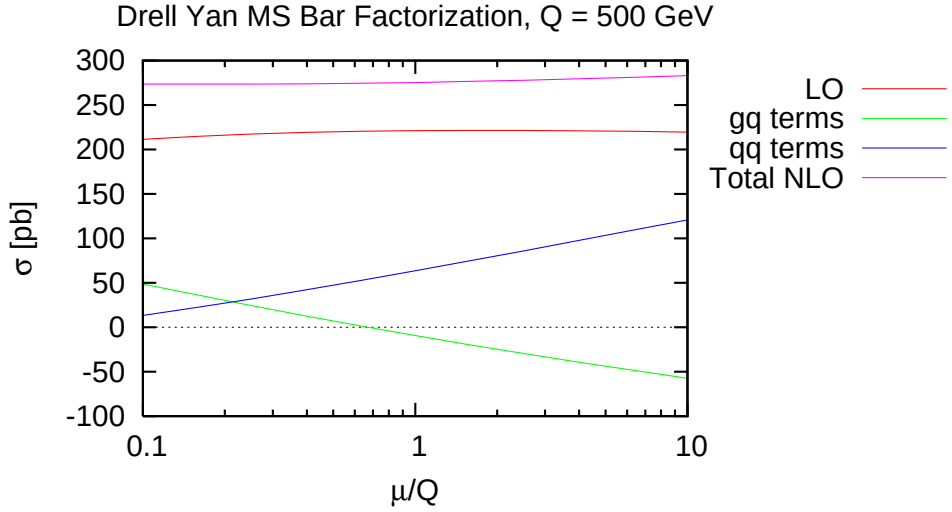

Figure 6.12: Virtual Z boson production with $Q = 500$ GeV cross section at the LHC calculated in the $\overline{\text{MS}}$ factorization scheme.

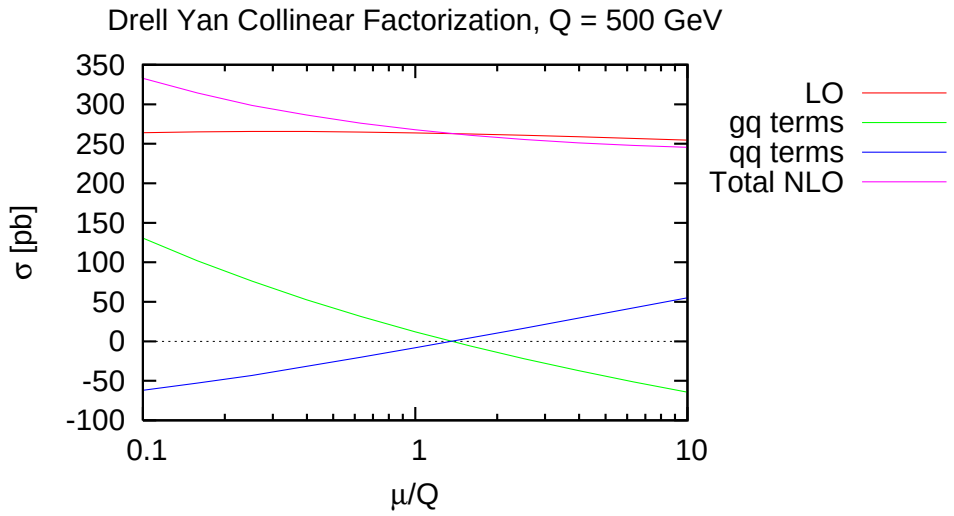

Figure 6.13: Virtual Z boson production with $Q = 500$ GeV cross section at the LHC calculated in the collinear factorization scheme.

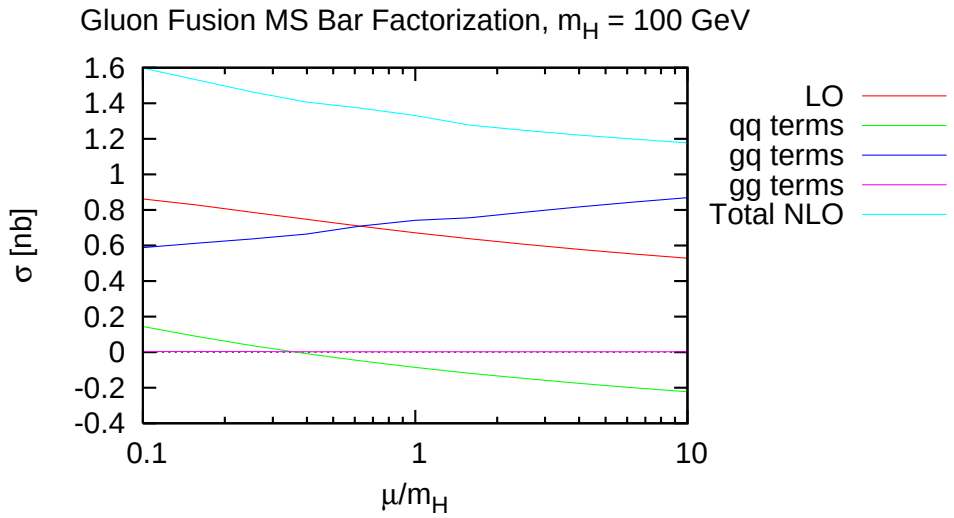

Figure 6.14: Higgs production by gluon fusion at the Tevatron with $m_H = 100$ GeV in the $\overline{\text{MS}}$ factorization scheme and $\overline{\text{MS}}$ renormalization scheme. The renormalization scale is chosen $\mu_{UV} = m_H$.

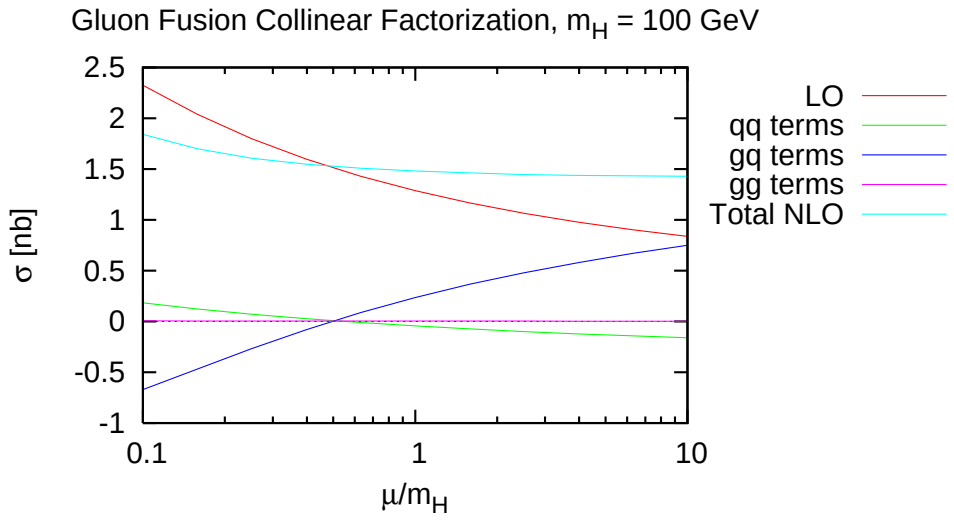

Figure 6.15: Higgs production by gluon fusion at the Tevatron with $m_H = 100$ GeV in the collinear factorization scheme and $\overline{\text{MS}}$ renormalization scheme. The renormalization scale is chosen $\mu_{UV} = m_H$.

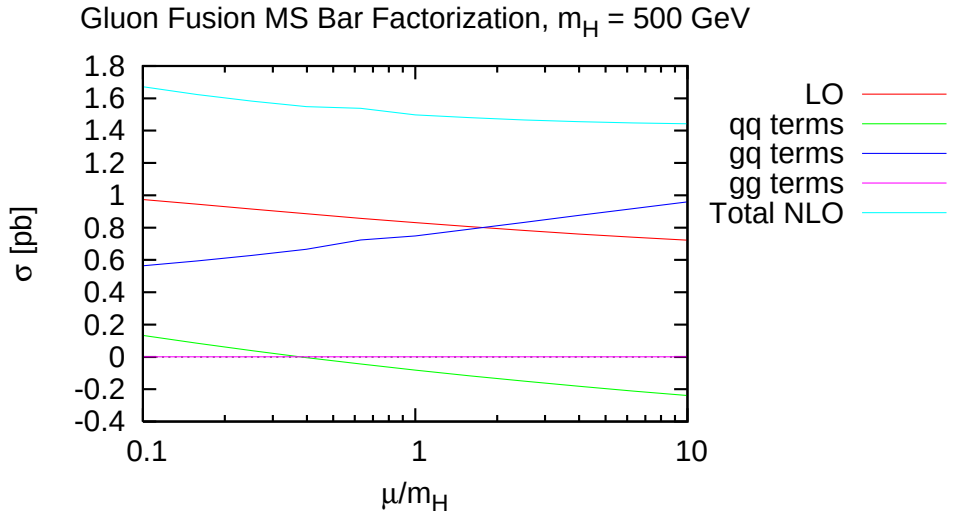

Figure 6.16: Higgs production by gluon fusion at the LHC with $m_H = 500$ GeV in the $\overline{\text{MS}}$ factorization scheme and $\overline{\text{MS}}$ renormalization scheme. The renormalization scale is chosen $\mu_{UV} = m_H$.

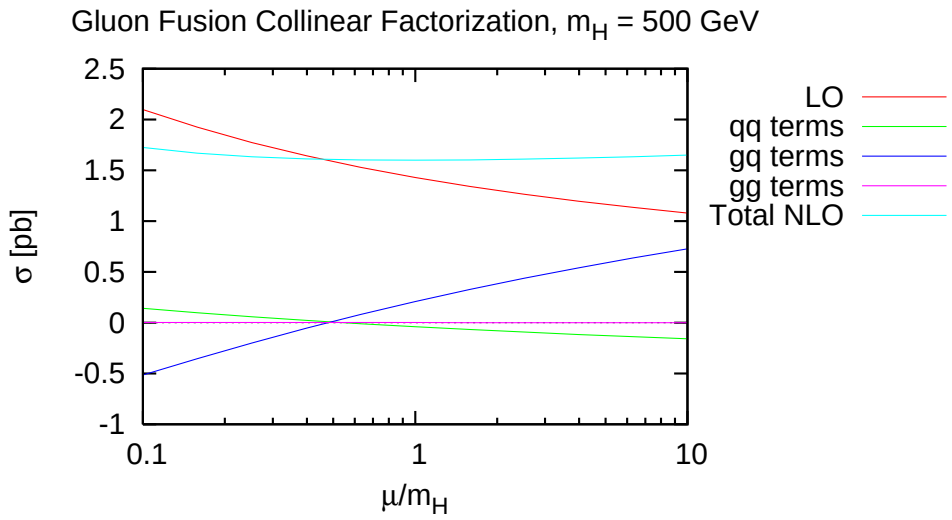

Figure 6.17: Higgs production by gluon fusion at the LHC with $m_H = 500$ GeV in the collinear factorization scheme and $\overline{\text{MS}}$ renormalization scheme. The renormalization scale is chosen $\mu_{UV} = m_H$.

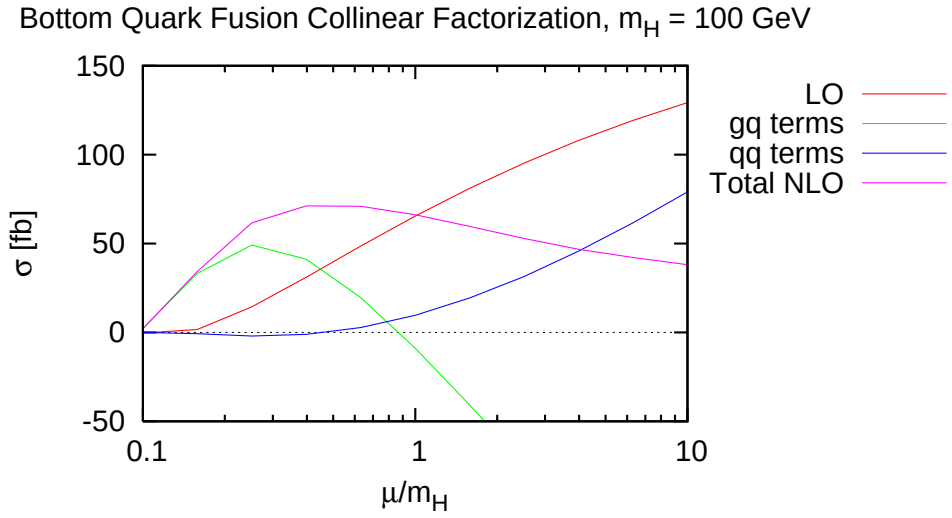

Figure 6.18: Higgs production by bottom quark fusion at the Tevatron with $m_H = 100$ GeV in the collinear factorization scheme and $\overline{\text{MS}}$ renormalization scheme. The renormalization scale is chosen $\mu_{UV} = m_H$.

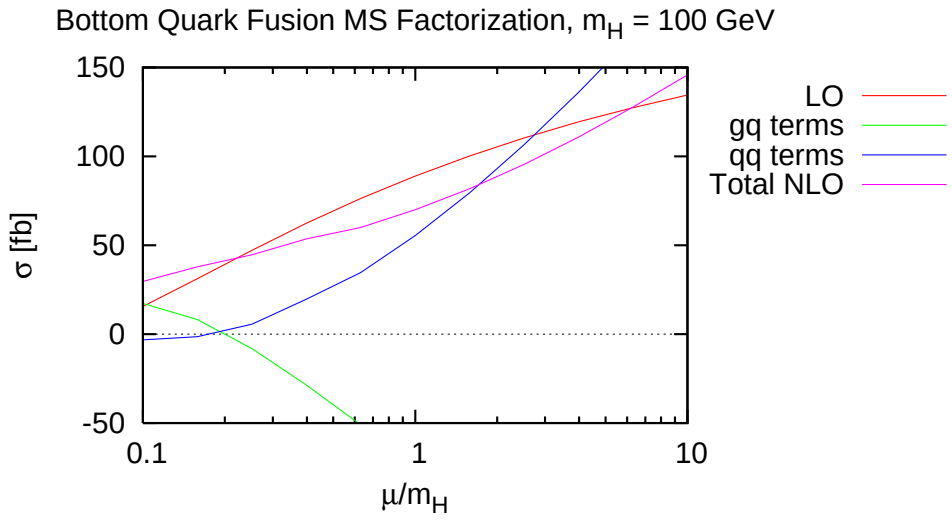

Figure 6.19: Higgs production by bottom quark fusion at the Tevatron with $m_H = 100$ GeV in the $\overline{\text{MS}}$ factorization scheme and $\overline{\text{MS}}$ renormalization scheme. The renormalization scale is chosen $\mu_{UV} = m_H$.

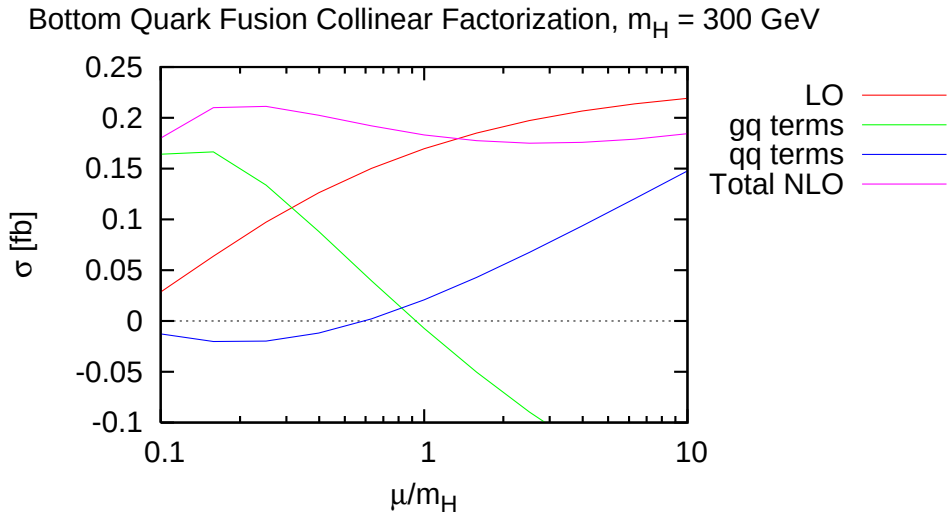

Figure 6.20: Higgs production by bottom quark fusion at the Tevatron with $m_H = 300$ GeV in the collinear factorization scheme and $\overline{\text{MS}}$ renormalization scheme. The renormalization scale is chosen $\mu_{UV} = m_H$.

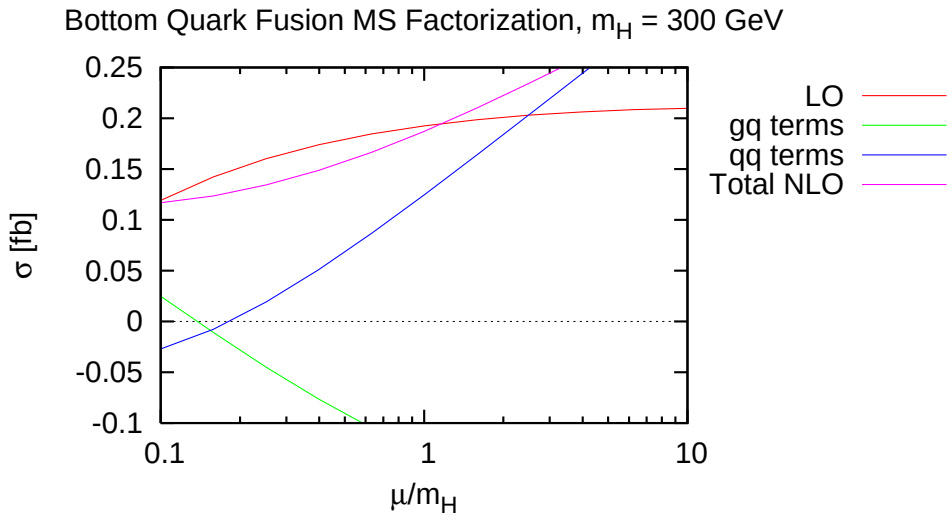

Figure 6.21: Higgs production by bottom quark fusion at the Tevatron with $m_H = 300$ GeV in the $\overline{\text{MS}}$ factorization scheme and $\overline{\text{MS}}$ renormalization scheme. The renormalization scale is chosen $\mu_{UV} = m_H$.

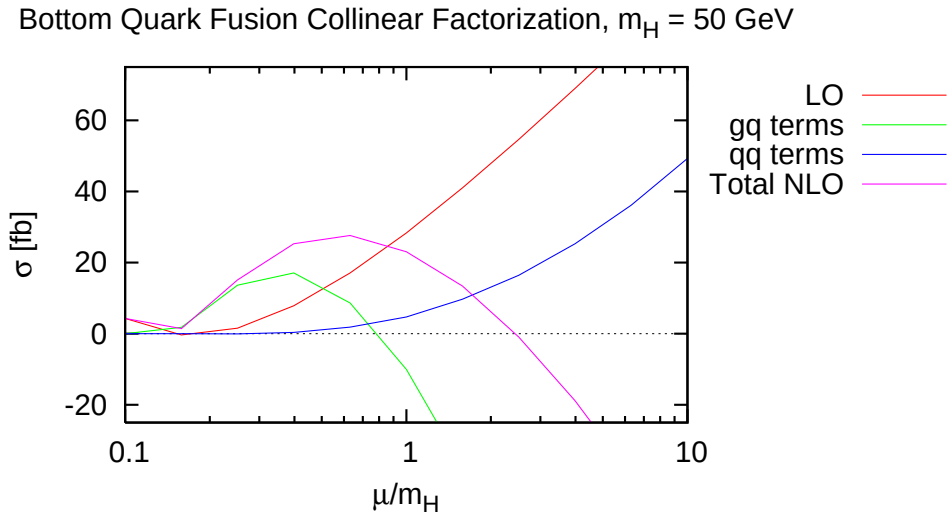

Figure 6.22: Higgs production by bottom quark fusion at the LHC with $m_H = 50$ GeV in the collinear factorization scheme and $\overline{\text{MS}}$ renormalization scheme. The renormalization scale is chosen $\mu_{UV} = m_H$.

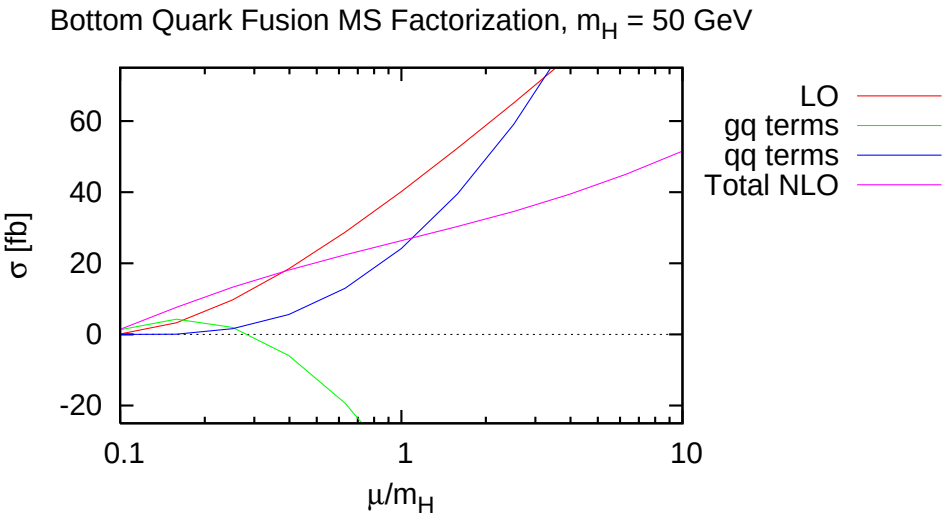

Figure 6.23: Higgs production by bottom quark fusion at the LHC with $m_H = 50$ GeV in the $\overline{\text{MS}}$ factorization scheme and $\overline{\text{MS}}$ renormalization scheme. The renormalization scale is chosen $\mu_{UV} = m_H$.

References

[1] Guido Altarelli and G. Parisi. Asymptotic Freedom in Parton Language. *Nucl. Phys.*, B126:298, 1977.

[2] Eduard Boos and Tilman Plehn. Higgs-boson production induced by bottom quarks. *Phys. Rev.*, D69:094005, 2004.

[3] J. C. Collins. Proceedings of the 25th rencontre de moriond: High energy hadronic interactions. 1990. Les Arcs, France, Mar 11-17, 1990, ed. J. Trân Thanh Vân (Editions Frontières, Gif-sur-Yvette, France.

[4] S. Dawson. Radiative corrections to Higgs boson production. *Nucl. Phys.*, B359:283–300, 1991.

[5] D. Dicus, T. Stelzer, Z. Sullivan, and S. Willenbrock. Higgs boson production in association with bottom quarks at next-to-leading order. *Phys. Rev.*, D59:094016, 1999.

[6] Yuri L. Dokshitzer. Calculation of the Structure Functions for Deep Inelastic Scattering and e+ e- Annihilation by Perturbation Theory in Quantum Chromodynamics. *Sov. Phys. JETP*, 46:641–653, 1977.

[7] V. N. Gribov and L. N. Lipatov. Deep inelastic e p scattering in perturbation theory. *Sov. J. Nucl. Phys.*, 15:438–450, 1972.

[8] B. W. Harris and J. F. Owens. The two cutoff phase space slicing method. *Phys. Rev.*, D65:094032, 2002.

[9] F. Maltoni, T. McElmurry, R. Putman, and S. Willenbrock. Choosing the Factorization Scale in Perturbative QCD. 2007.

[10] F. Maltoni, Z. Sullivan, and S. Willenbrock. Higgs-boson production via bottom-quark fusion. *Phys. Rev.*, D67:093005, 2003.

[11] Thomas James McElmurry. Collinear singularities and the factorization scale in perturbative QCD. UMI-32-42935.

[12] T. Plehn. Charged Higgs boson production in bottom-gluon fusion. Prepared for 10th International Conference on Supersymmetry and Unification of Fundamental Interactions (SUSY02), Hamburg, Germany, 17-23 Jun 2002.

[13] Paul M. Stevenson and H. David Politzer. OPTIMIZED PERTURBATION THEORY APPLIED TO FACTORIZATION SCHEME DEPENDENCE. *Nucl. Phys.*, B277:758, 1986.

[14] Scott Willenbrock. QCD CORRECTIONS TO p anti-p $\rightarrow$ W+ + X: A CASE STUDY. Presented at Theoretical Adv. Summer Inst. (TASI), Boulder, CO, Jun 4-30, 1989.